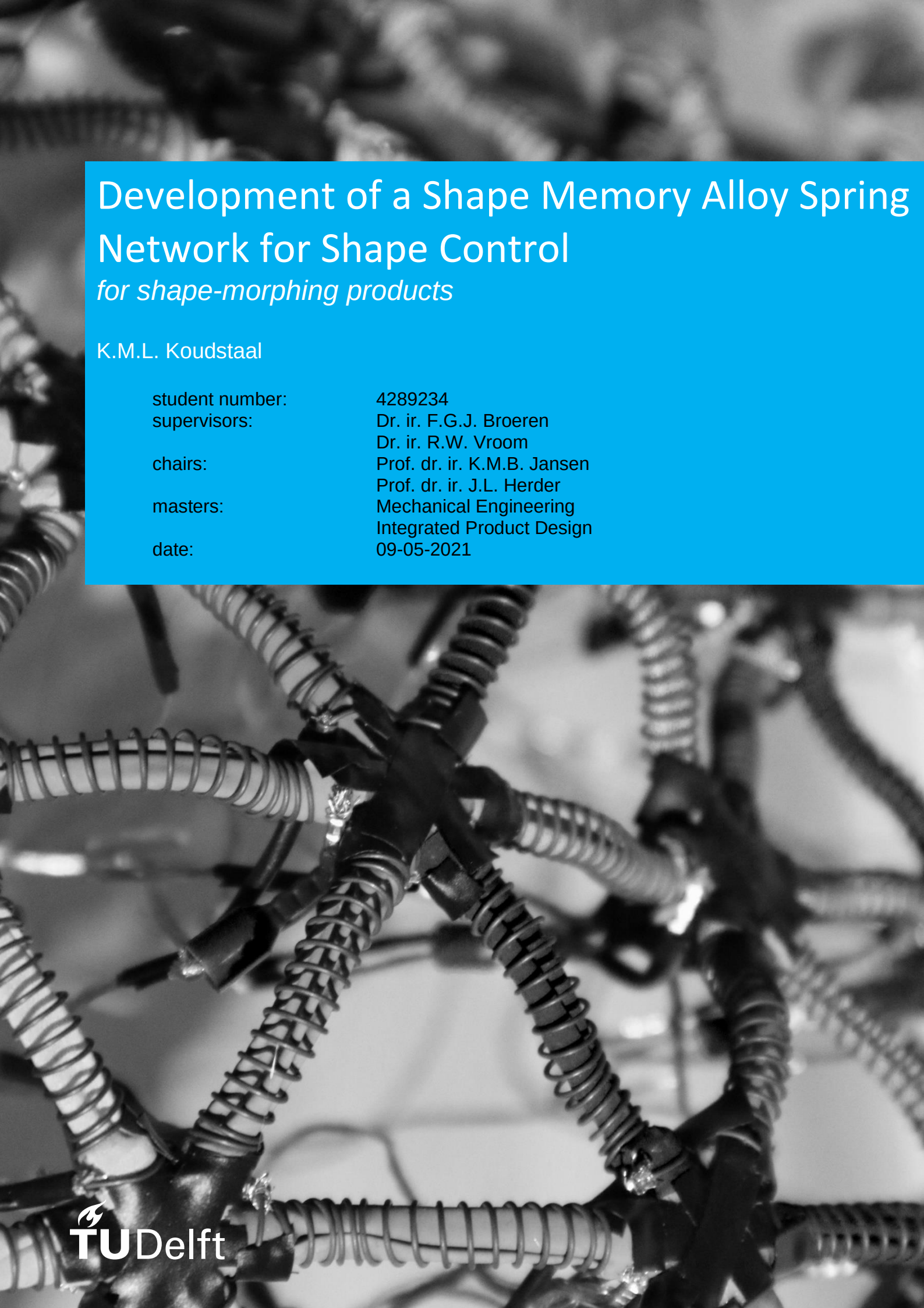

Development of a Shape Memory Alloy Spring Network for Shape Control

for shape-morphing products

K.M.L. Koudstaal

student number:	4289234
supervisors:	Dr. ir. F.G.J. Broeren
	Dr. ir. R.W. Vroom
chairs:	Prof. dr. ir. K.M.B. Jansen
	Prof. dr. ir. J.L. Herder
masters:	Mechanical Engineering
	Integrated Product Design
date:	09-05-2021

TU Delft

Development of a Shape Memory Alloy Spring Network for Shape Control

for shape-morphing products

By

K.M.L. Koudstaal

in partial fulfilment of the requirements for the degree of

Master of Science
in Mechanical Engineering and Integrated Product Design

at the Delft University of Technology,
to be defended publicly on Monday May 17, 2021 at 3:00 PM.

Thesis committee:	Dr. ir. F.G.J. Broeren,	TU Delft, supervisor
	Dr. ir. R.W. Vroom,	TU Delft, supervisor
	Prof. dr. ir. K.M.B. Jansen,	TU Delft, chair
	Prof. dr. J. Dankelman	TU Delft

TU Delft

Acknowledgements

First, I would like to thank my supervisors for putting together this assignment. I would also like to thank them for having fruitful meetings almost every week during the project. Their enthusiasm and helpfulness helped me in starting every week refreshed. In addition I would like to thank Jenny Dankelman for making time to participate in the examination committee.

Then, I would like to thank all the PMB stuff for kindly helping me with all kinds of questions, and for inviting me in their coffee breaks and chitchat, especially during the quiet summer.

I would also like to thank the Applied Labs staff. Especially Martin, without whom I would not have been able to set-up the electronics. I would like to thank Marcha and Tessa for their instructions of the various appliances that I used, and I would like to thank Elvis, who does not stop helping until the problem is solved.

I would like to thank Bertus Naagen for making time to patiently help me with 3Dscanning the network.

I would also like to thank Thijs Blad for making time to give me advice on modelling in Ansys.

Then, I would like to thank all of the people that participated in the brainstorm sessions, which resulted in interesting possible future applications.

And last but not least, I would like to thank Bram, my sister, my parents and my friends for their love and support, especially in the last phase of the project.

K. Koudstaal
Delft, May 2020

Summary

The interest in shape-shifting materials has increased over the past years. A part of this field concerns the shape-shifting of sheets from flat configuration into a double curved configuration, requiring nonuniform strain among the sheet. This functionality can be used for various purposes, in different application fields. For example, shape-changing properties are increasingly used in tangible user interfaces. For activating these sheets, shape memory alloys (SMAs) lend themselves well. That is why multiple shape-shifting sheets that are activated with SMAs already exist. However, a new design is developed and explored in this thesis, in which SMA springs are used as compressive bendable actuators. This is different from the designs that are found in literature, and the distributed low bending stiffness could potentially lead to smoother shapes.

The goal of the project is to create a SMA spring network that can deform out-of-plane into a specific shape and to explore possible applications. The idea is to prescribe this shape by prescribing the related nonuniform strain via controlling the springs individually. Through an iterative prototyping process such a network is developed. Flexures are included to impose the out-of-plane bending direction. Antagonist hoses are included to prevent these flexures from interacting with the springs and to draw the network back in plane upon cooling. In the final prototype, the shape of the network can be adjusted via binary activating the springs with Joule heating. More possible future applications of the network are explored through brainstorm sessions. In addition, a finite element model (FEM) is set-up to calculate the resulting shape upon an activation scheme. The important network parameters are tested and integrated in simple elements.

The demonstrator can successfully deform out of plane into different shapes upon different activation schemes, although the shape control is low, and the overall shape not very smooth due to excessive local bending of the network struts. This could be diminished by increasing the bending stiffness of the struts. However, this would lead to less overall deflection as well. The control over the strains or the bending should be improved for enhanced shape control. To evaluate the FEM, the prototype is 3Dscanned and compared with the result of the FEM. There is a significant difference in the amount of deformation, which may be due to inaccuracies in the model or in the prototype. The validity of these should be improved before further evaluating the effectiveness of the simplified model.

Contents

1 Introduction

1.1. Background

The interest in shape-shifting materials has increased over the past years [1]. A part of this field concerns the shape-shifting of sheets that can morph from a flat configuration in 2D into a double curved configuration in 3D. This shape-shifting technology can be used in various field. Example functionalities and application fields include the following:

- ease of packaging, transporting and storing
- ease of assembly [2]
- soft robotics [3] [4]
- tangibilizing digital information [5] [6]
- user interfaces [7] [8] [9] [10]
- adaptive optics [11]
- adaptive ergonomics [12] [13]
- adaptive architecture [14]
- adaptive aerodynamics [15]

In order for a flat sheet to deform into a double curved shape, it is necessary to stretch or shrink the sheet nonuniformly. This fact can be derived form *Theorema Egrigium* (which is Latin for Remarkable Theorem). The principle is often explained with creating a 2D map of the Earth; this cannot be done without distorting the sizes of countries. Following the same line of thought, it is possible to prescribe a shape with the amount of stretching or shrinking. This has previously been done at smaller scale in gel sheets [16].

Shape memory alloys (SMAs) can be used for shape-morphing features [17]. Especially SMA spring actuators are useful because of their ability to deform substantially. Therefore, multiple examples exist in which these are used to deform initially flat sheets. In the examples that are found in literature, the SMA spring actuators are programmed to contract upon activation, causing the actuation force to act in one line. The idea for this project is to use SMA springs in compression, and to allow them to bend as well, so that they can deform out of plane. It is expected that this distributed bending could lead to smoother surfaces.

1.2. Objective

The main objective is to design a shape memory alloy spring network that can deform out-of-plane into a prescribed shape upon a nonuniform stretch. Therefore, it is necessary to also create model that can calculate the required stretch. In addition, possible applications of the network will be explored. A demonstrator will be created to demonstrate the shape-morphing capabilities of the network.

The original Design Brief with the proposed project set-up can be found in Appendix X; the set-up that is described in here is refined after doing a literature research. The background information that is used for setting up the project can be found in the Literature Report, which can be found in Appendix XI.

1.3. Structure

The structure of the report is as follows. At first, a paper is presented, which can be seen as a conclusive summary of the project results, aside from the exploration of applications. At second, a more elaborate

report of the project as a whole is presented. This starts with describing the prototyping process throughout which the network design is developed in Chapter 3. A so called research-through-design process is used to iteratively develop the network upon gaining knowledge from prototypes. Hereafter, the exploration of applications is discussed in Chapter 4. An overview of the final demonstrator is given in Chapter 5. The modelling process and resulting simplified FEM model to predict resulting network shapes upon activation schemes is discussed in Chapter 6. This chapter has some overlap with the paper presented in Chapter 2. Finally, the report is closed off with a discussion, a conclusion and some recommendations.

2 Paper

Shape Control via a Shape Memory Alloy Spring Network

Authors

***Abstract* – The shape-shifting of flat sheets into a double curved sheet can be used for different purposes, such as multifunctionality and transport efficiency. In this paper, a design for a shape morphing sheet with bendable shape memory alloy (SMA) spring actuators is proposed and its behavior is analyzed. The shape of the sheet is controlled via binary electrical activation of the springs. A prototype is made and a simplified finite element model (FEM) is set-up. The result of the FEM is compared to a 3Dscan of the activated prototype. The result of the prototype shows that the network can deform out-of-plane into different curvatures. However a solution should be found for the local buckling of springs for smoother overall shapes, and the shape control could be improved. In addition, the FEM model should be set-up more accurately to improve its solution.**

***Keywords* – shape memory alloy, planar spring network, double curvature, shape morphing**

I. INTRODUCTION

The interest in shape changing features for a dynamic product interaction is increasing. An example product category in which a dynamic product interaction is essential is 'objects with intent'. These are everyday objects that are given a certain intelligence to fulfill a purpose through an enhanced relation with its user [1]. This is a growing category because of growing artificial intelligence. New shape changing capabilities augment the design space regarding product expressiveness here.

Shape change is a rather broad term; multiple types of shape change exist. Taxonomies to describe reconfigurable user interfaces have been established and refined [2]. The type of shape change of interest here is a change in intrinsic *curvature* enabled by nonuniform *stretchability* of a surface. Enabling a change in intrinsic curvature largely expands the shape changing capabilities compared to a change in merely extrinsic curvature.

Extensive research has been done on using shape changing mechanisms to adjust the intrinsic curvature of a surface. We can distinguish between surface normal actuators and surface parallel actuators (which is a typical distinction for deformable mirrors) for actuation types to distort the surface metric. An example of a user interface that uses surface normal actuators to change the surface curvature is inFORM [3]. A disadvantage of using surface normal actuators is the need of a reaction plate; the use of surface parallel actuators results in a more elegant system. Surface parallel actuators can be categorized based on the initial actuation principle, which is either bending or buckling [4]. Bending is caused by out-of-plane bending moments due to nonuniform stresses throughout the thickness of the sheet. Buckling is caused by compressive in-plane forces. Note that in the case of buckling, the initial buckling direction is usually undetermined. After initial transformation, the remaining bending moments and compressive stresses together determine the final shape of the sheet.

Different actuators can be used to provoke either bending or buckling in flat sheets. It is believed that smart materials could play an important role in the field of product interaction [5]. For shape changing features especially, embedded shape memory alloy (SMA) wires are promising [6]. Therefore, it should not come as a surprise that research has been dedicated to the use of SMA actuators to curve initially flat sheets. A commonly used technique is to a SMA spring actuator at two points on a sheet, causing the sheet to bend upon contraction, such as in the case of Surflex, Bosu, SMAAD Surface and NURBSforms [7] [8] [9] [10]. In some cases, the actuator is woven into a fabric, causing the fabric to ripple [11] [12]. SMA bending actuators do not only appear in linear form, but can also come as rotary actuators, which could for example be used to fold origami patterns in shape changing sheets [13].

Note that in the case of applying multidirectional bending moments on a sheet, an additional requirement is that the sheet can nonuniformly stretch to obtain a nonzero Gaussian curvature. In this paper, the idea is to integrate the activation mechanism and this requirement by prescribing the metric of a surface through nonuniformly stretching the surface, causing the sheet to buckle. A similar principle has previously been applied at smaller scale in gel sheets [14]. A SMA spring network is designed, enabling programming different shapes through binary activation of different springs. A simplified finite element model (FEM) to predict the

shapes is presented and the results are compared to a prototype. The prototype is a functional prototype and its design principles could be a source of inspiration for further research.

First, the network design is discussed. Thereafter, the fabrication of the springs, the setup of the FEM and of the prototype test are discussed in *Materials and Methods*. At last, the results of the prototype test are compared to the results of the model.

II. DESIGN

A. *Network lattice*

As the deformation mechanism is based on in-plane forces, a high in-plane lattice stiffness is desired, so that spring deformations are converted to in-plane stresses rather than in-plane motions. Therefore, a general triangular lattice is chosen for the network structure (see Figure 1A) which is a stretching-dominated lattice with no mechanism [15]. The network boundary blocks are fixated on a rigid plate.

B. *Network components*

The design of the network is explained here via descriptions of all component functions. A sideview of the components in one strut can be found in Figure 1B.

- **SMA springs** – The SMA springs are the actuators of the network that exert compressive forces or elongate upon heating. The springs are rather special actuators, as they can bend passively too. The spring parameters and characteristics are discussed in Materials and Methods.
- **Connectors** – The main function of the connectors is simply to connect the springs; they are the nodes of the lattice. Besides, the mass of the connectors introduces a gravity bias force that draws the network back in plane upon cooling. The connectors are 3D printed with ABS.

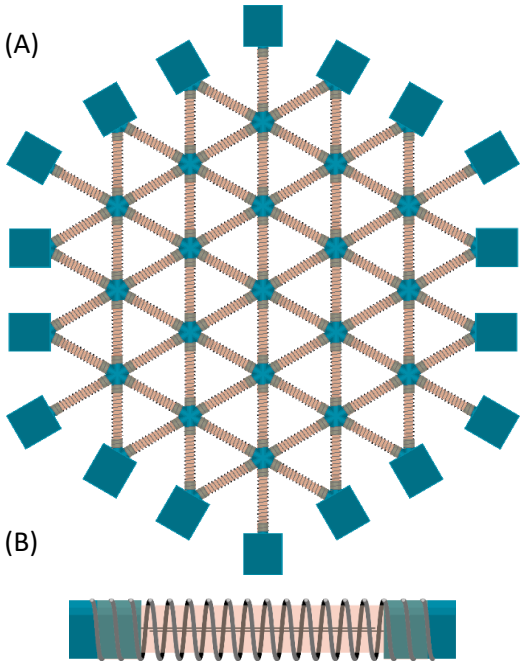

Fig. 1. (A) A top view of the overall design of the network. The network boundaries are fixated on a rigid plate. (B) A side view of a strut with a spring, connector ends, flexures and hose.

- **Flexures** – In each strut, there are two stainless steel flexures that can slide over each other. Each connector end has one flexure attached. The main function of the flexures is to impose out-of-plane deformations by obstructing in-plane rotational deformations. Besides, the flexural rigidity introduces a bias force. The flexures should remain in contact, so therefore they introduce a strain limit of the strut of 100%.
- **Elastic hose** – The main function of the elastic hose is to prevent the flexures from getting caught in between the spring windings. Besides, the elasticity introduces a bias force.

C. *Required spring force*

In order to take an initial guess of the required spring force, we have a look at the situation that is shown in Figure 2. The configuration is used to estimate the bias forces that have to be overcome. There are multiple end conditions in the network that could affect the interplay of forces. Therefore, the network will be examined through a finite element analysis of the total network later.

The spring force should be greater than the buckling force. The buckling force depends on the spring parameters. After buckling, the point of balance between the spring force and the bias forces prescribes the final shape. The weight of the

connectors is a constant bias force, but the elasticity of the hose, the rigidity of the flexures and the rigidity of the spring itself are nonlinear bias forces. The mass of one strut is approximately 1.5 g. The thickness of the flexures is 0.04 mm. These values result in relatively small bias forces, which are therefore neglected here. The bending stiffness of the spring can be neglected as well. Consequently, the sum of the bias forces is mainly defined by the elasticity of the hose. The force strain curve is plotted in Figure 3. The flexures impose a strain limit of 1, so the maximum force that could be exerted by the elastic hoses if they would not be prestrained is around 2 N.

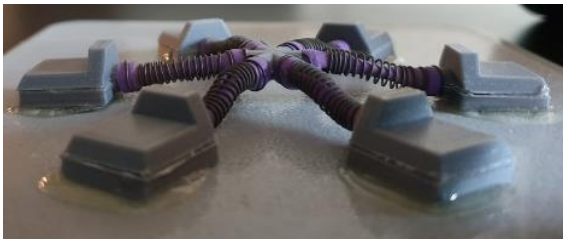

Fig. 2. Base configuration for force analysis.

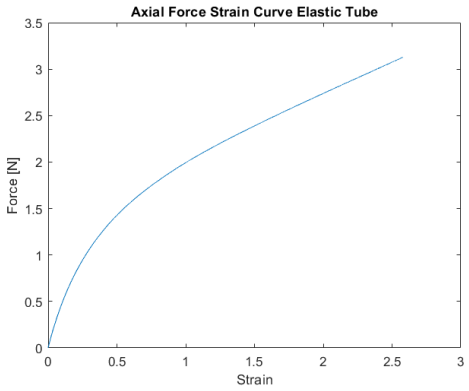

Fig. 3. The axial force caused by the elastic hose against the axial strain, to define the required spring force.

D. Spring parameters

To define the spring parameters (see Figure 4), an engineering design framework for a SMA coil spring actuator can be used [16]. The first step in the framework is to obtain the material properties after applying a specific annealing program. The annealing program influences the mechanical properties and the transformation temperatures [19]. A tensile test is performed on annealed springs with a wire diameter of 0.5 mm and a spring diameter of 5 mm to obtain the material properties. However, it could be readily observed from the data (see *Materials and Methods*) that the critical spring force is around 3 N in the austenite phase, so these spring parameters will be used right away. The initial pitch angle should be large enough to be able to compress the spring to half its own length. The number of windings influences the stroke. The springs have a pitch of 3.1 mm and 14 free windings.

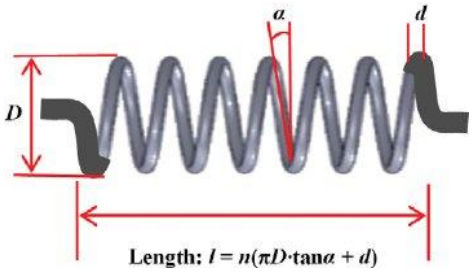

Fig. 4. The parameters of the SMA coil spring actuator. [16]

III. MATERIALS AND METHODS

A. Fabrication of springs

Flexmet^{TM} NiTiCu wires with a diameter of 0.5 mm are used to fabricate the springs. The springs are wound with a conventional manual spring winder, see Figure 5A. A threaded rod is used, because that makes it easier to avoid overlap of the windings without having to set a very large pitch angle, which results in more regular windings. The wound wire is placed on a smooth rod with a diameter of 4 mm. The pitch angle of the springs can be prescribed in a discrete manner with the number of wires that are wound around one rod. Here, we put six wires on one smooth rod. The wires are pulled tightly and are fixated onto the rod with terminal blocks before going into the ceramic oven. The springs are annealed at a temperature of 500 °C for 15 minutes. After coming out of the oven, the springs are quenched with water.

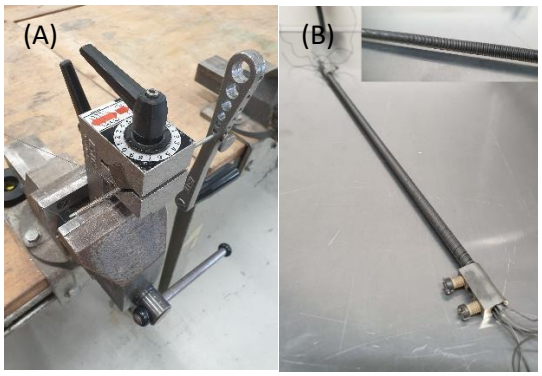

Fig. 5. (A) A manual spring winder is used for winding the springs. (B) The wires are clamped with terminal blocks on smooth rod for the annealing process. The pitch angle is prescribed by the number of wires wound around the rod.

B. Spring characteristics

We are interested in the spring characteristics, because we want to use these for the finite element model. Therefore, we will directly evaluate the spring characteristics, instead of evaluating the

material properties first. A tensile test is performed on the springs using a ZwickRoel™ Static Materials Testing Machine. It is assumed that the results will hold for compression as well. The springs are heated by means of resistive heating. The resulting force strain curves can be found in Figure 6.

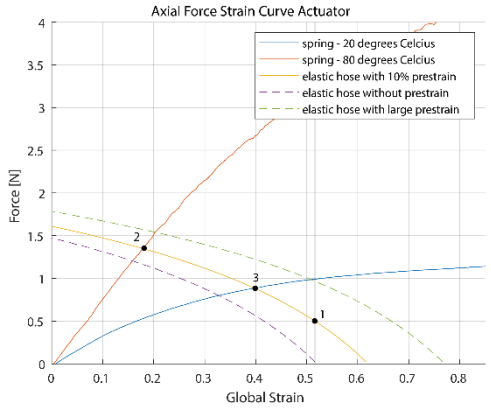

Fig. 6. The measured force strain curves. Point 1 is the initial flat state. Point 2 is the hot state. Point 3 is the cold state.

The bias force that is introduced by the elastic hose is included in Figure 6. Changing the amount of prestrain of the hose is like shifting the graph of the hose over the horizontal axis. Herewith, the stroke of the spring can be regulated. A prestrain of roughly 10% is set during the manufacturing process. The manufacturing process is as follows. The springs are compressed such that when let go, they are compressed up to 52% of their free austenite length (see point 1 in Figure 6) which results in an initial strut length of 21 mm. This is also the length of the flexures. Hoses are placed with some stretch alongside the springs. Upon initial activation, the springs grow from the compressed state at point 1 to the hot state at point 2, which is an elongation of 70% compared to the compressed state at point 1. Note that this is the strain that should stay below 100% due to the flexures. Upon cooling down, the springs are contracted towards the cold state at point 3, and will not go back to their originally compressed state at point 1; the strain between cold and hot state is between point 3 and point 2.

The global strain can be related to the material shear strain γ via the following equation

$$\gamma = \frac{1}{C}\frac{\cos^2\alpha_i\,(\sin\alpha_f - \sin\alpha_i)}{\cos^2\alpha_f\,(\cos^2\alpha_f + \frac{\sin^2\alpha_f}{1+\nu})} \quad (7)$$

where C is the spring index, α_i is the initial pitch angle, α_f is the final pitch angle and ν is the Poisson's ratio. To calculate the material shear strain, the global strain has to be translated to the final pitch angle first. For our spring parameters, a global strain of 40% (point 3) corresponds to a material shear strain of 1.1% and a global strain of 18% (point 2) corresponds to a material shear strain of 0.49%. Both the maximum and the minimum strain are within the typical limit strains that assure a maximum wire life for the martensite and the austenite phase respectively [20].

C. Effective bending stiffness

In the finite element analysis, the struts are modelled as beams. The bending of these beams is controlled with their thickness, such that the effective bending stiffness matches reality. The effective bending stiffness is composed off the resistivity induced by the spring itself and by the flexures. These stiffnesses are calculated here. The situation that is used is shown in Figure 2, where we are interested in the vertical stiffness of the connector.

Spring

The spring in Figure 2 is under combined lateral and axial load, which is shown schematically in Figure 7. The vertical deflection upon a lateral force depends on the bending rigidity and the shearing rigidity of the spring. If the axial load is neglected, the deflection can be calculated with

$$\delta_0 = \frac{Ql^3}{12\beta} + \frac{Ql}{\gamma} \quad (1)$$

in which Q is the lateral force, l is the compressed length under the axial load, β the flexural rigidity and γ the shearing rigidity [17]. The expressions for the flexural rigidity and the shearing rigidity are

$$\beta = \frac{2lEIG}{n\pi r(2G+E)} \quad (2)$$

$$\gamma = \frac{lEI}{\pi n r^3} \quad (3)$$

in which E is the Young's modulus, I is the moment of inertia, G is the shear modulus, n is the number of spring windings and r is the mean coil radius. The moment of inertia can be calculated with $I = \frac{\pi}{4}(r_2^4 - r_1^4)$, in which r_2 and r_1 are the outer and the inner radii of the spring, respectively. The shear

modulus can be calculated with $G = \frac{E}{2(1+\nu)}$ in which ν is the Poisson's ratio, which is taken as 0.44 [18].

To include the axial load, the deflection δ_0 has to be multiplied with a magnification factor that depends on the ratio between the axial load and the buckling load:

$$\delta = C_1 \delta_0 \tag{4}$$

$$C_1 = \frac{1}{1 - \frac{P}{P_{cr}}} \tag{5}$$

The axial load is introduced by the compression of the spring. Note that the axial load changes throughout the out-of-plane motion.

The critical buckling load can be calculated with

$$P_{cr} = \frac{\pi^2 \beta}{l^2} \left(\frac{1}{1 + \frac{\pi^2 \beta}{l^2 \gamma}}\right) \tag{6}$$

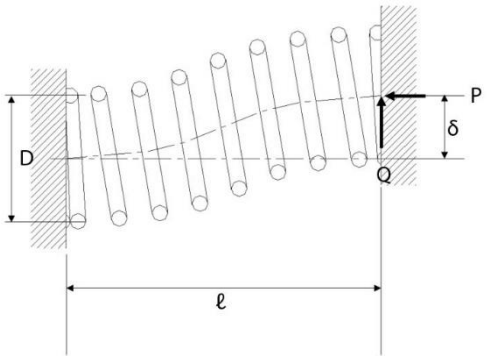

Fig. 7. A combined load on a coil spring.

Flexures

The two flexures within a strut are seen as one flexure under lateral load for the calculation here. It is assumed that there is no axial load on the flexures, because they can slide. The deflection can be calculated with

$$\delta_0 = \frac{Q l^3}{12 E I} \tag{7}$$

in which Q is the lateral force, l is the compressed length under the axial load, E is the Young's modulus and I is the moment of inertia. The moment of inertia can be calculated with $I = \frac{bh^3}{12}$ in which b and h are the width and the height of the flexures, respectively. The height of one flexure is 0.04 mm. The effective height variates between the thickness of two flexures and the thickness of one flexure throughout the out-of-plane motion. At an elongation of 70% (point 2 in Figure 6) compared to the initial state (point 1 in Figure 6), the amount of overlap is 18%, resulting in an effective thickness of 0.047 mm.

Thickness

The effective stiffness $\frac{Q}{\delta}$ of the spring and the flexures can now be calculated. The parameters that are used to calculate the effective stiffness can be found in Table 1. To calculate the thickness of the beam for the finite element analysis, Equation 4, 5, and 7 can be used again, but the critical buckling load should now be calculated with Equation 8, which is the critical buckling load for a beam with hinged ends. This end condition is used, because most struts in the network comply to this end condition, because the connector can rotate.

$$P_{cr} = \frac{EI\pi^2}{l^2} \tag{8}$$

Table 1 Parameters to calculate effective bending stiffness and therewith effective thickness, based on prototype parameters

Parameter	**Unit**	**Value**
Material		
Spring Poisson's ratio ν		0.44
Flexure elastic modulus E	[GPa]	190
Geometry		
Strut length (initial) l	[mm]	21
Number of spring windings		14
Spring inner radius r_1	[mm]	2.0
Spring outer radius r_2	[mm]	2.5
Flexure width b	[mm]	3.0
Flexure height average h	[mm]	0.047
Load		
Axial load P	[N]	1.35

It is difficult to mimic the effective stiffness of the real prestrained system with the modelled unprestrained system throughout the whole out-of-plane motion. This is because the prestrain introduces a constant force right from the start, which decreases the effective bending stiffness, and changes throughout the motion. This cannot be realized with the elastic modulus in the model alone. In addition, it is not possible to compressively prestrain the BEAM188 elements that are used in the finite element analysis to sufficient extent. Also, the flexures introduce a nonlinear bending stiffness throughout the motion. Therefore, we focus on the

equilibrium situation of the system in the final configuration. It is believed that if we make sure that the axial load and the effective bending stiffness of the final configuration resemble the axial load and the bending stiffness of the prototype at that point, the results of the simulation should be realistic.

From Figure 6, we can see that the axial load in the final configuration (point 2) is 1.35 N. It is assumed that this force acts on the springs and that the axial force on the flexures is zero. The model parameters that are free are E, b and h. These should be chosen such that the bending stiffness resembles the bending stiffness of the flexures and the spring, and the axial force at 70% strain is 1.35 N. Note that we focus on the axial stiffness versus the bending stiffness and neglect other stiffnesses. If the width b is chosen to be 15 mm, that is true for a thickness h of 12.8 mm and a modulus E of 10020 Pa. The width is constraint to be strictly larger than the thickness, such that the beam resembles the flexure shape. The width of the modelled beam is not constrained by the width of the flexure end, because beam elements (line elements) are used and their volumes can overlap.

D. Finite element model

The finite element model (FEM) is constructed and analyzed in Ansys Mechanical APDL.

Model

In the FEM, the lattice struts are represented by BEAM188 elements. The beam elements are connected with MPC184 general joint elements, which are well suited for large strain nonlinear applications. All relative six DoF of the joint are constrained. The length of the joint elements resembles the size of the connector. An overview of the input parameters can be found in Table 2.

Axial stress

The axial force is determined by the elastic modulus E, the strain ϵ and the cross-sectional area A. The previously calculated elastic modulus is taken for the linear elastic modulus in the model. To avoid zero stiffness at the critical stress, bilinear isotropic hardening is included, for which a critical stress and a tangent modulus have to be stated. The elongation due to the shape memory effect is represented by a thermal expansion of the beams. The amount of thermal expansion in cold and hot state is defined by the minimum and maximum axial strain of the spring with elastic hose, see Figure 6, so the beams will be prescribed to elongate up to 70% strain.

Bending stress

The bending stiffness of the springs and the flexures are included in the model through the geometry of the beam elements. The length of the strut is defined by its real value; the width and the height are effective parameters.

Table 2 FEM input parameters, based on prototype parameters

Parameter	**Unit**	**Value**
Material		
Elastic modulus	[Pa]	10020
Minimum strain		10%
Maximum strain		70%
Geometry		
Length connector end	[mm]	9.2
Length strut (initial)	[mm]	21.0
Height	[mm]	12.8
Width	[mm]	15.0

Load steps & Boundary conditions

In reality, the struts are initially compressed and then placed into the planar network. The thermal activation of the SMA springs causes the network to deform out of plane to a maximum. The cooling of the SMA springs causes the network to sink back to a minimum. Thermal cyclic loading will cause the network to deform in between these limits here.

In the analysis, the initial out-of-plane buckling is not simulated. The post-buckling situation is created by enforcing a small positive vertical displacement on the center connector of the network, and thereafter enforcing the resulting planar displacements of the outer ring on the outer ring, while releasing the constraint on the center connector. Thereafter, a small initial thermal load is applied to the whole network. All springs are activated up to a thermal load that relates to 10% axial strain, which is the estimated strain at the relaxed state in the prototype. Hereafter, it can be chosen what springs are activated.

E. Experimental set-up

A picture of the functional prototype in the test set-up can be found in Figure 8. A close-up of the "building blocks" that the network is composed of can be found in Figure 9A. The network ends are glued on a rigid open hexagon plate, so that the wires can be organized underneath the network. Each spring is connected to the power source with Litz wire, so that the springs can be heated via Joule heating. At each node, three springs are connected to the ground and three springs are connected to an individual LED driver module driver outlet, see Figure 9B. The springs are activated with an

effective voltage of around 1.5 V, depending on their specific resistance. Pulse-width modulation is used to regulate the effective voltage of each spring individually, such that the temperature measured at the surface of the spring is above 65 °C, which is the activation temperature of the springs prescribed by the manufacturer. Here, we assume that the activation temperature remains unchanged upon annealing, because no significant deformations are observed above this temperature, but the annealing temperature could in theory affect the activation temperature [19].

The activated network is scanned with a Artec™ Spider 3D scanner, so that the complete shape of the network is captured. A limitation is that only the top could be scanned due to the wires underneath and that the quality of the scan is diminished due to reflectiveness of some of the network parts. The scan data is an OBJ file. The scatter is manually cleaned up in both Meshmixer™ and Rhino™.

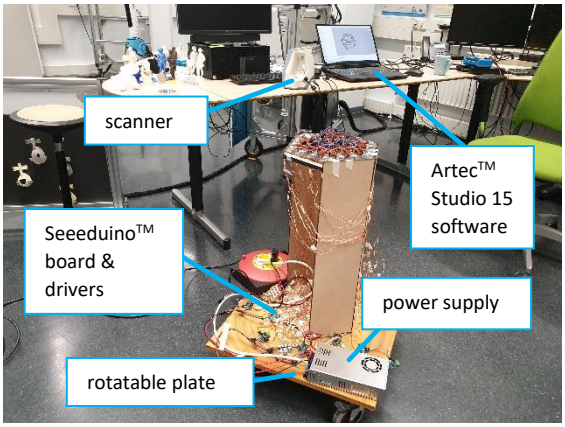

Fig. 8. The scan set-up. The network is activated and scanned. The rotatable plate allows for easy scanning around the network.

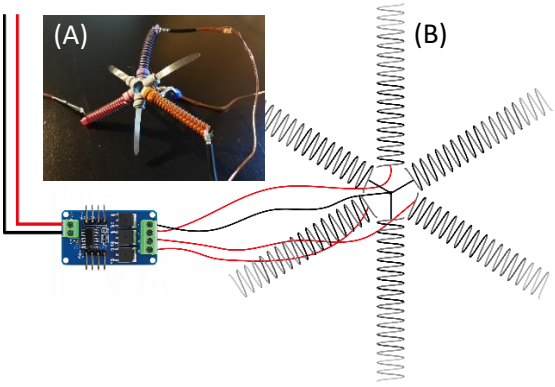

Fig. 9. (A) The "building blocks" of the network. (B) A schematic overview of an electrical node.

IV. RESULTS

Here, the results of the network itself and the results of the FEM are presented and compared.

A. *Prototype results*

Sideviews of the resulting shapes upon different activation schemes can be found in Figure 10.

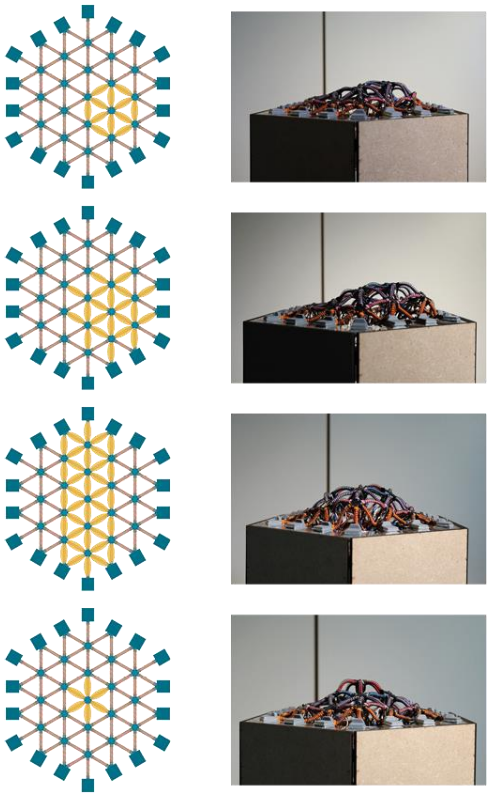

Fig. 10. Different shapes upon different activation schemes.

B. *FEM results*

To compare the FEM with the prototype, the first activation scheme of Figure 11 is used as an example case. The results of the FEM and the 3D scan are plotted together in Matlab. The result is shown in Figure 11. Due to convergence issues, the FEM has only run up to 55% strain instead of 70% strain. Different strains are shown in Figure 12 to show the development of the shape upon increasing the strain. As can be seen in Figure 11A, the FEM model expects a larger deformations than is reached in reality. In addition, there is a difference in buckling direction of some springs, see Figure 11B.

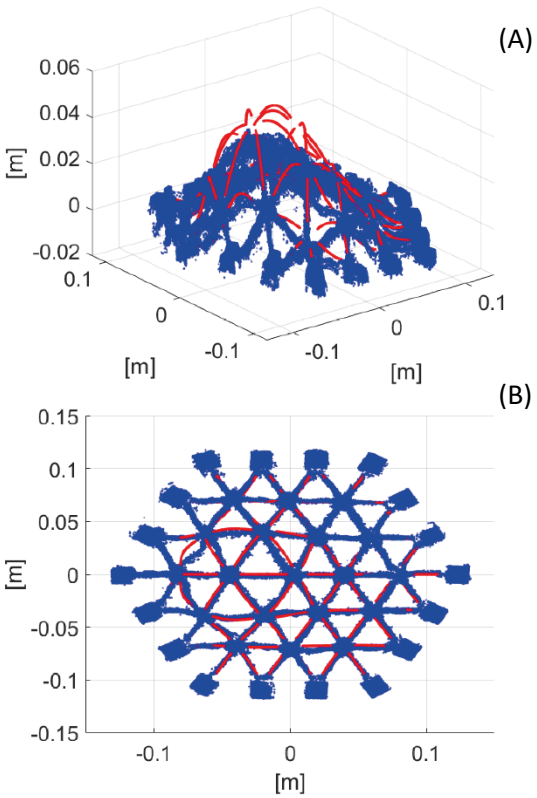

Fig. 11. The results of the FEM with 55% thermal strain and the prototype;. (A) isoparametric view (B) top view.

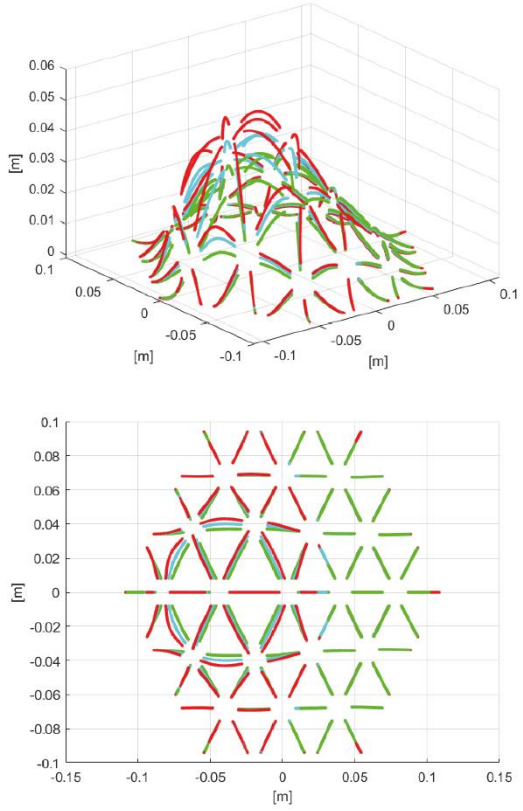

Fig. 12. Development of shape for increasing prescribed thermal strain. (green = 25%, blue = 40% and red = 55%)

V. Discussion

The prototype results show that it is possible to create different shapes upon different activation schemes. However, some springs bend locally, breaking with the overall shape. In addition, the buckling direction seems arbitrary sometimes.

The FEM results show that there is a significant difference in deflection; the maximum point in the FEM is higher than in the prototype. This difference would even been greater if the solution would have converged up to 70%. This means that the ratio between the stretching energy and the bending energy is different in both, but it is unknown if it is due to inaccuracies in the FEM or in the prototype or in both. Below, optional causes are listed.

FEM model

- All springs are modelled with the same bending stiffness. To calculate this bending stiffness an effective flexure thickness of 0.047 mm is used which is based on the 70% strain. However, most springs might actually strain less, resulting in more flexure overlap, so these springs should actually have a higher bending stiffness. To mimic the real situation best, the bending stiffness should actually be changing throughout the out-of-plane deformation.
- The elastic hoses in the prototype may shrink upon heating, similar to heat shrink tubing. This would result in a high contraction force being delivered by the elastic hoses. When looking at Figure 6, it can be seen that if the prestrain is increased (which is like shifting the curve towards the right), the strain from point 1 to point 2 is diminished.

Prototype

- The prototype could have been heated insufficiently, because it is possible that the annealing process has affected the activation temperature [19], although this effect was not observed visually.
- The wires may exert a not insignificant force on the network, which could either be pulling or pushing (due to some wire stiffness) on the network. If the wires pull more than anticipated on, this could be a explanation for the difference between the FEM and the prototype.
- Friction between the flexures and the hose and/or between the hose and the spring may prevent the network from deflecting more.

V. Conclusion

From the results of the prototype itself it can be concluded that the proposed design could be useful for shape control of surfaces; the inclined network can deform out-of-plane into different shapes upon nonuniform activation. A benefit of the design is that the actuation is integrated in the sheet itself. An interesting property is that the actuators are allowed to bend, which could hypothetically result in smoother shapes. However, the smoothness could be improved. It can be seen from the result of the prototype that, some springs buckle locally, and break with the overall shape of the network. This could be improved by using non-binary activation or by including bending control.

Modelling the behavior of the complete strut with a simple beam element could possibly be a useful method. However, the model parameters should be validated and the convergence issue should be solved before further evaluating the effectiveness of the simplified model.

VI. Recommendations

Regarding the network design, the shape-control could be improved by either including bending control or gradual strain control or both. Regarding the modelling, the values of the parameters should be examined more accurately. The stroke of the combination of the spring and the elastic hose should be checked at an elevated temperature, because the elastic hose may behave differently at elevated temperature than expected. If necessary, the model accuracy could be improved by distinguishing between the properties of activated and inactivated struts, by including a strain dependent bending stiffness and by analyzing the anisotropic behavior of the strut more carefully.

References

[1] Rozendaal, M. (2016). Objects with intent: a new paradigm for interaction design. *Interactions*, *23*(3), 62-65.

[2] Kim, H., Coutrix, C., & Roudaut, A. (2018, April). Morphees+ studying everyday reconfigurable objects for the design and taxonomy of reconfigurable uis. In *Proceedings of the 2018 CHI Conference on Human Factors in Computing Systems* (pp. 1-14).

[3] Follmer, S., Leithinger, D., Olwal, A., Hogge, A., & Ishii, H. (2013, October). inFORM: dynamic physical affordances and constraints through shape and object actuation. In *Uist* (Vol. 13, No. 10.1145, pp. 2501988-2502032).

[4] van Manen, T., Janbaz, S., & Zadpoor, A. A. (2018). Programming the shape-shifting of flat soft matter. *Materials Today*, *21*(2), 144-163.

[5] Vyas, D., Poelman, W., Nijholt, A., & De Bruijn, A. (2012). Smart material interfaces: a new form of physical interaction. In *CHI'12 Extended Abstracts on Human Factors in Computing Systems* (pp. 1721-1726).

[6] Jani, J. M., Leary, M., Subic, A., & Gibson, M. A. (2014). A review of shape memory alloy research, applications and opportunities. *Materials & Design (1980-2015)*, *56*, 1078-1113.

[7] Coelho, M., Ishii, H., & Maes, P. (2008). Surflex: a programmable surface for the design of tangible interfaces. In *CHI'08 extended abstracts on Human factors in computing systems* (pp. 3429-3434).

[8] Parkes, A., & Ishii, H. (2010, August). Bosu: a physical programmable design tool for transformability with soft mechanics. In *Proceedings of the 8th ACM Conference on Designing Interactive Systems* (pp. 189-198).

[9] Wakita, A., Nakano, A., & Ueno, M. (2011). SMAAD surface: A tangible interface for smart material aided architectural design.

[10] Tahouni, Y., Qamar, I. P., & Mueller, S. (2020, February). NURBSforms: A Modular Shape-Changing Interface for Prototyping Curved Surfaces. In *Proceedings of the Fourteenth International Conference on Tangible, Embedded, and Embodied Interaction* (pp. 403-409).

[11] Berzowska, J., & Coelho, M. (2005, October). Kukkia and vilkas: Kinetic electronic garments. In *Ninth IEEE International Symposium on Wearable Computers (ISWC'05)* (pp. 82-85). IEEE.

[12] Jun, G., Randhawa, J., & Baseta, E. (2017). Shape changing materials.

[13] Hawkes, E., An, B., Benbernou, N. M., Tanaka, H., Kim, S., Demaine, E. D., ... & Wood, R. J. (2010). Programmable matter by folding. *Proceedings of the National Academy of Sciences*, *107*(28), 12441-12445.

[14] Klein, Y., Efrati, E., & Sharon, E. (2007). Shaping of elastic sheets by prescription of non-Euclidean metrics. *Science*, *315*(5815), 1116-1120.

[15] Fleck, N. A., Deshpande, V. S., & Ashby, M. F. (2010). Micro-architectured materials: past, present and future. *Proceedings of the Royal Society A: Mathematical, Physical and Engineering Sciences*, *466*(2121), 2495-2516.

[16] An, S. M., Ryu, J., Cho, M., & Cho, K. J. (2012). Engineering design framework for a shape memory alloy coil spring actuator using a static two-state model. *Smart Materials and Structures*, *21*(5), 055009.

[17] Wahl, A. M. (1944). *Mechanical springs*. Penton Publishing Company.

[18] Fabregat-Sanjuan, A., Ferrando, F., & De la Flor, S. (2015). NiTiCu transverse to axial strain ratio analysis during tension/compression tests. *Materials Today: Proceedings*, *2*, S759-S762.

[19] Sadiq, H., Wong, M. B., Al-Mahaidi, R., & Zhao, X. L. (2010). The effects of heat treatment on the recovery stresses of shape memory alloys. *Smart Materials and Structures*, *19*(3), 035021.

[20] Gilbertson, R. (1993). Muscle Wires Project Book (San Rafael CA: Mondo-Tronics).

3 Prototyping

The final network design, which is discussed in Chapter 5, is developed throughout an iterative prototyping process. This chapter describes this process in chronological order. It concerns the steps taken to go from a simple SMA wire to a spring network that is capable of deforming out of plane and back. Background information on shape memory alloy materials and springs can be found in the Literature Report, see Appendix XI.

3.1. From wire to spring

The first step in making a spring network is to transform straight wires into springs. NiTiCu wire with a diameter of 0.5 mm is used for this, because of its processability and relatively low activation temperature. The latter is due to the addition of copper in the alloy [18]. An additional benefit is that copper has a positive effect on the thermal and geometrical stability of the material when used as actuator [19].

Multiple methods to make springs are discussed in the Literature Report. These are focused on springs with a small pitch angle or with a thin wire. However, a larger pitch angle is desired for a larger strain and a thicker wire for a larger force. Therefore, these methods are adjusted and evaluated here.

The first method is shown in Fig. 1A. The NiTiCu wire is wound around a steel rod, and its ends are wound around a bolt and then clamped with a nut on a perforated plate. The second method is shown in Fig. 1B. The second method is chosen, because it is easier with this one to pull the wires tight, and therefore to control the spring diameter. However, the first method could be beneficial if loop ends are needed.

Fig. 1 (A) Method 1: winding wire around rod and clamping with bolts and nuts on plate. (B) Method 2: winding wire around rod and clamping with terminal blocks. This method is chosen and improved.

A spring winder and threaded rod, see Fig. 2, are used to control the constructed pitch angle precisely and consistently. After winding the wire over the threaded rod, it is placed on a smooth rod. The wire is then pulled tight and fixated with terminal blocks. The pitch angle can be adjusted by varying the distance between the two terminal blocks. Even greater control over the pitch angle can be achieved by setting the pitch with the number of wires on the rod, see Fig. 3 The more wires in between a winding, the greater the pitch angle. Another advantage of this method is that the springs can be produced more space efficiently.

Fig. 2 The springs are wound manually with a spring winder.

Fig. 3 The pitch angle can be set with the number of windings that are placed on one rod.

3.2. From spring to network

The springs have to be connected to form a network. Several ideas are thought of to connect the springs, such as embedding the springs in an elastic material, waving the springs and connecting the springs via connectors. Using connectors is thought of as the most reliable and practical method.

The first connectors are 3Dprinted with PLA. The activation temperature of the springs is higher than the glass transition temperature of PLA, but it is used nevertheless for a quick first test. The springs are placed over the connector ends and then crimped, see Fig. 4. After heating the set-up, the ferrules are pulled open to detach the springs. However, the springs have fused with the connectors, because they have cut into the PLA.

Therefore, the next connectors are printed with threaded ends and with ABS, of which the glass transition temperature is above the activation temperature. The pitch angle of the thread is close to the programmed pitch angle of the spring, so that the forces exerted by the spring on the thread are limited when heated. These connectors work sufficiently.

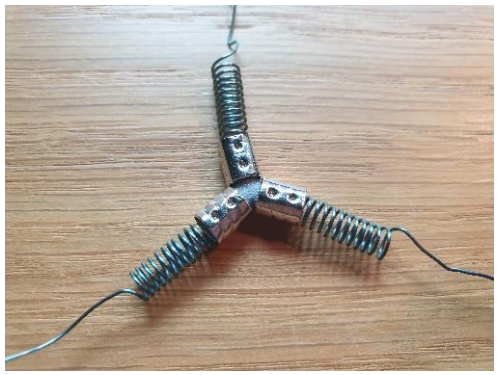

Fig. 4 The springs were initially connected with 3Dprinted connectors and ferrules. From this method it was learned that connectors with threaded ends are sufficient and ferrules are not needed.

3.3. Out-of-plane deformation

Problem: in-plane rotation

A network is required to test the out-of-plane deformation. Before creating a large network, an initial test is done with three springs to check if and how the springs deform out of plane. Three connected springs are compressed and clamped in between blocks. The set-up is placed in an aquarium with a layer of water. The water temperature is gradually increased up to 80 °C by adding boiling water. After the activation temperature is reached, the springs want to return to their programmed elongated length. It can be readily observed that the preferred bending direction of the springs is in-plane rather than out-of-plane, which can be seen in Fig. 5. Increasing the number of springs or decreasing the spring length do not prevent this from happening, as can be seen in Appendix I.

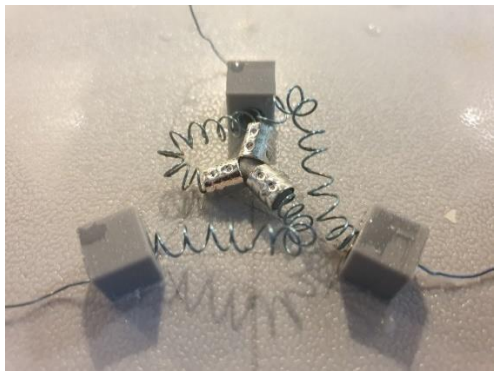

Fig. 5 Upon activation in hot water the connector starts rotating in-plane instead of deflecting out-of-plane.

Solution: flexures

A solution to this could be to constrain every DoF of the spring except for its axial translation and to design a hinged connector that allows for the out-of-plane bending. Another solution would be to increase the resistance in the unwanted DoF and to not constrain the useful out-of-plane bending. The latter is thought of as a more elegant solution. In addition, it may result in more smoothly rounded rather than sharply rounded shapes which would be the case if the springs would be enforced to remain straight.

The proposed solution can be realized by including plate flexures. The in-plane bending stiffness of the flexure is high compared to its out-of-plane bending stiffness. The flexures could be glued in-between the connector halves. To possibly exclude the gluing step, the first version of the solution is 3D printed in one go, see Fig. 6A. The thickness of the ABS plate flexures is 0.2 mm. The flexure bending stiffness is rather high compared to the spring bending stiffness. In addition, the connection points between the flexures and the connector is fragile.

Spring sheet metal flexures are glued in between the connector halves to eliminate these drawbacks. The use of spring sheet metal flexures with a thickness of 0.05 mm thickness results in a proper out-of-plane deformation mechanism, see Fig. 6B. An additional observation of the ABS plate flexure test is that the springs can still bend sideward where the flexures do not support the springs. Therefore, it is chosen to let the springs elongate to maximally twice their initial compressed length to prevent the connector from rotating, see Fig. 6B. The resulting connectors with flexures glued in between is shown in Fig. 7.

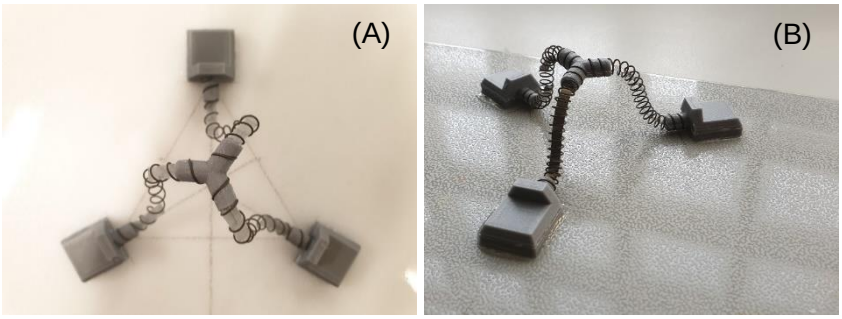

Fig. 6 Both pictures are after heating in a climate chamber. (A) ABS plate flexures are 3D printed in one go with the connector. Some rotation is still possible at the point where the flexures detach. (B) Spring sheet metal flexures of 0.05 mm are glued between the connector ends and block ends. The elongation is restrained to twice the flexure length which prevents rotation.

Fig. 7 The resulting connectors with threaded ends to connect the springs and with flexures glued in between to prevent in-plane rotation.

3.4. Reversibility

The reversibility is the ability of the network to be pushed or pulled back in place, either manually or automatically. For example, the network could be pushed back in place by hand or it could be pulled back in place by antagonist springs.

At first, a network is created to analyze the out-of-plane deformation of a whole network upon uniform heating. In contrast with the configurations in the initial tests, some springs have unclamped ends in the network. Upon external heating in a climate chamber, the network deforms into a predictable shape, see Fig. 8. The out-of-plane deformation starts off-center, but manages to grow into an axisymmetrical shape.

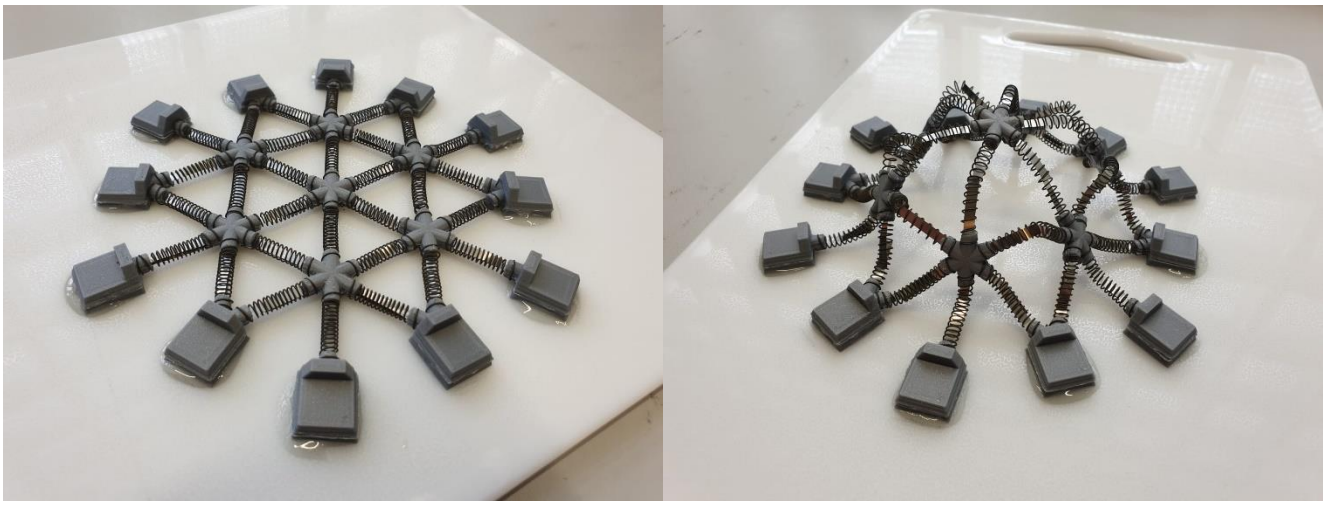

Fig. 8 The network deforms from flat state (left) to deflected state (right) upon uniform heating.

Problem: reverse deformation obstructed

The out-of-plane deformation of the network is satisfactory, yet it is difficult to push the network back in plane. This is caused by the flexures that hook in-between the spring windings, see Fig. 9. This happens most evidently in the springs that break with the overall shape of the whole network.

Fig. 9 The flexures hook in-between the spring windings, making it difficult to push the mechanism back in plane.

Solution: elastic hose

In the current design, the flexures are obstructing the downward motion; it is not possible to push back the current prototype in place, because the flexures hook in between the spring windings. Solutions can be aimed at either solving the problem or taking away what caused the problem, practically meaning that the problem can be solved by either mitigating the hooking or by taking away the combination of the flexures and the springs. It is not a solution to take away the SMA springs, as these are the base of the project. Taking away the flexures means that another solution has to be found for the sideways bending of the flexures upon activation. In the end, an elastic hose is used, which is discussed in the next section.

Two methods for mitigating the hooking are explored. The first method uses tubes in the form of bamboo straws to embrace the flexures, see Fig. 10A. The amount of out-of-plane deformation is diminished substantially due to the friction between the straws and the springs. In addition, the smooth character caused by the bendability of the springs is removed by the straws. The second method uses hoses in the form of balloons, see Fig. 10B. The elasticity of the balloon allows for the spring to bend and attain its smooth character. Another great benefit of the balloons is that they serve as passive antagonist springs, drawing the connector back in plane upon cooling down.

So, the threaded connectors with flexures will be provided with elastic hoses in the final network design, see Fig. 11. In addition, the flexures are rounded to prevent the flexures from perforating the balloons.

Fig. 10 Hoses are included to prevent the springs from hooking in between the spring windings. (A) rigid bamboo straws (B) stretchable balloons

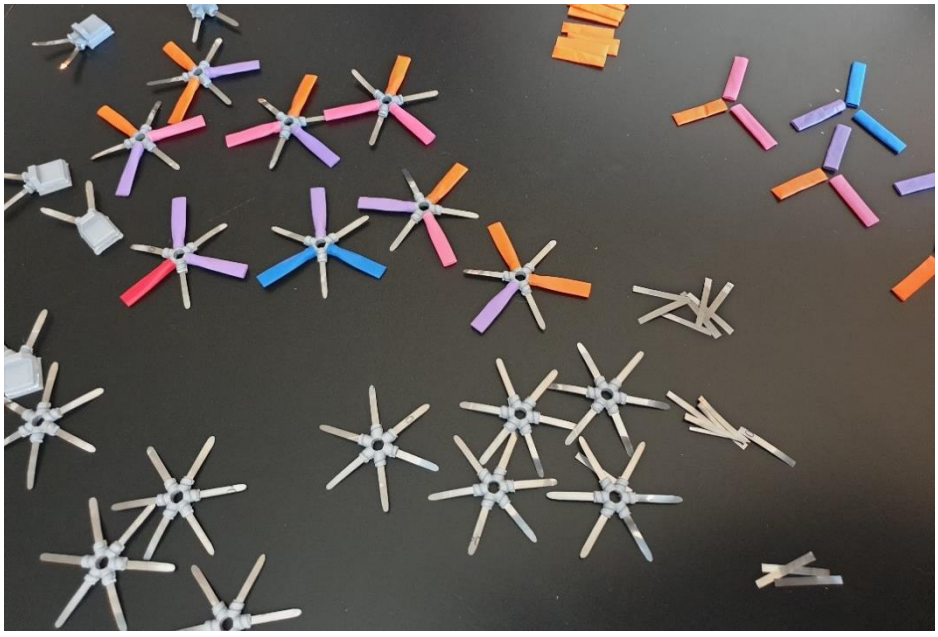

Fig. 11 The resulting threaded connectors with rounded flexures and elastic hoses.

4 Applications

Parallel to the technical development of the network, brainstorm sessions (Fig. 12), are organized to think about the possible applications of the network deformations. A brainstorm is typically set up around a specific problem, and the goal of the brainstorm is then to find solutions to this problem. However, you could say that in our case we start with a solution, and we try to find problems around it; we start with a "technology" and we try to find applications that require this technology. In his thesis called *"Technology Diffusion in Product Design: Towards an Integration of Technology Diffusion in the Design Process"*, W.A. Poelman states that matching opportunities of a technology ("supply") with functions of an application ("demand") is an extremely complex associative process, and should not be regarded as an individual activity [20]. Therefore, brainstorm sessions are organized. It fits the assumption that quantity leads to quality [21]. Background theory for the brainstorm method and the brainstorm method itself can be found in Appendix II.

Fig. 12 Brainstorms on applications.

The resulting ideas of the brainstorm are discussed in the beginning of this chapter. Out of these raw results, several ideas are selected to work out in concepts. The concepts are discussed in the last section. The boundary conditions and the criteria for ideas and concept selection are aimed at finding an application that lends itself well for demonstrating the capabilities of the network.

4.1. Ideas

The focus of the brainstorm sessions has been on literal applications directly and on more abstract aspects. The latter aims to gather more applications indirectly and encompasses associations, qualities, personal traits and emotions [7]. The abstract aspects can be especially useful for when designing dynamic product interactions or for products with hedonic aims. The resulting application ideas and abstract thoughts are discussed in this section.

Application ideas

The different backgrounds of the brainstorm participants led to diverse applications. For example, a participant with a father in bulk freight thought of trailers and transport of tall structures, a participant working in the chemical industry thought of process control techniques, a participant with a guitar thought of a variable acoustic chamber and a participant studying medicine thought of an adjustable gastric sleeve.

A complete list of the results can be found in Appendix III. The original idea of using the network as a cupholder for the demonstrator (see Design Brief in Appendix X) is included in this list as well. The list is divided into “functional aims” and “hedonic aims”. The functional aims are then subdivided in the functions that were initially thought of by the participants. However, it is interesting to note that some applications could actually make use of multiple functions or aims. For example, shape changing house furniture allows for efficient transport and easy assembly, but could also enable adaptive ergonomics. In addition, it could enable more complex, i.e. organic (rather than geometrical) shapes to be aesthetically pleasing, which would then be more of an hedonic aim. For the sake of clarity, all applications are listed under only one main function. The goal of the functions was not to categorize per se, but to inspire the participants to think of more applications within a function or to come up with new functions when they thought they could not think of anything more. In addition, the categorization gives an idea of whether all type of applications are covered.

Three ideas are selected from the list to work out into concepts. The selection process is discussed in Appendix IV.

Abstract thoughts

Here, the associations, qualities, personality traits and emotions that were named during the brainstorm are presented. These have also led to some application ideas, especially with hedonic aims. The abstract thoughts are divided in “associations”, “qualities and personality traits” and “emotions” [7]. The results are shown in Fig. 13. (The emotions that are shown were named at least twice.)

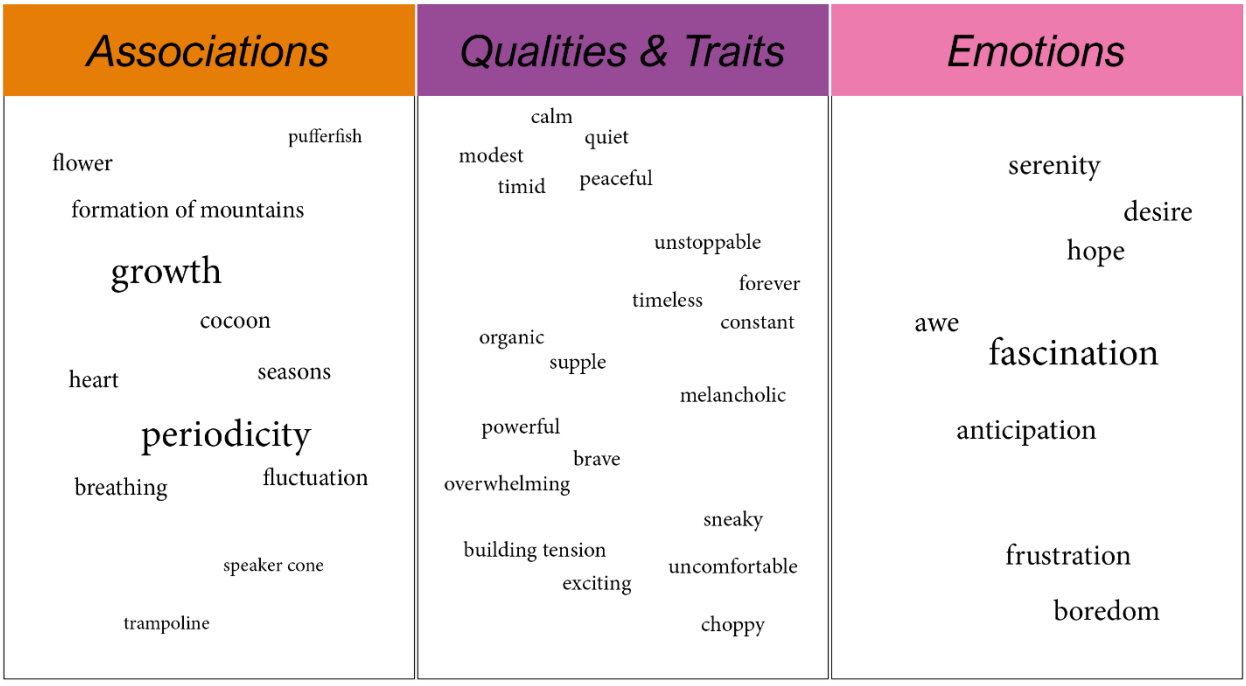

Fig. 13 Abstract aspects that were named during the brainstorm session.

Note that multiple words seem to be interrelated. For example, the qualities related to being unstoppable could be assigned to the association of growth. Another example is that the feeling of frustration could be elicit by the uncomfortable or tense character or the feeling of serenity could be elicit by the peaceful character. If the interrelations are ought to be true, they ratify the individual words named.

4.2. Concepts

The ideation phase resulted in three promising ideas for the demonstrator:

- light transmitter
- funhouse mirror
- (interactive) living / changing art / statue

The ideas are elaborated upon here, so that a more informed choice can be made. Attention is given to the feasibility of the concepts, as this is an important aspect to base the decision on.

Concept 1: light waves

Different ideas related to light transmittance are listed in Appendix III. A lamp is thought of as the most practical demonstrator because of its small size. The motion of the spot lights on a wall enlarge the shape-changing effect of the network. Therefore, this concept is like a shape-changing shadow casting lamp, of which its shadows can move, see Fig. 14.

A product idea for this concept is a breathing guider. The motions of the light would guide a paced breathing session to relax the user. It has been proven that doing a paced breathing exercise with a respiratory cycle of 10 s before going to sleep will help insomniacs to decrease their sleep latency and to increase their sleep efficiency [22]. The moving shadows could not only be used to guide the breathing session, but could also be used to create a dreamy atmosphere (perhaps the lights could generate a fireflies association), probably encouraging relaxation even more.

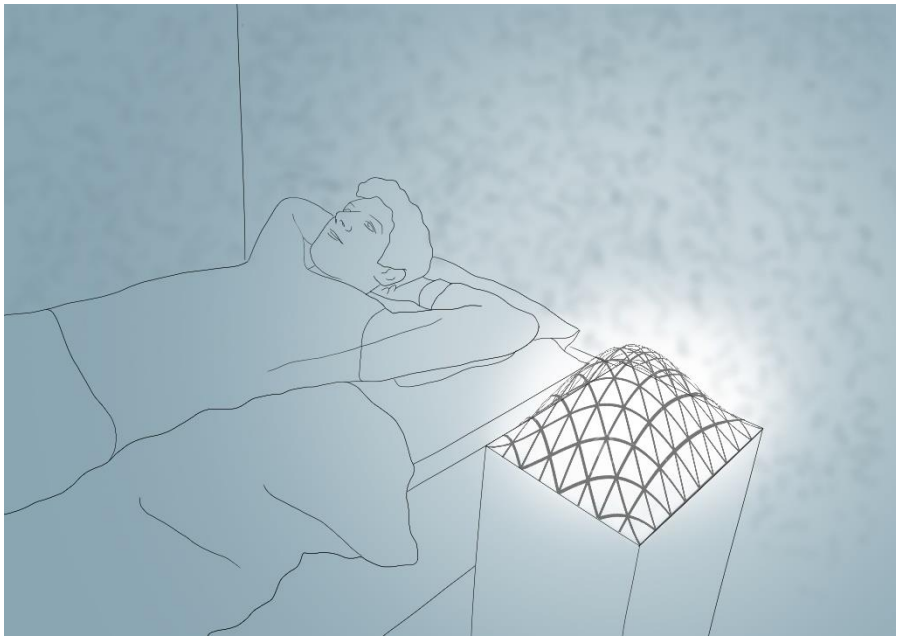

Fig. 14 Concept 1: The deformation of the network is displayed and enlarged with a lamp.

Concept 2: funhouse mirror

This concept for a demonstrator is a shape-changing funhouse mirror with which different types of distortions can be realized. The fact that the network is able to realize double curvatures next to single curvatures results in a larger range of possible distortions compared to a funhouse mirror that can curve in only one direction. In addition, it enables more extravagant distortions.

As a product, the mirror could be placed in public bathrooms, see Fig. 15, adding a spark of joy to an else ordinary place. The mirror could initially be flat, and for example be activated when the water tap is opened. The surprising effect could make it even more amusing than a static, predictable funhouse mirror. Several methods to realize a reflective deformable surface are discussed in Appendix VI. The most suitable method for this concept is to discretize the surface with mirror tiles.

Fig. 15 Concept 2: The changing curvature of the network is displayed with a funhouse mirror.

Concept 3: (interactive) living art

The idea is rather vague; anything is possible. Nonetheless, the product might have a hedonic aim. Therefore, the shape-changing effect could for example have an aesthetical, an emotional or a stimulatory aim. Regarding interaction, there are various options for shape-changing objects [7]:

- No interaction; shape-changing output only
- Indirect interaction; implicit input (e.g. weather) and shape-changing output
- Direct interaction; shape-changing input and (remote) output

I used these categorizations to think in different directions for working out the idea. This resulted eventually in the following two sub concepts. The first concept is *without interaction* (though it could be supplemented with indirect interaction) and the second concept is *with direct interaction*.

Concept 3A: living building

One of the emotions people ascribed during the brainstorm is ‘fascination’. That is a good quality for a piece of art. Here, I will discuss one of the concepts, and how I came to that concept.

Two overarching associations people had during the brainstorm are “growth” and “periodicity”. One more specific association that was named is “breathing”. One day, I stumbled upon a picture of The Shenzen Wave, which is a building with a double curved transparent roof. These things inspired me to think of the concept that is shown in Fig. 16. It is a breathing window, expressing the green character of a building. (When the sun is shining, the shadow casting effect could be similar to as in Concept 1.)

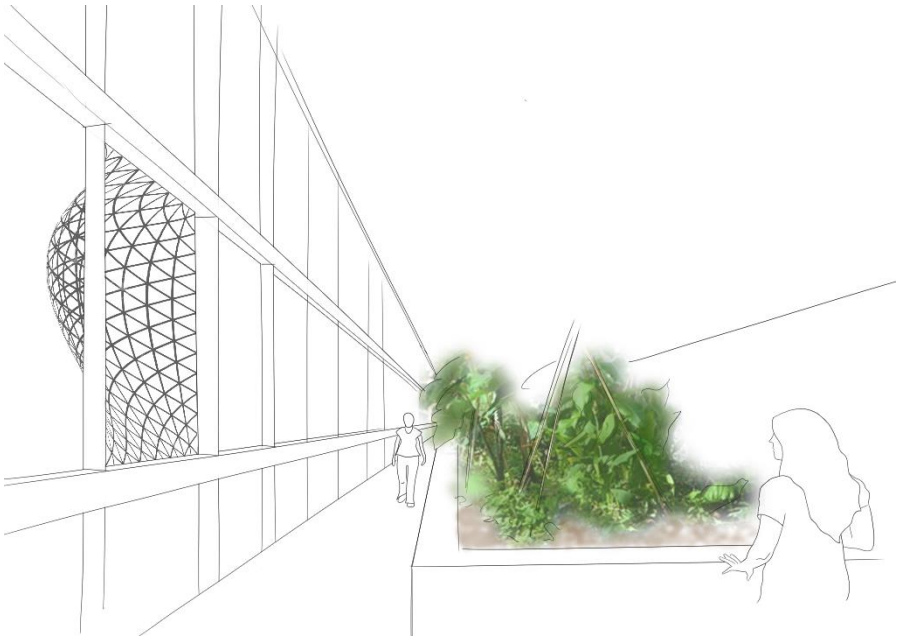

Fig. 16 Concept 3A: The deformation of the network is displayed with a breathing window.

Concept 3B: interactive board

In the concept here an interaction is included for giving the network an explorative aim [7]. The network could be integrated in a plateau, including a touchpad with which the network can be controlled. It could be placed at the faculty of Industrial Design Engineering as a source of inspiration for new types of products. Translating it into a game might encourage the user to become familiar with the material quicker. A game could be made out of it if you give the user a card on which a shape is shown that he/she has to rebuild, see Fig. 17. Perhaps the shape could also be checked somehow. If the network could shape-change fast enough, it is possible to evolve this game into a competitive marble track game, in which you have to manipulate a marble towards the goal of your opponent.

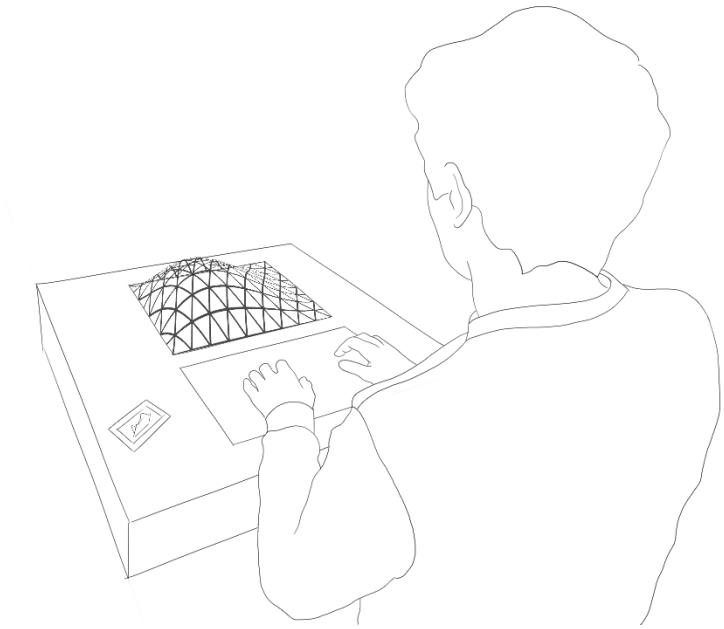

Fig. 17 The deformation of the network is displayed with a board game.

One concept is selected to work out into a demonstrator. The selection process is discussed in Appendix V. The concept that is chosen to use for the demonstrator is Concept 1: light waves.

5 Demonstrator

The demonstrator consists of the network supplemented with the aspects of Concept 1. The goal of the network is to examine and to display the shape-morphing behaviour of the network. Due to limited time, Concept 1 has not been developed into a breathing guider. Still, a light is included in the demonstrator to emphasize the shape-morphing behaviour. In this chapter, all aspects of the demonstrator are discussed separately at first. The description of network design is like a conclusive summary of the prototyping process. The parts that are new to the final prototype are the electrical activation and the housing. The demonstrator is shown as a whole at the end of this chapter.

5.1. Network design

An overview of the final network design is given in Fig. 18. The screwed connectors allow for the springs to be connected to each other. The flexures enforce an out-of-plane deformation by obstructing the in-plane rotation. The elastic hoses ensure that the flexures do not hook in-between the spring windings, and they also retract the mechanism upon deactivation. The springs that are used in the final network have a pitch of 3.1 mm (6 wires are wound together on one rod) in their austenite state, and have 14 free spring windings in the network. They are compressed up to 21 mm in the flat state of the network.

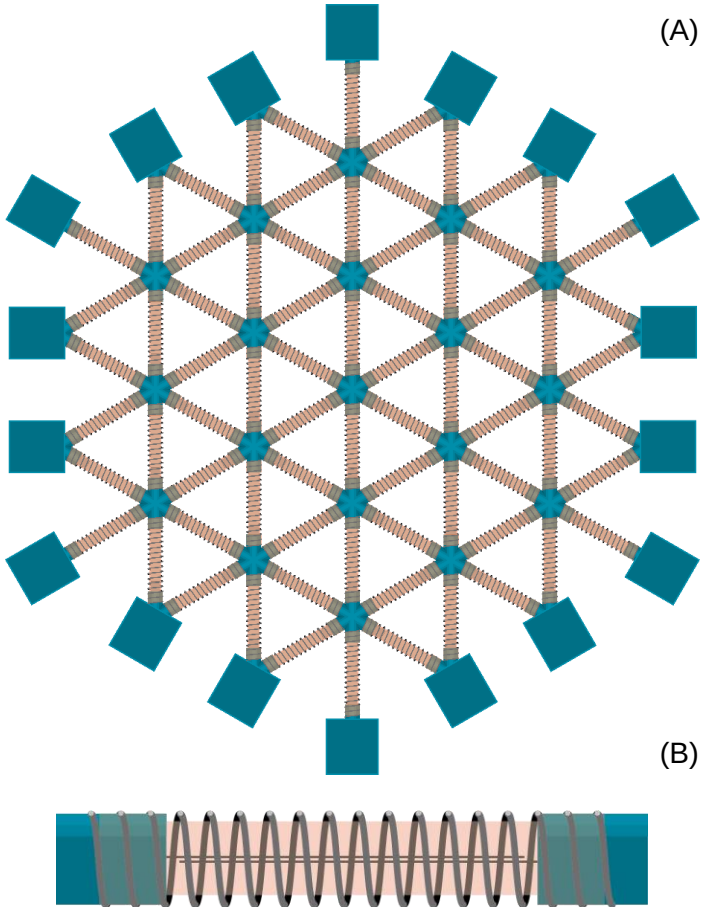

Fig. 18 (A) Top view of final network design. (B) Sideview of strut, including spring, connector ends, flexures and elastic hose.

5.2. Electrical Activation

Global heating in a climate chamber was used to activate the springs during the prototyping process. Now we want to be able to activate the springs individually, which cannot be done with the climate chamber. Instead, Joule heating is used in the final prototype. Here, the electrical circuit and the power that is supplied to the springs are discussed.

Electrical circuit

All springs are connected in parallel, which can be seen in Fig. 19, so the required voltage is prescribed by the required voltage of one spring. The power supply that is used is a 132 W power supply with a 3.3 V DC voltage output. Only three of the four groups that can be seen in Fig. 19 can be connected to the power supply, so 54 of the 72 springs can be connected to the power supply at the same time. The AC voltage applied to each spring is controlled via LED driver modules, in combination with a Seeeduino Lotus board. The driver modules all have three output ports and one ground port. In between the driver modules, the springs are wired with Litz wire. This is a more pliant wire than a conventional PVC insulated wire, which is useful because it will therefore less likely disturb the deformation of the network.

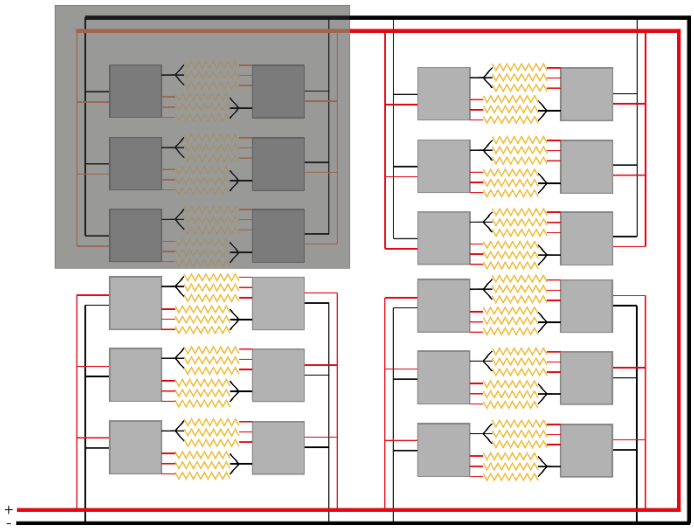

Fig. 19 Schematic overview of the electrical network. The grey squares resemble the LED driver modules. 54 springs can be connected at the same time, because 3 groups can be connected at the same time.

The overview in Fig. 19 is a schematic overview to explain the electrical circuit. In reality, the spring ends distributed more crisscross over the LED driver modules because of the network shape. At each node, six spring ends come together, of which three are connected together to one ground port and three to individual output ports. This is shown in Fig. 20A. In Fig. 20B, the building block of the network is shown. It contains three springs, of which the ground is located at the node and the free ends are related to other nodes.

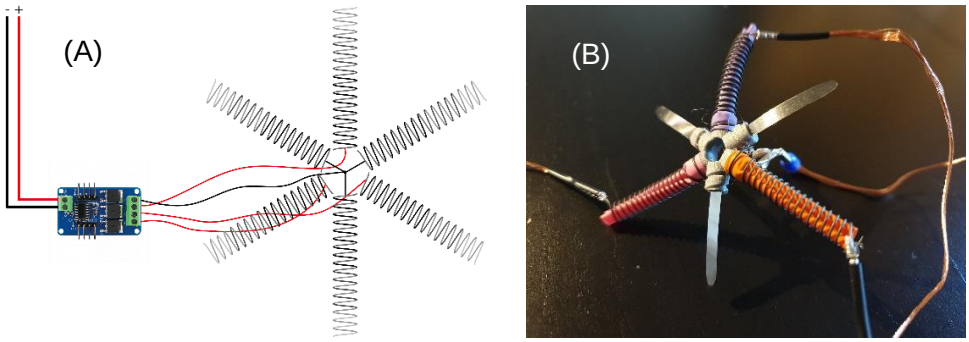

Fig. 20 (A) Electrical connections at one node. (B) Building block of the network.

Power

To find the required power to heat up the springs, wired springs are connected to a power supply with manual voltage or amperage control. The temperature is measured with a K-type thermocouple at the surface of the springs. The springs are heated up to 70 °C to 80 °C, which is above the activation temperature of 65 °C specified by the manufacturer, but below the melt temperature of the elastic hoses. The power to heat up a spring sufficiently is 1.5 W to 1.7 W.

However, this is the ideal case. In the network, there are multiple connection points which could increase the required power because of their increased resistance. In addition, a difference in resistance per circuit could lead to uneven heating of springs, and possibly even overheating of springs. To ensure that the springs are evenly heated, several measures are taken, which are discussed below.

Connection points

Because of the risk of overheating the SMA wire, they cannot be soldered. Therefore, they are crimped. However, crimping results in a highly varying resistance, and sometimes even in no connection, because of the insulation lacquer on the Litz wire. A solution to this is to burn off this lacquer and coat the Litz wire with tin at first, and then crimp it to the SMA spring, which can be seen in Fig. 21. After crimping, the springs are connected to the power supply to check if their resistances are practically the same. The same is done after crimping the ground wires, see Fig. 20B, together.

Fig. 21 SMA spring crimped with tinned Litz wire to ensure sufficient electrical connection

The remaining points that are checked are the soldered ramifications from the power supply and the LED driver module outputs. They are checked by connecting one spring to each driver module output and check the resulting current under a set voltage. Resultingly, a few outputs did not work, so these are excluded.

PWM

The power supply that is used in the final prototype has a DC voltage output of 3.3 V, which can only be slightly adjusted on the power supply. A DC voltage output of 3.3 V results in a too high temperature. Therefore, PWM is used to diminish the power that is supplied to the springs. In addition, PWM is used to slightly variate the power between the springs, upon measuring the temperature at the spring surfaces.

5.3. Housing

An overview of the housing is given in Fig. 22. The plastic blocks that the network ends are connected to are glued onto the plastic hexagonal ring, which can be placed on the rim on top of the housing. The wires underneath the network should first go towards the sides and then towards the bottom of the housing, where the driver modules are. This way, the interference of the wires with the light is reduced as much as possible, since the light source is placed on the middle plate. This enlarges the deformations through casting shadows. The height of the middle plate can be chosen, according to the desired shadow sharpness.

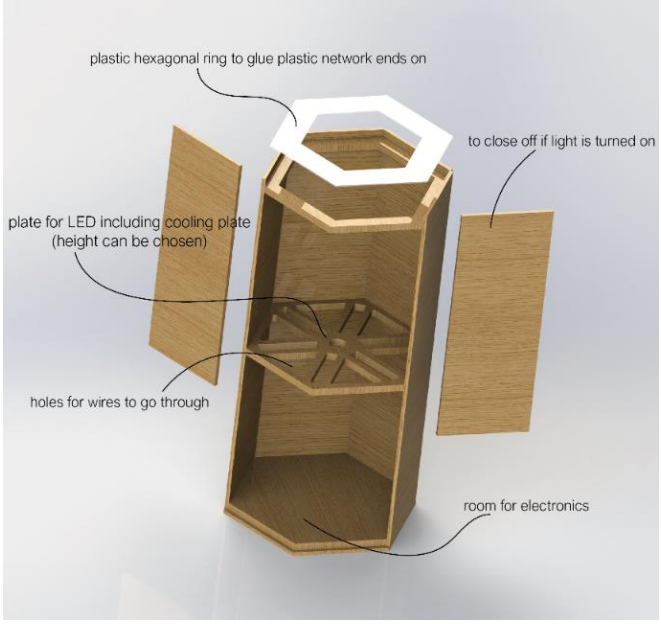

Fig. 22 An overview of the housing. The network will be glued on the plastic ring. The light will be placed on the middle ring.

5.4. Final Prototype

Pictures of the final prototype and a shadow projection of the network can be found in Fig. 23.

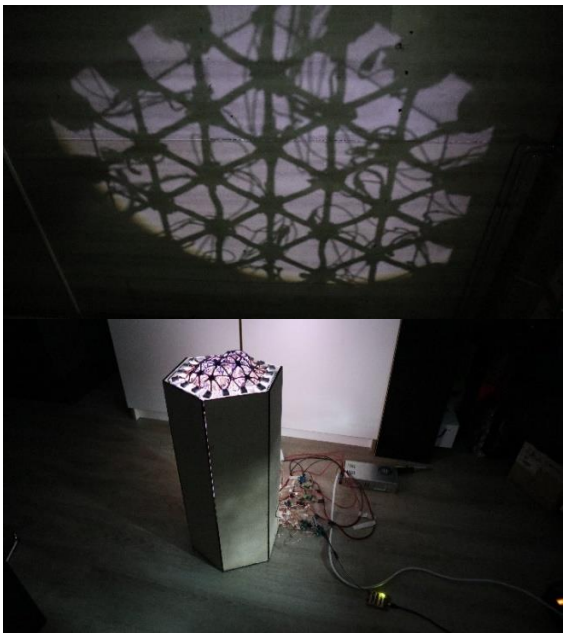

Fig. 23 The demonstrator (below) and a shadow projection (above).

Results

The initial activation is done in a climate chamber at 70 °C, so that all springs are activated at the same time, see Fig. 24A. The resulting permanent deformation can be seen in Fig. 24B.

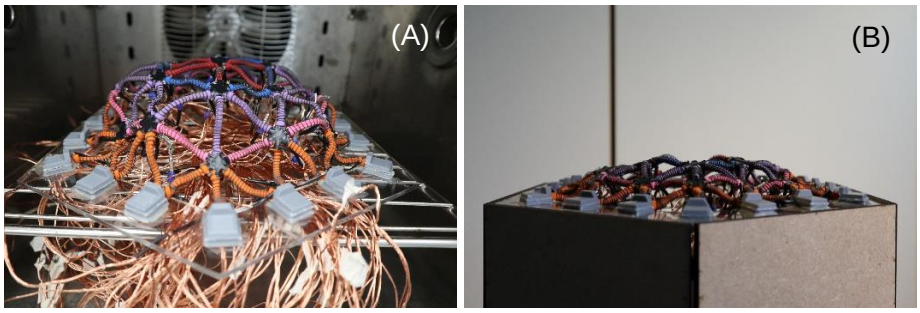

Fig. 24 (A) All springs are heated in a climate chamber at 70 °C. (B) The resulting equilibrium state after heating.

Hereafter, different sets of springs are activated via Joule heating, resulting in different network shapes. Four activation schemes (describing what springs are switched on) and the resulting shapes are shown in Fig. 25.

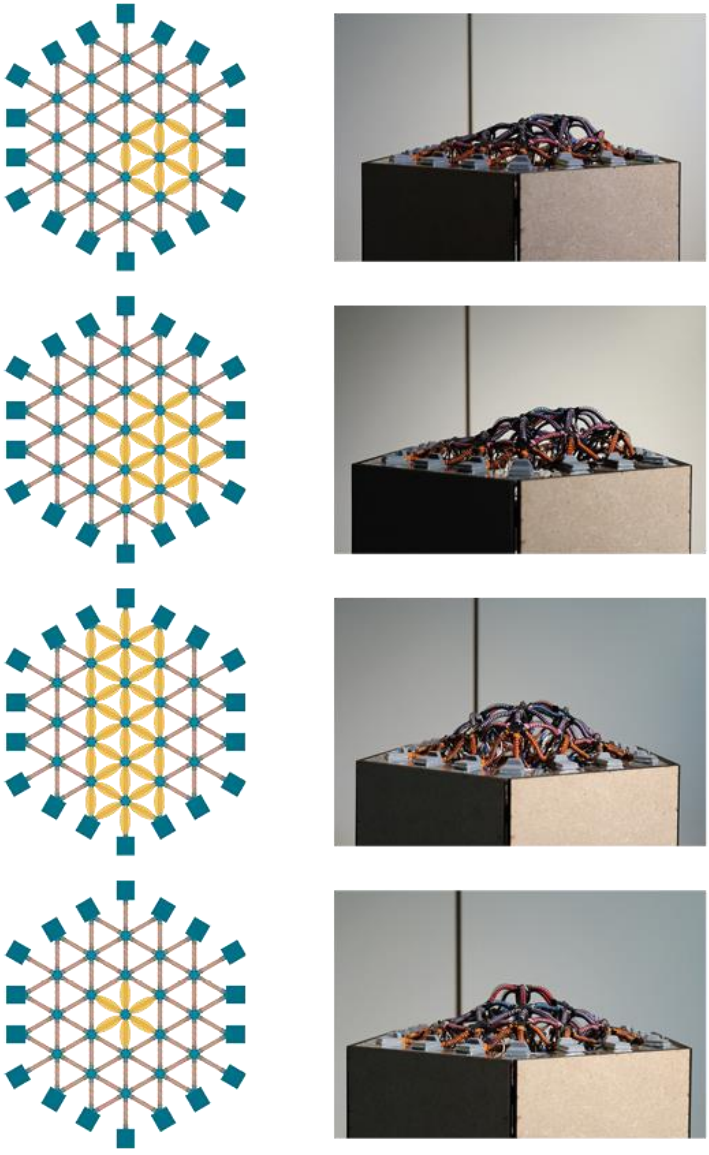

Fig. 25 Activation of springs and resulting sideviews.

The first two activation schemes in Fig. 25 are asymmetric, and the last two activation schemes are symmetric. The sideviews of the symmetric schemes are rather symmetric as well. However, when looking at the top, the network is not completely symmetric, see Fig. 26. When comparing the left springs with the related right springs, it can be seen that some springs bend in different curves, sometimes even in opposite direction, resulting in the highlighted node on the left to be pushed downwards rather than upwards. A slight asymmetry of the network can be observed in inactivated state as well.

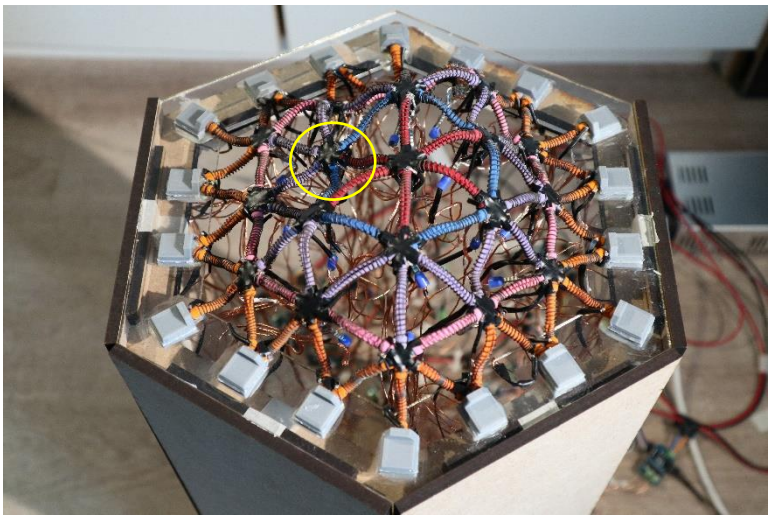

Fig. 26 A top view of the third activation scheme in Fig. 25.

6 Modelling

A model is required to translate a desired shape of the network into an activation scheme, i.e. a description of which springs should be switched on to create a shape that is as close as possible to the desired shape. A start has been made on such a model, see 6.1. Kinematic model. For practical reasons that are explained in the section, this model has not been elaborated upon. The goal has shifted towards creating a model that calculates the resulting shape upon an activation scheme. A finite element model (FEM) is created for this in Ansys. The development and the set-up of this model are discussed from 6.2 to 6.4. At the end of this chapter, the result of this model is compared to a 3D scan of the activated prototype.

6.1. Kinematic model

A kinematic model is created in Matlab to calculate the required spring strains for a desired shape with the help of an available conformal map algorithm [23]. Background information on conformal maps can be found in the Literature Report (see Appendix XI). The desired shape can be put in in the form of an STL file, and the required strains of the struts in the triangular lattice pattern will then be calculated by the algorithm. The algorithm is described in more detail in Appendix VII. However, it results in very specific strains, which is impractical. Therefore, the idea is to reverse the model, so that you can provide strains as input and check the resulting shape.

This is not straightforward because multiple shape solutions often exist for one set of strains. Another downside of this kinematic model is that it is not capable of capturing bending and twisting effects of the struts. Therefore, it is chosen to perform a static structural finite element analysis (FEA). Ansys APDL is used for this, because with Ansys APDL it is easy to adjust parameters and quickly run a simulation again with adjusted parameters.

6.2. Ansys shape memory effect model

A SMA material model for both pseudoelasticity and shape memory effect is available in Ansys. The background information on this model can be found in the ANSYS Mechanical APDL Material Reference [24]. An overview of the practical input parameters can be found in Fig. 27 [25].

Modelling all spring geometries results in a very large model, and there is a maximum number of elements that can be used in the student version of Ansys APDL. Therefore, the idea is to model the springs and the elastic hoses with BEAM elements, with their measured effective global stiffnesses inputted as material stiffnesses. The bending direction imposed by the flexures is controlled with the ration between the width and the thickness of the beams. In addition, the bending stiffness of the beams should be the same as the real bending stiffness of the struts. In the network, the struts are initially compressed, and they elongate upon thermal activation. This is done by prestraining the elastic hose elements, which are manually meshed over the nodes of the spring elements.

Density : ρ		SMA density
Isotropic Elasticity	Young's Modulus E_A	It's the Young's modulus of Austenite
	Poisson's Ratio ϑ_A	It's the Poisson's ratio of Austenite
Shape Memeory Effect	Hardening Parameter : H	It is the slope of the stress-strain curve during martensitic transformation
	Reference Temperature T_{ref}	It's the temperature at which the SMA properties, that you will introduce, are measured (it is the test temperature)
	Elastic limit : σ_s^{AM+}	It's the start stress for Austenite to martensite transformation
	Temperation Scaling Parameter : C	It's the slope of band transformation considered the same for the twice sens of transformation : austenite to martensite and martensite to austenite
	Maximum transformation strain : ε_{tr}^{max}	The maximum strain due to martensitic transformation
	Martensite Modulus : E_M	It's the Young's modulus of Martenite
	Lode dependency parameter : β	it's a parameter measuring asymmetric behaviour of SMA under compression and tensile loadings. In the case of symmetric behaviour β=0

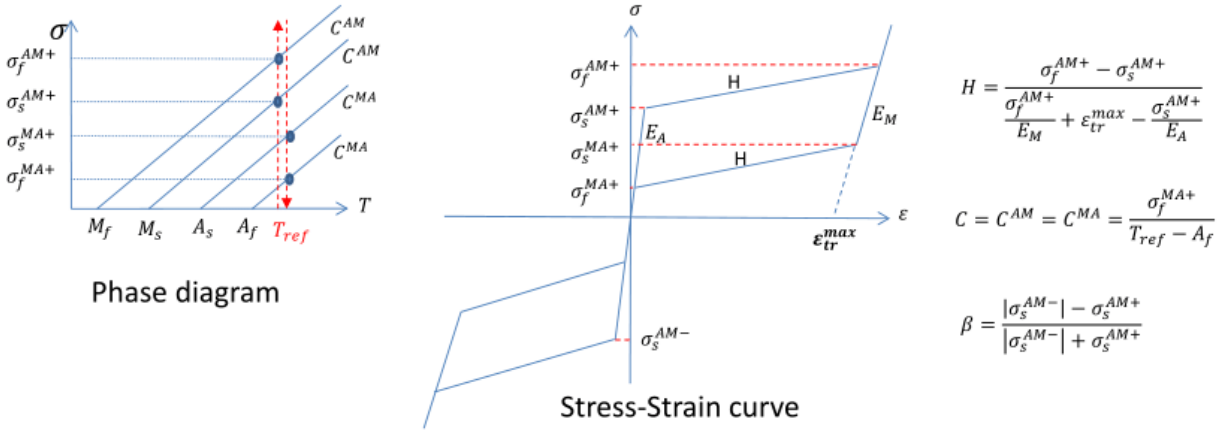

Fig. 27 Overview of input parameters for shape memory effect [25].

However, it turns out that BEAM elements cannot be axially compressed to sufficient extent. Therefore, SOLID elements are used hereafter. These increase the model size, because they consist of more nodes, and all nodes at the interfaces with the connectors have to be constrained. (Different methods exist to connect the beams with the connectors. It should be ensured that the type of contact that is used is suitable for large nonlinear deformations.) Nonetheless, it turns out that these elements allow for a sufficiently large compression. However, it is impossible to manually mesh the "elastic hose elements" over the nodes of the "spring elements" due to the high number of nodes, and no automatic solution could be found for this. Another solution would be to set a prestrain on the spring elements themselves, but this is not possible for the shape memory alloy material model [26]. If you would want to prestrain these elements, you have to displace and constrain all nodes manually. Because of these difficulties and limited time, it is chosen to follow another, more reliable though less elegant approach, which is discussed in the next section.

6.3. Final model set-up

In the new model set-up, the focus is on the balance of forces in the activated configuration. The idea is that if the modelled forces resemble the real forces in this state, the result of the simulation will represent the real activated configuration. The forces may be different than in reality throughout the out-of-plane deformation. The focus is on the austenite state, because it is difficult to make the model consistent for the whole stroke, and the activated configuration is the configuration of interest.

The upward force is provided by the SMA springs, and it is assumed that the downward forces are primarily caused the elastic hoses, the bending resistance of the flexures and the springs and the weight of the mechanism. The point of balance between these forces determines the amount of deflection. Therefore, we want the axial force provided by the springs, the bending stiffness of the struts and the weight of the mechanism to be the same in the model, at least at the point of balance for the austenite state.

Axial force and strain

An important difference with the approach described in the previous section is that the shape memory effect strain is mimicked with a thermal expansion strain [27]. So, there is no initial compression which can then be recovered; the length of the modelled strut increases upon a thermal load. Because there is no prestrain, the more simple beam elements can be used instead of the more complex solid elements. The amount of elongation is determined by the combination of the spring and the elastic hose, see Fig. 28, which can be seen as two parallel springs. The stiffness of the elastic hose is constant, but the stiffness of the spring depends on the temperature, causing the strut to have an equilibrium in both martensite and austenite state. A prestrain of the elastic hose influences the points of both these equilibrium states. The elastic hose also influences the axial compressive force in the austenite state which we are interested in. Instead of including the elastic hose with separate elements as previously done, they are included via prescribing the prestrain and prescribing this axial compressive force.

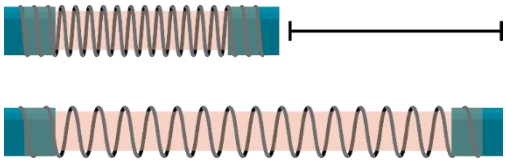

Fig. 28 The combination of the spring and the elastic hose are modelled together with one element. The imposed thermal strain is determined by the difference between the equilibrium in martensite (above) and austenite (below).

In order to know these equilibrium points, the characteristics of the spring and the hose should be known. The results of tensile tests on a spring at room temperature, a heated spring and an elastic hose are shown in Fig. 29. More elaborate results can be found in Appendix VIII. At zero strain, the spring is in austenite state. The related length of the 14 spring windings that are free in the final network is 43.4 mm. The spring is compressed up to 21 mm (which is also the flexure length) for the initial flat configuration of the network, resulting in a global spring strain of 52%, see the vertical line in Fig. 29. At this length, the elastic hose is placed alongside the spring with a prestrain of around 10%. The strut is now at point 1, see Fig. 29, with the amount of prestrain of the hose presented by the part of the curve on the right side of the vertical line. Upon heating, the strut elongates towards point 2, which is an elongation strain of 70%. Upon cooling, the strut shrinks towards point 3, so some strain remains; the network does not go back to its initial flat configuration. It can be seen in Fig. 29 that the force in the austenite state at point 2 is 1.35 N, so at a strain of 70% the axial compressive force on the strut should be 1.35 N in the model as well.

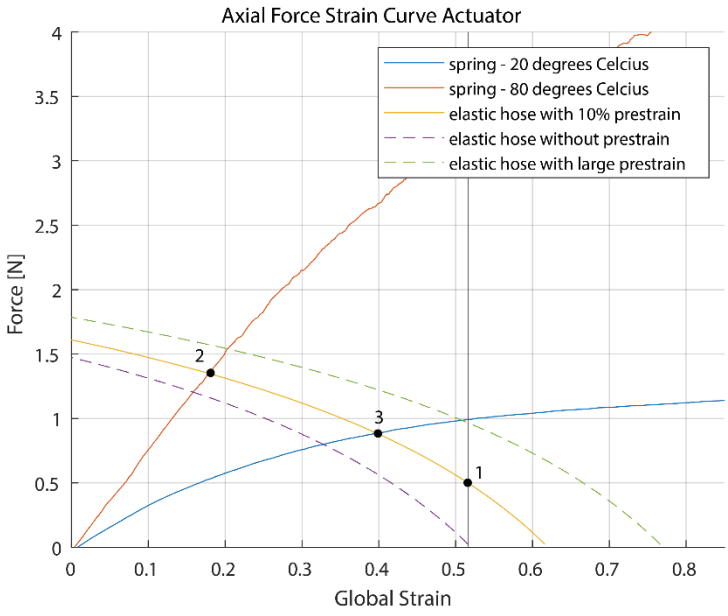

Fig. 29. The measured force strain curves. Point 1 is the initial flat state. Point 2 is the hot, austenite state. Point 3 is the cold, martensite state.

The stroke can be increased by increasing the prestrain. Nonetheless, it should be ensured that the strain from point 1 to point 2 is not larger than the flexure length. The stroke is chosen such that it is sufficiently large, but not too close to this limit. In addition, it is checked if the global spring strains do not result in too large material strains. The global strain can be related to the material shear strain via the following equation

$$\gamma = \frac{1}{C}\frac{\cos^2\alpha_i\,(\sin\alpha_f - \sin\alpha_i)}{\cos^2\alpha_f\,(\cos^2\alpha_f + \frac{\sin^2\alpha_f}{1+\nu})} \qquad \text{Eq. 1}$$

in which C is the spring index, α_i is the initial pitch angle, α_f is the final pitch angle and ν is the Poisson's ratio. To calculate the material shear strain, the global strain has to be translated to the final pitch angle first. For the used springs, a global strain of 40% (from the origin to point 3) is related to a material shear strain of 1.1% and a global strain of 18% (from the origin to point 2) is related to a material shear strain of 0.49%. Both the maximum and the minimum strain are within the typical limit strains that assure a maximum wire life for the martensite and the austenite phase respectively [28].

Bending stiffness

In the finite element analysis, the struts are modelled as beams. The thickness of the beams represents the effective bending stiffness of the struts. The effective bending stiffness is composed off the resistivity induced by the spring itself and by the flexures. The calculation of these stiffnesses is explained here. The situation that is looked at for this is shown in Fig. 30A, where we are interested in the vertical stiffness of the connector.

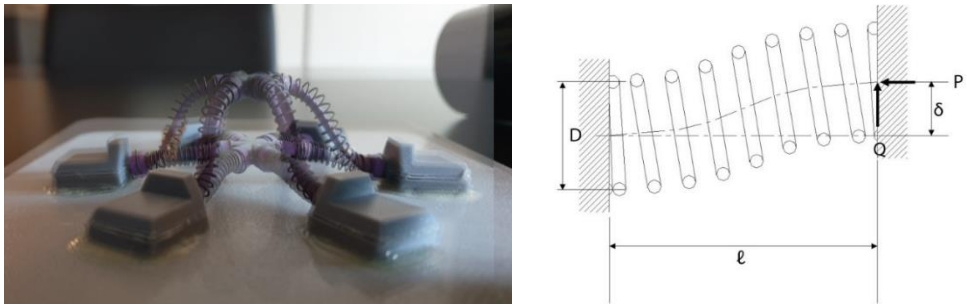

Fig. 30 (A) The situation that is looked at for calculating the effective bending stiffness. (B) The springs are under combined lateral and axial load **[29]**.

Spring

The spring in Fig. 30A is under combined lateral and axial load, which is shown schematically in Fig. 30B The vertical deflection upon a lateral force depends on the bending rigidity and the shearing rigidity of the spring. If the axial load is neglected, the deflection can be calculated with

$$\delta_0 = \frac{Ql^3}{12\beta} + \frac{Ql}{\gamma} \qquad \text{Eq. 2}$$

in which Q is the lateral force, l is the compressed length under the axial load, β the flexural rigidity and γ the shearing rigidity [30]. The expressions for the flexural rigidity and the shearing rigidity are

$$\beta = \frac{2lEIG}{n\pi r(2G+E)} \qquad \text{Eq. 3}$$

$$\gamma = \frac{lEI}{\pi n r^3} \qquad \text{Eq. 4}$$

in which E is the Young's modulus, I is the moment of inertia, G is the shear modulus, n is the number of spring windings and r is the mean coil radius. The moment of inertia can be calculated with $I = \frac{\pi}{4}(r_2^4 - r_1^4)$, in which r_2 and r_1 are the outer and the inner radii of the spring, respectively. The shear modulus can be calculated with $G = \frac{E}{2(1+\nu)}$ in which ν is the Poisson's ratio, which is taken as 0.44 [31].

To include the axial load, the deflection δ_0 has to be multiplied with a magnification factor that depends on the ratio between the axial load and the buckling load:

$$\delta = C_1 \delta_0 \qquad \text{Eq. 5}$$

$$C_1 = \frac{1}{1 - \frac{P}{P_{cr}}} \qquad \text{Eq. 6}$$

The critical buckling load can be calculated with

$$P_{cr} = \frac{\pi^2 \beta}{l^2} \left(\frac{1}{1 + \frac{\pi^2 \beta}{l^2 \gamma}}\right) \qquad \text{Eq. 7}$$

Flexures

The two flexures within a strut are seen as one flexure under lateral load for the calculation here. It is assumed that there is no axial load on the flexures, because they can slide. The deflection can be calculated with

$$\delta_0 = \frac{Q l^3}{12 E I} \qquad \text{Eq. 8}$$

in which Q is the lateral force, l is the compressed length under the axial load, E is the Young's modulus and I is the moment of inertia. The moment of inertia can be calculated with $I = \frac{b h^3}{12}$ in which b and h are the width and the height of the flexures, respectively. The height of one flexure is 0.04 mm. The effective height variates between the thickness of two flexures and the thickness of one flexure throughout the out-of-plane motion. At an elongation of 70% (point 2 in Fig. 29) compared to the initial state (point 1 in Fig. 29), the amount of overlap is 18%, resulting in an effective thickness of 0.047 mm.

The parameters that are used to calculate the effective stiffness can be found in Table 1.

Table 1 Parameters to calculate effective bending stiffness and therewith effective thickness

Parameter	Unit	Value
Material		
Spring Poisson's ratio v		0.44
Flexure elastic modulus E	[GPa]	190
Geometry		
Strut length (initial) l	[mm]	21
Number of spring windings		14
Spring inner radius r_1	[mm]	2.0
Spring outer radius r_2	[mm]	2.5
Flexure width b	[mm]	3.0
Flexure height average h	[mm]	0.047
Load		
Axial load P (on spring)	[N]	1.35

Thickness of beam in FEM

To calculate the thickness of the beam element in the FEM, Equation 5, 6, and 8 can be used again, because the beam elements have a similar geometry as the flexures. The critical buckling load should be calculated with Equation 9, which is the critical buckling load for a beam with hinged ends. This end condition is used, because most struts in the network comply to this end condition, because the connectors can rotate.

$$P_{cr} = \frac{EI\pi^2}{l^2} \qquad \text{Eq. 9}$$

The free parameters are the modulus E, the beam width b and the beam thickness h. These should be chosen such that the bending stiffness and the axial force are in agreement with reality. If the width b is chosen to be 0.015, that is true for a thickness h of 0.0128 mm and a modulus E of 10020 Pa. The width is chosen sufficiently large such that the thickness is smaller, so that the beam resembles the flexure shape. Because beam elements are used, the width of the modelled beam is not constrained by the width of the flexure end, because the volumes of the beam elements (which are actually line elements) can overlap.

In initial models, the counteracting elastic hose force was taken along in the thickness as well, which resulted in overly thick beams. Because solid elements were used, no overlap was possible, which made it impossible to make the width larger than the height for the required thickness.

6.4. Implementation in Ansys

The lattice struts are represented by BEAM188 elements in the FEM. The beam elements are connected with MPC184 general joint elements, which are well suited for large strain nonlinear applications. All six relative DoF of the joint are constrained. The length of the joint elements resembles the size of the connector. An overview of the input parameters can be found in Table 2. The APDL code up to the load steps can be found in Appendix IX.

Table 2. FEM input parameters based on real values or effective values

Parameter	Unit	Value
Material		
Elastic modulus austenite (effective)	[Pa]	10020
Minimum strain (real, from prototype)		10%
Maximum strain (real, from tensile test data)		70%
Geometry		
Length connector end (real)	[mm]	9.2
Length strut, initial (real)	[mm]	21.0
Height (effective)	[mm]	12.8
Width (effective)	[mm]	15.0

The initial out-of-plane buckling is not simulated. The post-buckling situation is created by enforcing a small positive vertical displacement on the center connector of the network, and thereafter enforcing the resulting planar displacements of the outer ring on the outer ring, while releasing the constraint on the center connector after a small thermal load is applied as well. Thereafter, the thermal load is increased up to the initial strain, which is the remaining strain after the initial global activation in reality. The calculated initial strain is 24%, which is the strain from point 1 to point 3 in Fig. 29. However, this results in a deflection that does not resemble the real result in Fig. 24B. Therefore, an estimated initial strain of 10% based on the real situation is applied to all beams in the model. Now that the network has a slight positive deflection, gravity is activated. Hereafter, it can be chosen what springs are activated. The springs can be "activated" by increasing the strain up to 70%, which is the strain at point 2 in Fig. 29 compared to point 1. It is necessary to apply the thermal loads in multiple load steps to assure convergence. For nonlinear problems, it is more useful to increase the number of load steps rather than increasing the number of substeps [32].

Results

Despite the high number of load steps that is used, the solution has not converged beyond a strain of 55%. This strain results in a higher deflection than the prototype though, which can be seen in the next section. To provide an idea of how the shape converges upon an increasing strain, the results for three different strains are displayed together in Fig. 31. The activation scheme that is used for these is the first activation scheme of Fig. 25. In the sideview in Fig. 31D it can be seen that a higher strain does not only increase the maximum deflection, but also moves the "hill" towards the left. In the top view in Fig. 31C it can be seen that the springs on the left bend more upon an increasing strain.

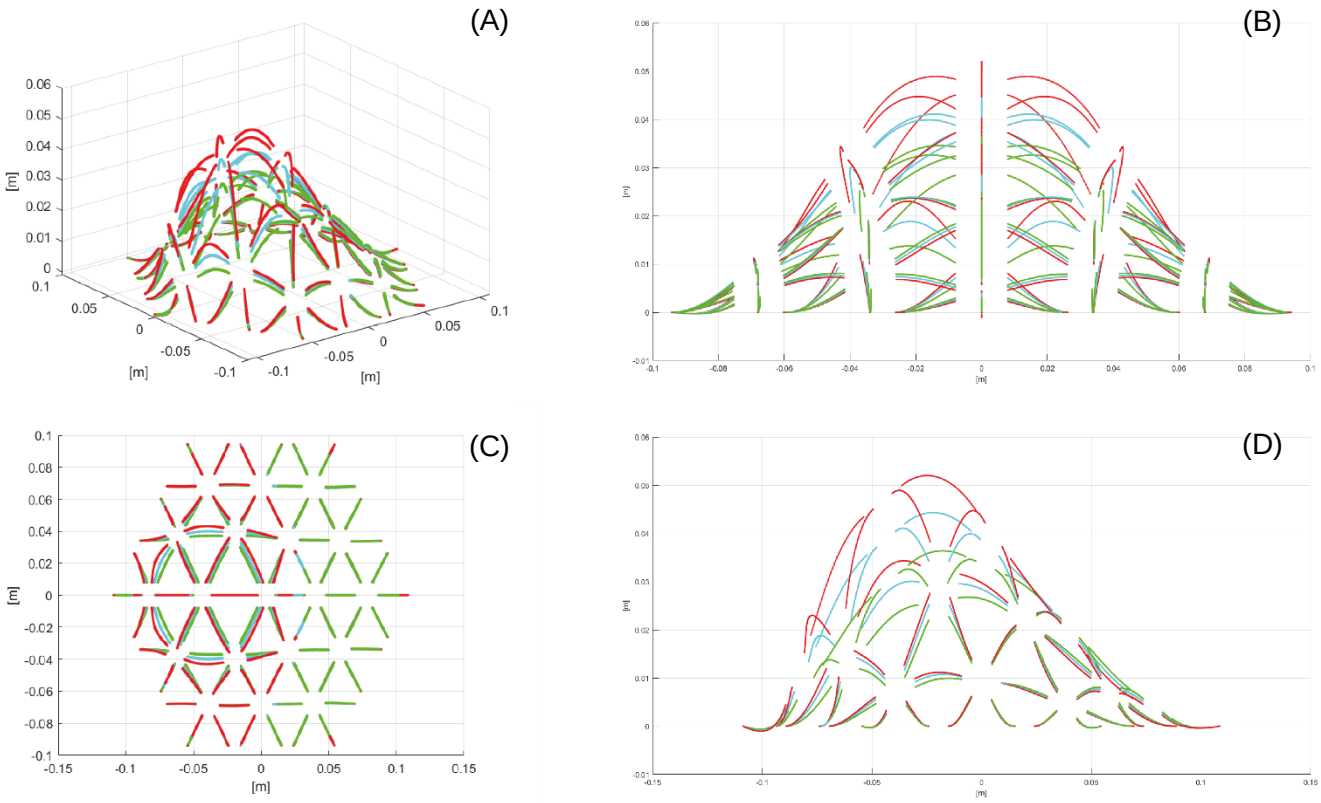

Fig. 31 Different views of different Ansys results to analyze deformation: 25% strain (green), 40% strain (blue) and 55% strain (red)

6.5. Model validation

The first activation scheme Fig. 25 is also used to compare the solution of the finite element analysis to the result of the prototype. The result of the activated prototype is captured with an Artec Spider 3D hand scanner and the Artec Studio15 software, see the set-up in Fig. 32. 3D scanning is used so that the complete shape of the network can be compared. A limitation is that only the top could be scanned due to the wires underneath and that the quality of the scan is diminished due to the reflectiveness of some of the network parts. The resulting OBJ file is manually cleaned up in both Meshmixer and Rhino.

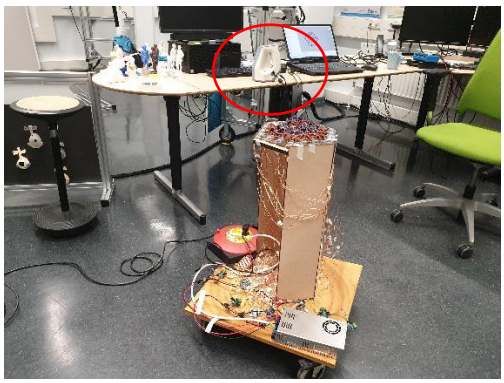

Fig. 32 The set-up for scanning the activated prototype with the Artec Spider 3D hand scanner (encircled).

The result of the FEM for a 55% strain and the 3D scan are plotted together in Matlab. Different views of the result are shown in Fig. 33.

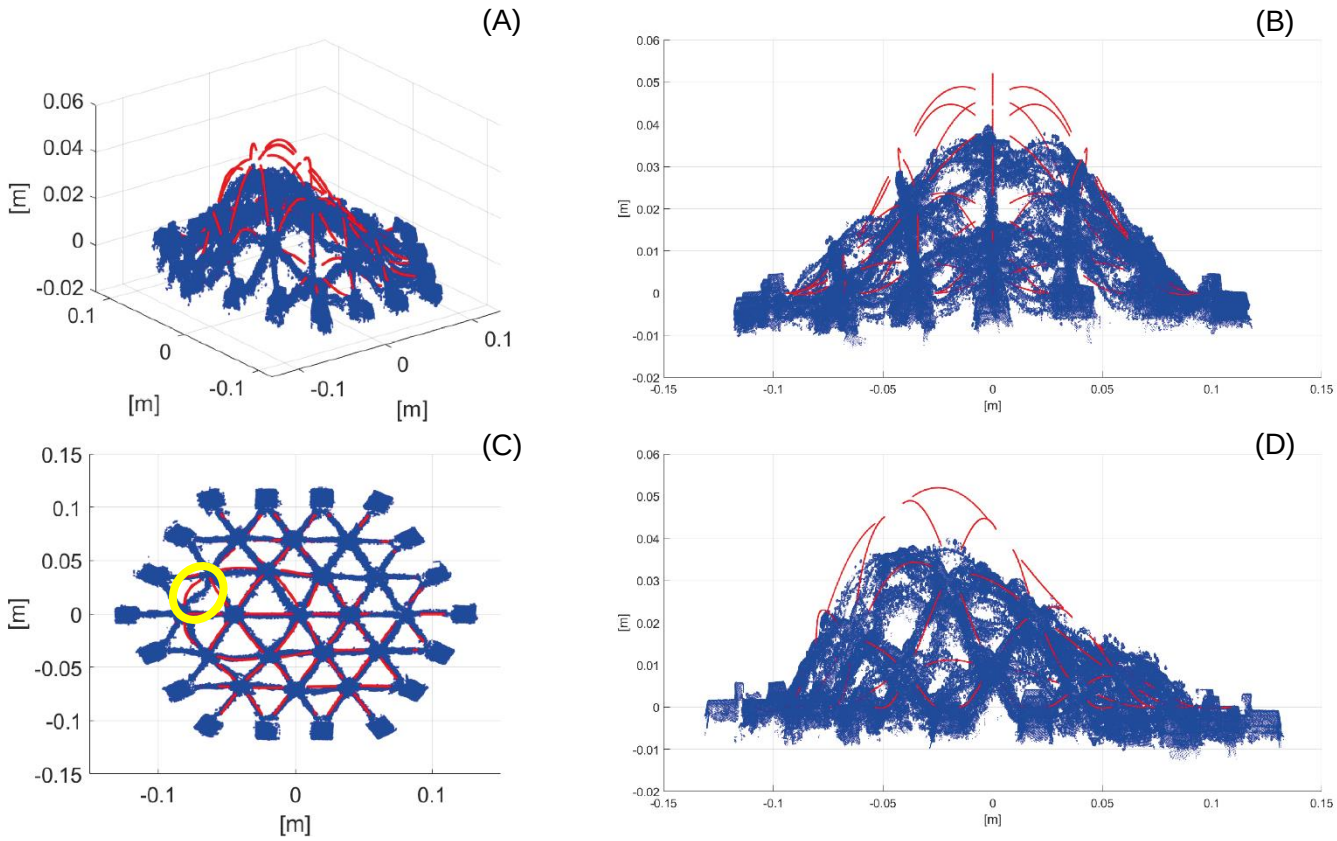

Fig. 33 Different views of 3D scan (blue) and Ansys result for 55% strain (red)

Taking into account that the activated section should actually have strained even more, there is a large difference in deflection between the FEM and the prototype. In addition, there is a difference in overall shape. There is an asymmetry in the network in Fig. 33B although the activation scheme is symmetric in this view. This could be related to the downward buckling of the node that could be seen in Fig. 26. There is also a difference in local shape, as can be seen from the highlighted section in in Fig. 33C. The spring bends outward in the FEM and inward in the prototype. The difference in local shape is even clearer in the screenshot in Fig. 34. In the FEM, the struts remain more straight or bend into a C-shape. In the prototype, the struts bend more, and often in a S-shape instead of a C-shape.

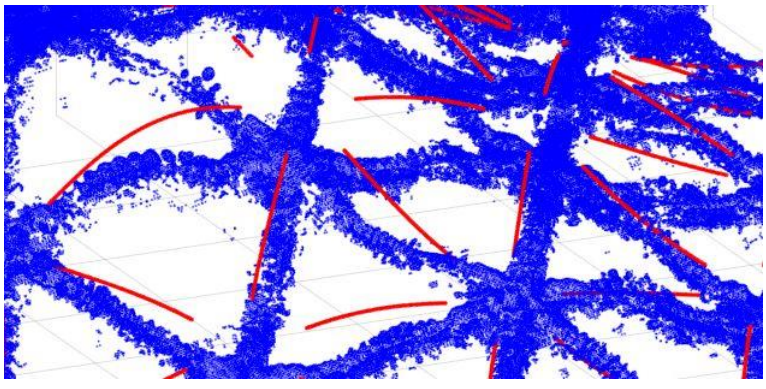

Fig. 34 Different bending shapes in 3D scan (blue) and Ansys result for 55% strain (red)

7 Discussion

All project results are discussed in this chapter. First, possible reasons for the differences between the FEM and the prototype are discussed, including limitations of the model. Second, the network design and its results are discussed. Third, the brainstorm process and the applications are discussed.

Model

Difference in resulting strain

The differences in strain between the FEM and the prototype could be caused by inaccuracies in the FEM or imperfections in the prototype or both.

When looking at the prototype, the bias forces could be too high and/or the axial strain could be too low. The bias forces in the prototype could be higher because it weighs more than anticipated on. In addition, friction could prevent the network from deflecting more. On the other hand, the strain could be too low, because an annealing process can affect the activation temperature [18]. However this effect was not observed visually; the spring shape did not change upon increasing the temperature above 80 °C.

When looking at the FEM, the bias forces could be too low and/or the axial strain could be too high. The bending stiffness of the beam elements could be too low to resemble the bending stiffness of the struts. The bending stiffness is a function of the strain, because the flexure overlap decreases throughout the out-of-plane motion. However, a static effective flexure thickness of 0.047 mm is used to resemble the bending stiffness. This thickness is based on the flexure overlap at 70% strain which is the activated strain of the strut if there is no bias force. The springs might actually strain less, resulting in more flexure overlap, and therefor in a higher effective thickness. To resemble the real situation more accurately, the bending stiffness should actually decrease throughout the out-of-plane motion / upon increasing strain. On the other the other hand, the prescribed axial strain could be too high. It could be that the elastic hoses in the prototype shrink upon heating, similar to heat shrink tubing. This would then be like as if the prestrain of the elastic hoses is increased. When looking at Fig. 29, it can be seen that if the prestrain is increased, which is like shifting the elastic hose curve towards the right and shifting point one above along the vertical line, the strain from point 1 to point 2 is diminished somewhat.

The large difference in strain between the FEM and the prototype was also the reason why the initial strain on all springs was taken from the prototype and not from the model. This contributes to that the difference is most vivid in the activated region.

Difference in local buckling shapes

It is argued above that the enhanced strain in the model could be a result of an unforeseen prestrain of the elastic hoses in the prototype. If this is true, the axial compressive force at point 2 in Fig. 29 would be increased as well upon shifting the elastic hose curve towards the right. This higher compressive force could then also be an explanation for the difference in buckling mode between the real and the modelled spring in the highlighted section in Fig. 34. However, there are two other possible explanations for this. Firstly, it is possible that the result of the FEM would be closer to the S-shape at a strain of 70%. Secondly, it is quite possible that the difference in shape is caused by the flexures. Two flexures are modelled as one. In reality, the flexure ends may have some interaction with the elastic hose, and not slide completely

smoothly in the hose despite their rounded edges, causing the strut to bend into an S-shape rather than a C-shape at some points in the network.

Model limitations

A limitation of the model is that all springs are modelled with the same stiffness, whereas the inactivated springs are in martensite state and should have a lower stiffness. The model should be improved by making a distinction between the martensite and the austenite strut properties. This could also diminish the difference. This is not straightforward in the current model set-up, because the elastic modulus is used together with the beam dimensions to mimic the axial force (caused by the spring and the elastic hose) and the bending stiffness (of the flexures and the spring) of the real situation. Therefore, one cannot simply scale the elastic modulus according to the ratio between the austenite and the martensite modulus of the springs. To mimic reality best, the stiffness should change upon activation. Ansys material models are available to do this, but it is difficult to axially prestrain beam elements.

The strategy of making the width of the beam larger than the height of the beams to mimic the flexures works quite well if the goal is to get an idea of the resulting shape; the beams virtually bend in the same plane as their real counterpart, but are sometimes mirrored. However, if more accurate results are required, the anisotropic stiffnesses should be analyzed more closely.

Network design

Above, possible causes for the differences between the FEM and the prototype are discussed, of which some are due to the prototype. These prototype observations are supplemented here with some observations of the prototype, without comparing it to the FEM necessarily.

Asymmetry

The asymmetry of the network in Fig. 33B is probably caused by the downward deflection of the highlighted node in Fig. 26. For all states, including the inactivated state, the preferred bending direction of this node is downward. This difference in buckling direction can also be observed at smaller scale in the highlighted section in Fig. 33C. Despite efforts to reduce inconsistencies in the manufacturing process as much as possible, flaws in the prototype could prescribe the bending directions. A solution to this could be to automize the manufacturing process, resulting in more control over irregularities. A more robust solution would be to include bending control.

Smoothness

In general, the network does not have a very smooth shape; some springs bend locally. This bending could be obstructed by localizing the bending in a hinge, but this may result in more jerky shapes. The special aspect of the design is that the actuator can bend itself, because this may result in smoother shapes. A solution could therefore be to increase the bending stiffness to a certain extent. However, increasing the bending stiffness also decreases the overall deflection of the network, so this is a trade-off. The smoothness of the shape could also be increased by increasing the control over the amount of strain or over the amount of bending per strut.

Activation

It takes roughly 40 seconds to activate the prototype. The activation speed is controlled with the applied voltage, which is set at a constant that prevents the elastic hoses from overheating. For some applications it may be necessary to speed up the activation. Two options for this are described here. The first way is to set a higher constant voltage and use a material that can withstand the higher temperature. The second way is to set a higher voltage initially, such that the activation temperature is reached quickly, and then decrease the voltage. It is recommended to include a control loop for the latter, because with feed-forward control it might be difficult to achieve the correct temperatures, since these heavily depend on the environment.

Applications

At the moment of the brainstorm, the “opportunities” provided by the “technology” [20] were unknown. These opportunities could have been defined more clearly if the technology would have been developed further. However, developing it further without having an idea of the desired functionalities could result in a useless technology. Therefore, it was chosen to organize a brainstorm session after creating the first network. At this moment, the technology could speak already to the imagination regarding the opportunities.

If we look at the resulting ideas, we can see that properties such as strength, speed and accuracy might become limiting factors. There was too little time during this project to improve on these properties, so this is interesting for future research. For improving on the speed, two optional solutions are discussed in the section above. For improving on the accuracy, a first step would be to translate the basis of the design to a design that can be manufactured automatically and therefore more consistently. In addition, the network density could be increased. For improving on the strength somewhat, the spring characteristics could be adjusted. Note that this also influences the thermal activation characteristics [17]. For improving on the strength significantly, the design has to be adjusted, allowing for a mechanism to be highly deformable as well as stiff in the end state(s). Nonetheless, it is useful to keep close connection with possible applications and their requirements. When focusing on a specific application, the design should be compared to other designs.

For this project, an application with required functionalities close to the current network capabilities was implemented in a demonstrator. Unfortunately, the anticipated shadow effect of the lamp turned out much smaller, and could therefore not be used to enlarge the shape-morphing effect. Nonetheless, the deformations of the network itself could be inspiring as well.

8 Conclusion

The original project goal was to create a SMA spring network that could deform from a flat configuration in 2D into a specific double curved configuration in 3D and to explore possible applications. A design for such a spring network is developed throughout a prototyping process, which resulted in a network that can successfully deform out of plane into different double curved shapes. Flexures are used to impose the out-of-plane bending direction. Antagonist hoses are used to prevent these flexures from interacting with the springs and to draw the network back in plane upon cooling. During the project, the focus has shifted from creating a sheet with one embedded shape towards a universal sheet that can deform into different curvatures upon different activation schemes. In the final functional prototype, the network is able to deform into different curvatures via binary activating the springs with Joule heating. However, the shape control is low, and the overall shape not very smooth due to excessive local bending of the network struts. This could be diminished by increasing the bending stiffness of the struts. However, this would lead to less overall deflection as well. Instead, shape control could be improved by including bending control or gradual strain control.

A related goal was to create a model which could calculate the required activation for a certain shape. A start to reach this goal was made (see Appendix VII), but it resulted in very specific strains which would be very difficult to realize. Therefore, the focus shifted towards creating a model which could calculate the shape for a certain activation, so that manufactured strains could be inputted. A FEM model to predict resulting shapes upon activation is proposed. The important strut parameters are measured and integrated in a simple beam element. Unfortunately, it has not converged completely. To evaluate the FEM nonetheless, one of the resulting shapes is 3Dscanned and compared with the result of the FEM. There is a significant difference in the amount of deformation, which may be due to inaccuracies of the parameters. The validity of these should be improved before further evaluating the effectiveness of the simplified model.

Along the development of the network and its model, brainstorm sessions were held to complement the applications named in the introduction. The results of the brainstorm could be a source of inspiration for both finding the important properties of the network that should be improved and for finding (demonstrative) applications for shape-morphing products. Important properties seem to be accuracy, speed and strength. There is room for optimizing the parameters of the network design regarding these. One of the applications, the light wave, was chosen as a demonstrator to enhance the shape-morphing behaviour with. However, the effect was not as large as expected, but the final prototype including the light resulted in a working demonstrator nonetheless.

9 Recommendations

Some recommendations regarding future research are listed in this final chapter of the report.

Network design

- The shape-control could be improved via including bending control or via improving strain control. In the current design, the activation is binary. For more accurate shape control, an actuator with which the strain can be chosen more gradually should be designed. This could prevent the struts from local bending and breaking with the global shape of the network. If not using such actuators, another solution to prevent the local bending could be (to control) the strut bending stiffness.

- It could be interesting to look at the influence of subsequent activation, especially if there is no control over the bending direction; can different shapes be achieved by different order of activation?

- It could be interesting to look at other inclination shapes instead of a hexagonal shape, as this influences the behaviour of the network. In addition, it would be interesting to look at inclination shapes that are not planar, as this may be useful for certain applications. Especially if the configuration of the network can change, it might become necessary to be able to control the buckling / bending direction actively for the network to result in a predictable shape.

- The current manufacturing process of the network is laborious and not accurate enough. It could be useful to look into manufacturing processes of shape memory alloy hybrids, as a means to connect the springs and possibly to increase the strength in the end state(s). In addition, the upcoming field of stretchable electronics could be useful in the manufacturing process as well.

- The desired properties of promising applications should be clarified for further development.

Model

- To rule out any inaccuracies regarding the parameters of the model, it is recommended to perform more tensile tests, in which the elastic hose is also tested at an elevated temperature. In addition, a distinction should be made between the martensite and the austenite strut properties. (Currently, the distinction between martensite and austenite is only integrated via the prescribed strain.)

- The model could be improved by making the bending stiffness strain dependent.

- Instead of mimicking the anisotropic stiffness of the strut by making the width larger than the height, all stiffnesses should be determined exactly if a more accurate result is desired. Besides, it would be interesting to look at the effect of changing these stiffnesses upon the resulting shapes.

- If the predictive model is to be used in a practical situation, it is recommended to use a kinematic model as a base for an even simpler FEM, because the current FEM is computationally expensive. The bendability of the struts allows for more round shapes, but makes it also more difficult to model the mechanism. The bendability of the struts could be mimicked with a hinge with a certain stiffness in the kinematic model, like in a pseudo-rigid-body model.

Bibliography

[1] Dunbar, "Emerging technologies insights: Shape-shifting materials.," American Chemical Society , 27 September 2018. [Online]. Available: https://www.cas.org/resource/blog/emerging-technology-insights-shape-shifting-materials. [Accessed 22 May 2020].

[2] R. Guseinov, C. McMahan, J. Pérez, C. Daraio and B. Bickel, "Programming temporal morphing of self-actuated shells," *Natrue Communications ,* vol. 11, no. 1, pp. 1-7, 2020.

[3] S. Ceron, I. Cohen, R. Shepherd, J. Pikul and C. Harnett, "Fiber embroidery of self-sensing soft actuators," *Biomimetics ,* vol. 3, no. 3, p. 24, 2018.

[4] E. Palleau, D. Morales, M. Dickey and O. Velev, "Reversible patterning and actuation of hydrogels by electrically assisted ionpringing," *Nature communications ,* vol. 4, no. 1, pp. 1-7, 2013.

[5] F. Hemmert, "The shape-shifting future of the mobile phone," February 2010. [Online]. Available: https://www.ted.com/talks/fabian_hemmert_the_shape_shifting_future_of_the_mobile_phone?language=en. [Accessed April 2020].

[6] H. Wang, D. Kaleas, R. Ruuspakka and R. Tartz, "Haptics using a smart material for eyes free interaction in mobile devices," *2012 IEEE Haptics Symposium (HAPTICS),* pp. 523-526, 2012.

[7] M. Rasmussen, E. P. M. Pedersen and K. Hornbaek, "Shape-changing interfaces: a review of the design space and open research questions," *Proceedings of theSIGCHI Conference on Human Factors in Computing Systems ,* pp. 735-744, 2012.

[8] J. Alexander, A. Roudaut, J. Steimle, K. Hornbaek, M. Bruns Alonso, S. Follmer and T. Merritt, "Grand challenges in shape-changing interface research," *Proceedings of the 2018 CHI conference on human factors in computing systems ,* pp. 1-14, 2018 .

[9] A. Boem and G. Troiano, "Non-rigid HCI: A review of deformable interfaces and input," *Proceedings of th 2019 on Designing Interactive Systems Conference ,* pp. 885-906, 2019.

[10] M. Coelho and J. Zigelbaum, "Shape-changing interfaces," *Personal and Ubiquitous Computing ,* vol. 15, no. 2, pp. 161-173, 2011.

[11] W. Liu and J. Talghader, "Current-controlled curvature of coated micromirrors," *Optics letters,* vol. 28, no. 11, pp. 932-934, 2003.

[12] S. Follmer, D. Leithinger, A. Olwal, A. Hogge and H. Ishii, "inFORM: dynamic physical affordances and constraints through shape and object actuation," *User Interface Software and Technology,* vol. 13, no. 10, pp. 2501988-2502032, 2013.

[13] S. Follmer, "Shape-shifting tech will change work as we know it," October 2015. [Online]. Available: https://www.ted.com/talks/sean_follmer_shape_shifting_tech_will_change_work_as_we_know_it?language=en#t-465934. [Accessed April 2020].

[14] E. Baseta, E. Tankal and R. Shambayati, "Translated geometries," Institute for advanced architecture of Catalonia, 2014. [Online]. Available: https://iaac.net/project/translated-geometries/. [Accessed 2020].

[15] NASA, "What is MADCAT? Flexing wings for efficient flight," NASA, Earth Science Communications Team, 5 April 2019. [Online]. Available: https://climate.nasa.gov/news/2858/what-is-madcat-flexing-wings-for-efficient-flight/. [Accessed 20 April 2020].

[16] Y. Klein, E. Efrati and E. Sharon, "Shaping of elastic sheets by prescription of non-Euclidean metrics," *Science ,* vol. 315, no. 5815, pp. 1116-1120, 2007.

[17] J. Jani, M. Leary, A. Subic and M. Gibson, "A review of shape memory alloy research, applications and opportunities," *Materials & Design ,* vol. 56, pp. 1078-1113, 1980-2015.

[18] S. U. Rehman, M. Kahn, A. N. Khan, K. Alam, S. H. I. Jaffery, L. Ali and A. Khan, "Influence of Cu addition on transformation temperature and thermal stability of TiNiPd high temperature shape memory alloys.," *Proceedings of the Institution of Mechanical Engineers, Part L: Journal of Materials: Design and Applications,* vol. 233, no. 5, pp. 800-808, 2019.

[19] C. Grossmann, J. Frenzel, V. Sampath, T. Denka and G. Eggeler, "Elementary transformation and deformation processes and the cyclic stability of NiTi and NiTiCu shape memory spring actuators.," *Metallurgical and Materials Transactions A,* vol. 40, no. 11, pp. 2530-2544.

[20] W. Poelman, "Technology Diffusion in the Design Process," 24 5 2005. [Online]. Available: http://resolver.tudelft.nl/uuid:d9850382-00c6-4f16-ab3f-3336aa39df01. [Accessed 20 August 2020].

[21] A. van Boeijen, J. Daalhuizen, J. Zijlstra and R. van der Schoor, Delft Design Guide, Amsterdam : BIS Publishers , 2013.

[22] H. Tsai, T. Kuo and G. Y. C. Lee, "Efficiacy of paced braething for insomnia: enhances vagal activity and improves sleep quality," *Psychophysiology ,* vol. 52, no. 3, pp. 388-396, 2015.

[23] T. W. Meng, G. P.-T. Choi and L. M. Lui, "TEMPO: Feature-Endowed Teichmüller Extremal Mapping of Point Clouds," *SIAM Journal on Imaging Sciences,* vol. 9, no. 4, pp. 1922-1962, 2016.

[24] I. Ansys, "Mechanical APDL Material Reference Ansys," November 2013. [Online]. Available: https://www.yumpu.com/en/document/view/7801539/mechanical-apdl-material-reference-ansys. [Accessed November 2020].

[25] M. Ben Jaber, "Ansys parameters for shape memory alloys (Aurricchio Model)," March 2018. [Online]. Available: https://www.researchgate.net/publication/323883785_Ansys_parameters_for_shape_memory_alloys_Aurricchio_Model. [Accessed November 2020].

[26] I. Ansys, "INISTATE," Release 18.2. [Online]. Available: https://www.mm.bme.hu/~gyebro/files/ans_help_v182/ans_cmd/Hlp_C_INISTATE.html. [Accessed 2021].

[27] F. Elteren, "Ansys learning forum - How to model SMA bending actuator?," Ansys, Inc. , January 2018. [Online]. Available: https://forum.ansys.com/discussion/717/how-to-model-sma-bending-actuator. [Accessed March 2021].

[28] R. Gilbertson, Muscle Wires Project Book, San Rafael CA: Mondo-Tronics, 1993.

[29] Hermano, "Lateral spring stiffness," Physicsforum, 8 June 2019. [Online]. Available: https://www.physicsforums.com/threads/lateral-spring-stiffness.973149/. [Accessed 20 January 2021].

[30] A. M. Wahl, Mechanical Springs, Penton Publishing Company , 1944.

[31] A. Fabregat-Sanjuan, F. Ferrando and S. De la Flor, "NiTiCu transverse to axial strain ratio analysis during tension / compression tests.," *Materials Today: Proceedings ,* vol. 2, pp. S759-S762, 2015.

[32] M. Benvidi, "How to get over the convergence problem related to shape memory alloy (nonlinear)?," 13 November 2019. [Online]. Available: https://www.researchgate.net/post/How-to-get-over-the-convergence-problem-related-to-shape-memory-alloy-nonlinear. [Accessed 28 December 2020].

[33] M. Tassoul, Creative Fascilitation, VSSD, 2012.

[34] I. Asimov, "How do people get new ideas?," *MIT Technology Review,* 2014.

[35] P. Desmet and S. Fokkinga, "Human Experience Catalog: Five Typologies of Human Experiences," Emotion Studio , 2019.

[36] Wikipedia, "Deformable Mirror," 14 June 2020. [Online]. Available: https://en.wikipedia.org/wiki/Deformable_mirror. [Accessed 24 September 2020].

[37] P. Madec, "Overview of deformable mirror technologies for adaptive optics and astronomy.," *Adaptive Optics Systems III,* vol. 8447, p. 844705, 2012.

[38] Amazon, "Hexagonal mirror mosaic tiles craft mirror pieces bulk 100 pieces for craft projects home decor," Amazon, 2020. [Online]. Available: https://www.amazon.com/Hexagonal-Mirror-Mosaic-Pieces-Projects/dp/B07PHXBTQ1. [Accessed 2020].

[39] M. Madelaire, "MATLAB Answers," 31 July 2019. [Online]. Available: https://nl.mathworks.com/matlabcentral/answers/474193-how-to-generate-points-in-triangular-lattice-pattern. [Accessed 31 July 2020].

Appendix I – Preventing rotation with more or shorter springs?

It could be observed during one of the first tests during the prototyping phase that the connector prefers to rotate in-plane rather than deflect out-of-plane. Here, it can be seen that the same happens with more and shorter springs and also without the water load in the aquarium that was initially used.

More springs

It is unlikely that all springs bended sideways in the same direction by chance, but it could be possible that one spring starts to rotate sideways and takes along the other springs via rotating the connector, which then magnifies the effect. Therefore, six springs are connected (which will also be the case in the final network), so that the in-plane rotational stiffness of the mechanism is increased. However, does it increase faster than the effective vertical stiffness of the mechanism? The results of a quick test can be seen in Fig. 1. The springs lift the connector to some extent, but still rotate the connector as well, so it is not a sufficient solution.

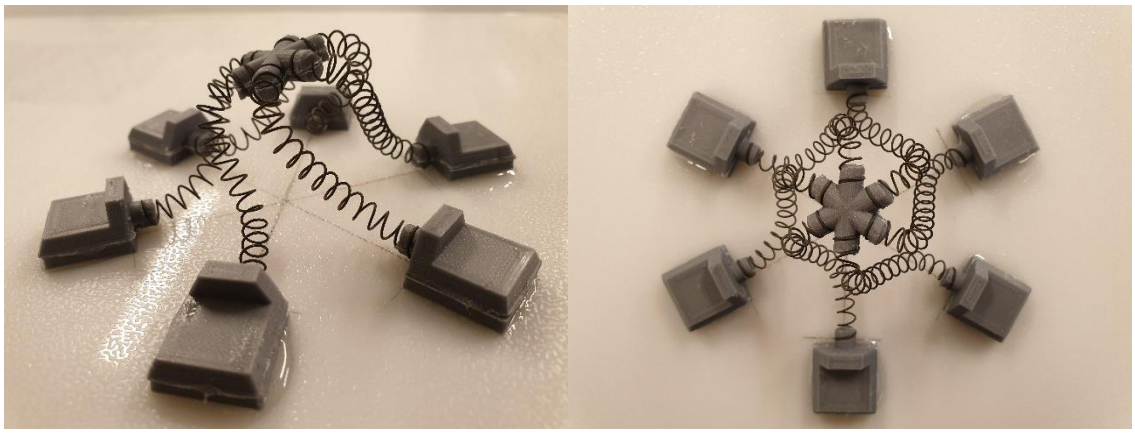

Fig. 1 The results of using six springs instead of three. There is some vertical deflection and some rotation.

It could be that the springs exert forces slightly off centered caused by their winding direction. A solution could be to alternate the winding direction. However, in a later test, the connector rotated in the other direction. Therefore, alternating the winding direction is not a robust solution.

Shorter springs

Here, shorter springs are used to increase the bending stiffness of the springs. The results are shown in Fig. 2 The results of using shorter springs. (A) 10 free windings (B) 7 free windings (C) 4 free windings. For any number of spring windings, the connector is rotated. The lower the number of windings, the smaller the rotation, but also the smaller the out-of-plane effect. Therefore, decreasing the number of spring windings is not effective. .

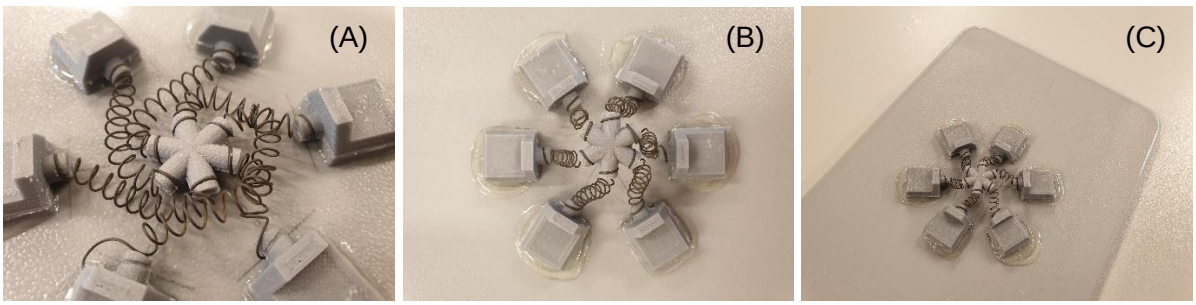

Fig. 2 The results of using shorter springs. (A) 10 free windings (B) 7 free windings (C) 4 free windings

Appendix II – Brainstorm method

Brainstorm method theory

This section provides some in-depth information on how the brainstorm sessions are setup; it explains the reasoning behind some parts of the method, which is discussed hereafter.

Flower association

Two different association processes can be distinguished. The first one concerns generating associations close to a first term (the technology in our case), which is called a flower association. The second one concerns generating association upon association to move away from the first term, which is called a chain association [33]. Our goal is to come up with a lot of diverse ideas, while maintaining relevance. Successive associations might lose their relevance here. For example, if one has thought of a self-deploying circus tent, the second association could be a clown, which is completely irrelevant in this case. The circus tent could be a source of inspiration though, which is explained in the next section. As the goal is to find neighboring concepts, the brainstorm session is focused on finding as many as possible different associations close to the technology.

Lateral and vertical thinking

The circus tent named above could be a source of inspiration by specifying the opportunity that the technology provides within this concept. You could describe the opportunity as “easy assembly at site”. From there, you could then think of other applications which could make use of this opportunity as well. Of course, participants could also think directly of opportunities. However, it may be easier for them to first think of a more tangible phenomenon. Thinking of these direct associations in the first instance could in some way be described as lateral thinking; it is meant to “dig a hole in a different place”. Using these associations to come up with other ideas could then be described as vertical thinking; it is meant to “dig the same hole deeper” [33].

Functional and hedonic aim

Focusing on the opportunities of the technology may result in rather practical applications, depending on the first associations of the participants though. Besides functional aims, there could also be hedonic aims. Hedonic aims “focus primarily on non-instrumental goals such as stimulation, aesthetics, identification, and fun” [7]. The brainstorm is split up into two parts: one part focusing on functional aims and one part focusing on hedonic aims. Therefore, the first part is more focused on defining opportunities of the technology and the second part is more focused on defining qualities and personality traits of the technology.

Individually and together

When in isolation, people can think without interruption and can shuffle great amounts of information in their mind at a time, which could lead to creative ideas [34]. However, the benefit of brainstorming in a group is that people can hitch-hike on each other’s ideas [33]. Therefore, space is created for both in the brainstorm sessions. At first, the participants have some time to think for themselves without being distracted by the ideas of others. Thereafter, the brainstorm sessions continue as a more collective process.

Brainstorm method practically

The trial session was to examine the brainstorm method on the resulting creativity of the participants. Some minor points of improvement were found regarding the brainstorm flow and the clarity of some terms, but many relevant ideas were found already, so these were added to the results.

Participants

Thirteen people (of which five female, all in the age range from 24 to 55 years old), participated in the brainstorm in total. Eight of them were students or graduates from Industrial Design Engineering (IDE) or Mechanical Engineering (ME), though one student with a background in architectural engineering and another student with a background in electrical engineering. The remaining participants were either studying or working in the field of medicine, chemical industry or management. The benefit of IDE and ME students is that they are familiar with thinking abstractly and brainstorming. The benefit of having different backgrounds in the group is that this might lead to diverse associations. The participants were asked to participate in a brainstorm session in exchange for a meal.

Setting

Because of COVID-19 it was not possible to reserve a room at the faculty, three brainstorm sessions were held at home in small groups: a trial session and two “real” sessions. The IDE and ME participants were mixed to realize more diverse groups. I served as facilitator and another person served as host.

Steps

(1) Dinner (45 min): The participants and the facilitator first had dinner together to start the brainstorm session in a casual ambiance. Also, SMA springs and hot water were put on the table for the participants to play with to get familiar with the SMA.
(2) Introduction (5 min): The setup of the project was explained and a movie of the spring network coming out of plane was shown to the participants. The important feature, which is the deformation from 2D to 3D, possibly into a double curvature, was highlighted. The goal of the brainstorm, to find applications that make use of this technology, was stated.

<u>Session 1 (focused on functional aims)</u>

(3) Warming up (5 min): Examples of shape-changing everyday objects were shown, see Fig. 3. The participants were asked to state which objects had a similar deformation, how they would describe this deformation, if they could think of another product with this deformation and to describe the function of the deformation in these products.

Fig. 3 The participants were asked to describe the deformations, think of other products with the same deformations and describe the functions of the deformations in these products as a warming-up.

(4) Possibilities (5 min): The participants were shown animated movies of different type of deformations that are enabled by the technology to inspire their imagination. For example, one animation showed sequential activation allowing for more complex shapes. In addition, the participants were made aware of the following variations:

- The deformation could take up the whole sheet, or a part of the sheet.
- The deformation could move faster or move slower.
- The sheet can be horizontal or vertical.
- The sheet can be large or small.
- The sheet can be open or closed.
- The activation can be by means of anything.

(5) Round 1 (10 min): The participants were asked to write down any first thoughts individually on separate sticky notes. What did the deformations make them think of? These thoughts could be anything (e.g. phenomenon, analogy, product, application, function, etc.); it was meant to not forget about something that could be useful throughout the brainstorm and to clear their mind. In the end, the participants were asked to explain their thoughts in turn and put their sticky notes on a white sheet in three categories: applications, functions and other.

(6) Round 2 (30 min): The participants were asked to think of more applications, also while taking inspiration from what was already on the white sheet. In the end, the participants were asked to group all applications together based on more abstract functions. If the function description was not yet on the sheet, a new function group was created.

(7) Motion (5 min): During the trial session, participants were likely to come up with functions concerning the shape-change: the function of going from shape A to shape B (and vice versa). However, the motion itself of the shape-change could elicit a different set of functions. Therefore, the participants were shown several GIFs, see Fig. 4, to give examples of functions of motions. An additional set of animated movies in which the focus was on the motion of the network rather than the shape-change was shown hereafter. For example, one animation showed the propagation of a wave throughout a sheet.

Fig. 4 The participants were shown examples of functions of motions.

(8) Round 3 (20 min): The participants were asked to think directly of missing functions, either concerning a shape-change or a motion of a shape-change. After the participants were done thinking about functions, the facilitator added a function that was thought of during the project and was not yet on the white sheet. Hereafter, the participants were asked to add applications that they could think of by looking at the function descriptions.

Session 2 (focused on hedonic aims)

(3) Round 1 (10 min): The participants were talked through what the other participants had been doing last week. The resulting list of ideas was shown to the participants, and they were asked if they could think of any additional applications or functions.
(4) Round 2 (10 min): The participants were introduced to the concept of **hedonic aims** and showing several examples. Then, they wrote down any initial ideas.
(5) Round 3 (5 min): The participants were asked to write down their **associations** regarding the displayed stimuli. In addition, they were specifically asked if they could think of biomimetic associations. The participants were shown a slide with images of several resulting shapes, animated movies of motions and a movie of the real network played twice as fast. (The speed was increased to make the movie more vivid and therewith more inspiring. It was assumed that the speed of the deformation could be readily increased through activation well above the activation temperature instead of heating up gradually.)
(6) Qualities & Personality traits (5 min): The participants were shown several GIFs, see Fig. 5, to give examples of qualities and personality traits of motions.

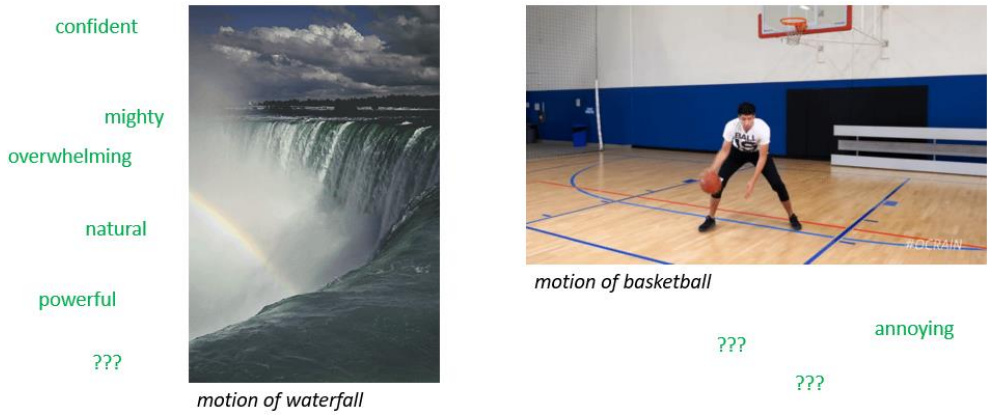

Fig. 5 The participants were shown examples of qualities and personality traits of motions.

(7) Round 4 (5 min): The participants were asked to write down **qualities and personality traits** that they would ascribe to the motion in the movie of the real network played twice as fast or to the association(s) that they had thought of in Round 3.
(8) Round 5 (5 min): How did the motion (in the movie of the real network played twice as fast) make the participant feel? The participants were shown a set of positive and negative emotions that were taken from the Human Experience Catalog [35] for inspiration, but they were allowed to describe their **emotion(s)** differently.
(9) Round 6 (10 min): The participants were asked to think of hedonic (stimulation, aesthetics, identification, fun) applications based on the associations, qualities and personality traits and emotions that were lying (in different colors) on the white sheet in front of them. To help the participants on the way, example train of thoughts were given with random qualities or personality traits and emotions. For example, if a quality is “peaceful”, you could think of an application in the field of meditation, so you could think of a yoga mat.

Appendix III – Brainstorm results

All of the plain resulting ideas for applications of the brainstorm are listed here.

Functional Aims

For multi-functionality

- Any sports ball (e.g. rugby ball and football)
- Any dish bowl (from flat plate to soup bowl)
- Car seat neck rest for different postures (and maybe different lengths)
- Office floor with pop-up seats and tables
- Living building / home according to event
- Cutlery (e.g. spoon that can be fork as well)
- Cooking utensils (e.g. spoon that can be spatula as well)
- Cutting board that can change into bowl
- Cap / hat that changes according to sun / body heat
- Lounger (for sitting any way you like)
- All-size-in-one measuring cup
- Cutting board that becomes dish washbowl upon rinsing it with hot water
- Popup bridge (for animals?)
- Haptic interface (for blind people)

To change height / size gradually (not specifically shape)

- Shoe soles of doctors assisting surgery (table height is set to chief physician)
- Rollercoaster seats (so that no minimum length is required)
- Airplane seats for different human sizes

To deploy

- Stents and other implants
- Expandable catheter

To efficiently store and transport and / or For easy assembly (due to part reduction) at site

- Pots and pans for camping
- Self-deploying festival / circus tent
- Expandable shelter or tent (for refugees)
- Any temporary structure
- Umbrella
- Deployable heat shield
- Furniture (in separate packages that fit into your mailbox)
- Objects that do not fit under (highway) bridges during transportation
- Extractor hood becoming larger when in use
- Table top with adjustable surface area

To manufacture complex shapes

- Organic architectures like the Sydney Opera House
- Concrete reinforcement of more complex shapes

To embrace / fit other shapes

- Cupholder
- Helmet and other sports protection
- Body shaping apparels
- Clothing that fits many sizes and shapes
- Packaging
- Universal charger / power plug
- Any object grabber (eliminating high pressure points)
- Blood pressure band
- Growing-along shoes
- Earphones
- Car chair
- Key
- Radiation mask

To change volume / space

- Submarine in which amount of air density is regulated by volumetric change
- Any surface tires (regulating pressure)
- Expansion balloons for plaque removal
- Airbags
- Resonance box with adjustable vibration field
- Adjustable gastric sleeve

To change stiffness

- To prestress (long) trailers depending on load
- To statically balance
- To change frequency of tuned mass damper because of stiffness change
- To increase damping by increasing force on damper because of higher stiffness
- Adjustable speed bump
- Smart bubble wrap for shipping (size of bubble is adjusted according to pressure at that spot)
- Mattress

To change permeability
- Filter (change according to the liquid flowing through it or according to the size of the particles that have to be filtered out)
- Sieve
- Shower nozzle (regulating water jet speed)
- Lamp cap (regulating amount of illuminance)
- Building façade (regulating amount of sunlight)
- Blinds (regulating amount of sunlight)
- Beach umbrella (regulating amount of sunlight)
- Windshield (regulating amount of breeze)
- Sail on sailboat (regulating wind pressure)
- Air filter (to filter air from polluting gasses or fine dust)
- Water filtering system
- Selective membrane
- Regulating chemical reactions (by regulating supply)
- Tent (or roof) that opens when the sun shines and closes when it rains
- Valves in water pipes (e.g. to regulate hot water supply)
- (Sports) clothes that open up when it is hot
- Flower pot that holds or releases water
- Fishing net with holes according to fish size
- Spaghetti / churros maker (setting profile shape)
- Sunglasses that can change light intensity
- Window which automatically regulates sun / wind (with pieces of glass that can open up)
- Pram cap (+ grow along with child)

To change texture or surface curvature
- Adjustable terrain
- Pop-up buttons of touch screen (haptics)
- Grater (from fine to coarse)
- Knife with adjustable sharpness
- Adjustable aerodynamics

To supply (cyclic) actuation
- Massage mat
- Posture correcting mattress
- To lift things
- To launch things
- To push out things
- Stabilizing platform
- Pump (like a heart)
- Wavemaker
- To lift eggs from boiling water
- Artificial pericardium / myocardium to assist heart pump function
  (from meeting with Jenny Dankelman)

To store energy
- Converting thermal energy to height energy

Education
- Mecano building blocks (applying electricity to change shape or move stuff)
- Formation of mountains

To change slope / reflection direction
- Solar panel (flat when sun is high, curved when sun is low)

“Hedonic Aims”

- Long and short dress
- Light show by changing permeability / direction
- Ceiling lamp
- Furniture that can change shape for aesthetical purposes
- Wine bottle
- (growing / moving) artificial plant
- Changing laughing mirror
- Sculpting material (tool)
- Toy (different activation = different shape)
- Board marble track
- Adaptive game board
- Type of beach animal
- “supercool” blinds
- Living / changing statue
- Statue that expresses fluctuation of …
- Fashionable armpit ventilation
- Breathing aid (preventing hyperventilation) around your body
- Belly that grows along with belly during pregnancy (for long distance relationships?)
- Corset
- Summer / winter roof (changing insulation)
- Hor
- Fountain with more / less water (smaller holes → higher fountain)
- Clock
- Kitchen timer
- Changing jewelry
- Decoration
- Living art
- Door knobs that are not visible when not being used (aesthetic pleasure)
- Golf course that changes over time

Appendix IV – Idea selection

Here, the ideas from the brainstorm (see Appendix III) are assessed, and three of them are chosen.

Boundary conditions

At first, all ideas are selected based on whether they fit with the technical result of the prototyping phase of the project, so that is if the ideas make use of the 2D to 3D deformation. In addition, there should be no obvious or existing other solution, so that our “material” enables the application. However, an exemption to this rule is made if the application could also have a hedonic aim. For example, fabricating a roof that can open up out of our material may be quite cumbersome regarding the desired function. However, because of its possible artistic value it is kept in the list. Note that not only the ideas that need multiple memory shapes but also the ideas that need only one memory shape are included in the list. The functional requirements are repeated below.

- It makes use of the 2D to 3D deformation.
- There is no obvious or existing other solution. OR The solution has a hedonic aim.

Criteria

After the ideas are taken out of the list, similar ideas are combined in one description, and the list in Table is formed. These ideas are assessed with the help of The Weighted Objectives Method [21]. Even though this method could be seen as rather cumbersome for a relatively large number of ideas, it is chosen to use this method anyway because of the ability to assess the ideas on a chosen number of criteria in a relatively accurate way. The criteria are discussed below.

Weakness / strength inaccuracy
This criterium is included to assess the ideas based on the required stiffness in the end shapes or the required accuracy with which the stiffness can be regulated (through the amount of deformation). As the maximum stiffness of the future design and the exact required stiffnesses of the ideas are not clear, this aspect is included as a criterium, and not as a functional requirement. Note that the load can be either compressive or tensile. A low required stiffness or accuracy results in a high score.

Slowness / time inaccuracy
This criterium is included to assess the ideas based on the required speed or the required accuracy of the speed of the deformation. According to a similar line of thought as for the first criterium, this aspect is included as a criterium. A low required speed or accuracy results in a high score.

Shape inaccuracy
This criterium is included to assess the ideas based on the required shape accuracy; how tight should the spring network follow a certain shape? A low required shape accuracy results in a high score.

Demonstratability
This criterium is included to assess the ideas based on their demonstrability. The demonstrability is composed of two aspects. The first aspect concerns the inspirational level of the demonstrator. Does the application need or could it benefit from using multiple memory shapes (so that it can show the capabilities of the material)? Is the application understandable? The second aspect concerns the practicality of the demonstrator. For example, demonstrators that require a liquid flow are not very practical. The practicality also concerns the size of the demonstrator. Applications that require a large spring network score low on the demonstrability. Size is not included as a boundary condition, because the option exists to create a scale model, but this is not desirable.

Weights

All four criteria are considered comparably important. However, the weakness and the slowness could be seen as unspecified functional requirements, so these might be more critical than the shape inaccuracy and the demonstrability, which are more like performance criteria. (A better shape accuracy or demonstrability will in general gradually improve the performance.) Therefore, the weakness and the slowness are given somewhat higher weights than the other two.

Results

The results are shown in Table 1. The top three ideas are an (interactive) living / changing art / statue, a laughing mirror and adaptive permeable light shield (in unspecified form).

Table 1. The remaining ideas are assessed by means of the Weighted Criteria Method.

	weakness (compressive & tensile) / strength inaccuracy		slowliness / time inaccuracy		inaccuracy of shape		demonstratability (including size) + demonstrative value		
weight factor	30		30		20		20		
(interactive) living / changing art / statue	5	150	5	150	5	100	5	100	500
laughing mirror	5	150	5	150	4	80	5	100	480
all ideas related to permability of light *(a lot of different ideas!)*	5	150	5	150	3	60	5	100	460
adaptive game board	5	150	4	120	5	100	4	80	450
living building	5	150	5	150	5	100	2	40	440
boiling egg lifter	4	120	4	120	5	100	5	100	440
cutting board / bowl or sink	4	120	4	120	5	100	5	100	440
dish bowl	4	120	4	120	4	80	5	100	420
any deformable tent / shelter / structure	4	120	5	150	5	100	2	40	410
board marble track	5	150	2	60	5	100	5	100	410
any popup tent / shelter / structure	4	120	5	150	5	100	1	20	390
cap with extandable flap	5	150	4	120	3	60	3	60	390
adjustable / growing terrain	3	90	5	150	5	100	2	40	380
adjustable resonance chamber	5	150	3	90	4	80	3	60	380
dynamic affordances (e.g. door knobs)	4	120	3	90	3	60	5	100	370
all-size-in-one measurement cup	4	120	3	90	3	60	5	100	370
popup / growing terrain	3	90	5	150	5	100	1	20	360
energy converter	3	90	5	150	5	100	1	20	360
artificial (growing) plant	5	150	3	90	3	60	3	60	360
growing belly	5	150	3	90	3	60	3	60	360
(car) chair / neck rest	2	60	4	120	4	80	4	80	340
cupholder	4	120	2	60	3	60	5	100	340
aerodynamics	4	120	3	90	3	60	3	60	330
radiation mask	5	150	3	90	1	20	3	60	320
time measurement system	5	150	1	30	5	100	1	20	300
popup bridge (for animals)	1	30	5	150	5	100	1	20	300
haptic interface	3	90	3	90	4	80	2	40	300
deformable mold	1	30	5	150	1	20	5	100	300
lounger	1	30	4	120	5	100	2	40	290
mattress	1	30	4	120	5	100	2	40	290
all ideas related to permability of fluids *(a lot of different ideas!)*	4	120	3	90	2	40	2	40	290
popup furniture	1	30	4	120	3	60	2	40	250
deformable furniture	1	30	4	120	3	60	2	40	250
office floor	1	30	4	120	3	60	2	40	250
wavemaker	3	90	1	30	4	80	2	40	240
tunable variable stiffness	1	30	2	60	5	100	2	40	230
stabilizing platform	1	30	2	60	5	100	1	20	210
speed bump	1	30	1	30	5	100	1	20	180

Appendix V – Concept selection

Here, the concepts are assessed, and one of them is chosen.

Harris profiles are made for every concept. Harris profiles are chosen because herewith multiple criteria can be included and the graphic representation allows for a discussion. In a Harris profile, the criteria are listed in the order of most important to least important. The performance criteria are divided into three categories: 'prototype feasibility', 'using material's capabilities' and 'demonstrative value'. (The criteria are slightly adjusted compared to the criteria that are used for the idea selection.) A concept makes use of the specific material's capabilities if it makes use of the multiple shapes function and of the smoothness of the shapes. The demonstrator is believed to be a good demonstrator if it is attractive, explanatory and inspiring.

Results

The results are represented in Table 2. An argumentation for the profiles is given below.

Table 2 The concepts are assessed by means of Harris profiles.

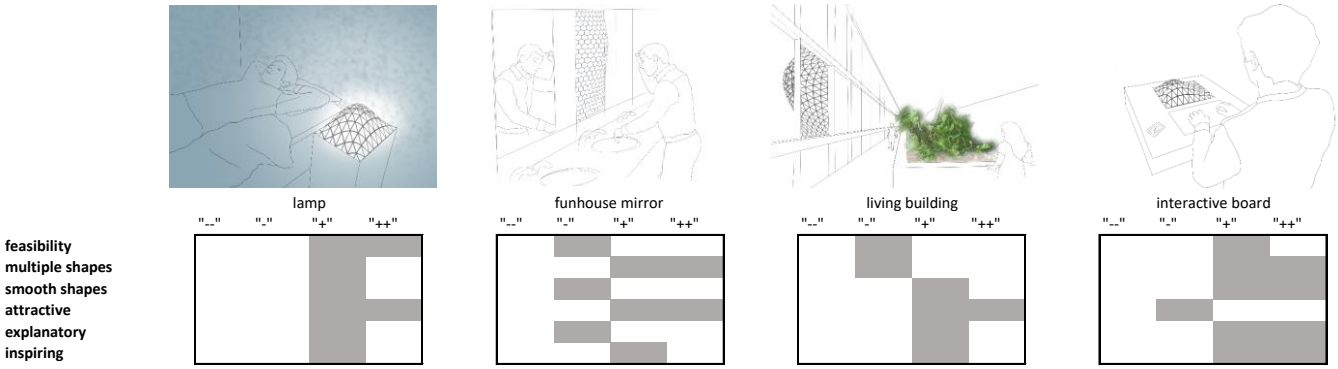

Feasibility

Gravity influences the behavior of the network. Up to now, the network has been kept horizontal, with the network growing upwards. The balloons prevent the flexures from sticking out of the springs, but also pullback the mechanism. However, they cannot pullback the mechanism completely flat. Therefore, it could possibly be useful to make use of gravity. We can only make use of gravity if we keep the network horizontal. The lamp and the interactive board are horizontal, so these are considered to be more feasible initially, as they resemble the prototype configuration. However, the interactive gameboard requires an interface, which is considered less feasible than integrating a lamp in the demonstrator.

Multiple shapes

The funhouse mirror and the interactive board depend on the ability to create multiple shapes. In addition, what shape exactly can be made is essential. For the lamp, it is desirable that multiple shapes can be made. However, what shapes exactly is less pressing. For the living building, some kind of wave motion could be beneficial, but furthermore, a variety in shapes would only break with its periodic character, so the living building would not demonstrate this function well.

Smooth shapes

The funhouse mirror scores lowest, because the smoothness of the shape is disrupted by the discretization of the surface. (It could be created with surface normal actuators as well.) The interactive board scores highest, because the smoothness could be useful for when trying to make certain shapes.

Attractive

All concepts that do not require manual activation and move automatically or have some kind of decorative function are considered more attractive. Therefore, the interactive game board scores lowest here.

Explanatory
The funhouse mirror scores lowest here, because for this concept the network might not be visible. The interactive gameboard is believed to be extra explanatory, because the user controls the input him or herself and is able to observe the output.

Inspiring
Here, it is assumed that the more generic the concept, i.e. the less expressive the application, the more likely it is that the concept inspires new applications. The interactive gameboard is considered the most generic and the rest is considered more specific.

Discussion

During a discussion with the supervisors, it was named that one of the disadvantages of the mirror would be that it only requires very small deformations, whereas the network can enable very large deformations, so the mirror would not utilize the material. The size of the deformation was not included in the initial set of performance criteria. However, the size of the deformation does not differ much among the remaining concepts, so it would not influence the decision. From the Harris profiles, the lamp and the interactive board seem to be the best concepts. The interactive board seems to be the best if one would only look at the amount of positive colored blocks. However, the feasibility was stated to be the most important criterium, on which the lamp scores highest. During the discussion, it was decided that the lamp wins from the interactive board because of the feasibility. If time would be left, an interface could be added to the lamp concept.

Appendix VI – A reflective surface with adjustable curvature

Here, the ideas to create a reflective surface with adjustable curvature for Concept 2 are discussed.

As said before, for a flat sheet to morph into a double curved sheet, the material has to stretch. The following abstract solutions are thought of to realize / mimic the stretching effect:

1. Use a (highly) stretchable reflective material or fabric
2. Use a reflective liquid (a change in thickness enables a change in surface area)
3. Discretize the surface and use flat pieces of mirror with variable distances between them

Stretchable material

A typical field of application of deformable mirrors is adaptive optics [36]. One of the design strategies here to make the mirrors deformable is to make them very thin. This makes them expensive. In addition, the strokes are typically relatively small; the strokes are in the order of µm for a surface diameter in the order of m [37].Therefore, a continuous solid material is not a suitable solution in this project.

Stretchable fabric

Different reflective stretchable fabrics can be found online. From online pictures it can be seen that these fabrics diffuse the light to great extent. This results in a blurred reflection, which is undesirable. Therefore, this is not a suitable solution.

Liquid

An example of a material that could serve as a reflective liquid is Gallium. Gallium is a liquid above 30 °C, so it will melt in a person's hand. However, using a liquid might actually be cumbersome.

Discretization

The idea here is to discretize the surface with flat pieces of mirror. Mirror tiles, see Fig. 6, could be attached to every connector. If mirror tiles turn out to be too heavy, mirror stickers could be used. Even though this solution breaks with the fluent character of the spring network, it is nominated as the most suitable solution for this project based on practicality, mirror quality and price.

Fig. 6 Mirror tiles can be used for creating a reflective surface with adjustable curvature **[38]**.

Appendix VII - Kinematic Model

From shape to elongations

Conformal map

To calculate the elongations of the lattice struts that result in a certain shape, a Matlab file is created. The desired shape is created in Rhino, and the related STL file is the input for the Matlab file. From the *stlread* function in combination with the *patchlim* function, two vectors are created: one with the 3D node coordinates and one with the node numbers describing the connectivity. A plot of the mesh is shown in Fig. 7A. The vectors are the input for the conformal map algorithm. The conformal map algorithm translates the 3D coordinates to 2D coordinates while locally preserving angles as much as possible by distorting lengths. An existing Matlab algorithm called *Rectangular Conformal Map* is used to create a conformal map of the triangulated shape [23]. (A version that creates a circular conformal map is also available.) The resulting conformal map of the desired shape is given in Fig. 7B.

Lattice

Now we could actually calculate how much the triangle edges in the conformal map should grow in order to result in the desired shape, because we have the triangle node coordinates in both 2D and 3D. However, we use a rougher and periodic mesh as opposed to the mesh of the conformal map. An existing algorithm is used to calculate the coordinates of a triangular lattice pattern [39], for which the input parameters are the width (and the height) of one triangle and the total horizontal and vertical lengths. The algorithm is supplemented with a code that generates the connectivity vector of the lattice triangles. It is ensured that the base square of the conformal map of the triangulated shape is aligned with the lattice square.

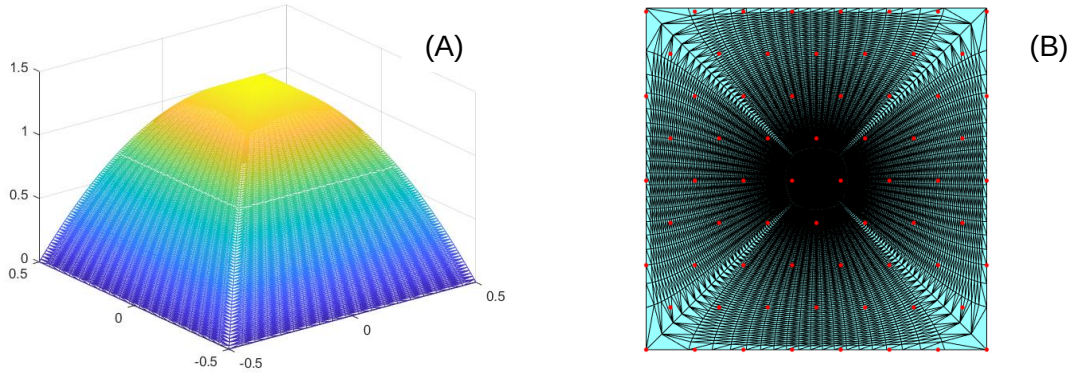

Fig. 7 (A) A plot of the mesh of the desired shape. (B) A conformal map of the mesh, with the lattice nodes plotted on top.

Overlay and elongations

The planar state is the neutral state of the lattice; no deformations have taken place yet. The planar lattice is so to speak placed over the conformal map, see Fig. 7B. Then, for each node in the lattice, the closest node in the conformal map is found. The nodes are not lying exactly on top of each other, so there is an error here. Using a finer triangulation for the STL file results in a smaller error in this step. The original 3D node coordinates of the found conformal map nodes are known. Therewith, the required length change of the lattice struts can be calculated.

From elongations to shape

The method described above results in very specific growth factors. With the used manufacturing method it impossible to realize such specific growth factors. We would round them up. Therefore, what we actually want to have is a geometric model that allows us to specify the elongation of each lattice strut and show us the resulting shape. An attempt is made using the *fsolve* function, which can solve a large set of nonlinear equations. The equations are describing the lattice strut lengths in terms of the 3D coordinates of the lattice nodes. However, this code does not work, probably because multiple solutions exist, so the code would need more constraints. The result that you would want to have is similar to the dome shown in Fig. 8. However, here the plot is made by taking the 3D node coordinates of the STL file that are related to the conformal map nodes that resemble the lattice nodes.

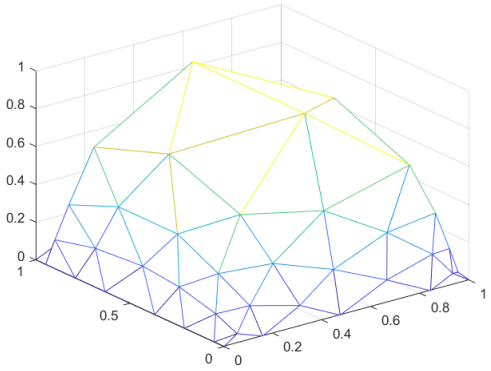

Fig. 8 Only the coordinates of the STL file that are related to the conformal map nodes that resemble the lattice nodes are plotted here.

Appendix VIII – Tensile tests & results

Tensile test – elastic hoses

Tensile tests are performed on the hoses to see if there are any differences between colors and to find the force strain curve for the modelling. The results for differently colored samples are shown in Fig. 9. The two outliers were neglected for calculating the average. In Fig. 10, the results for same colored (green) samples are shown. As can be seen, they cover more or less the same range as the differently colored samples. Therefore, no distinction can be made between colors, and the average of Fig. 9 is used .

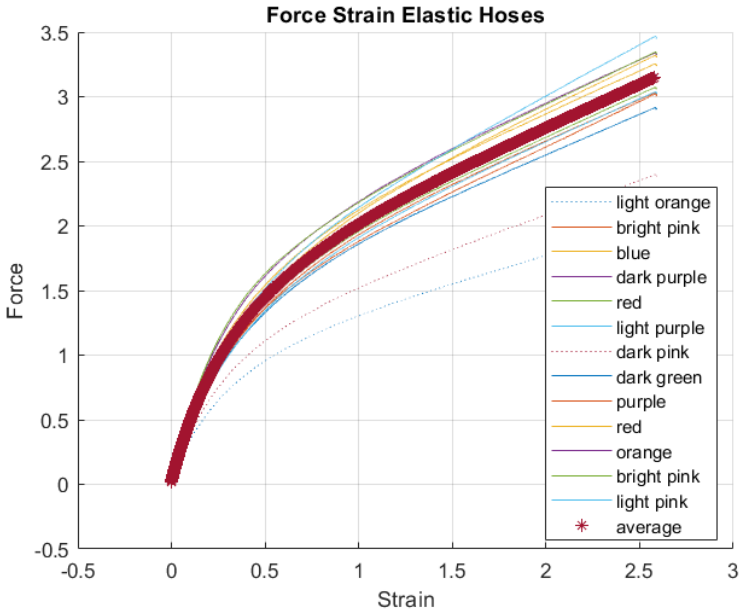

Fig. 9 Tensile test results of elastic hoses of different colors.

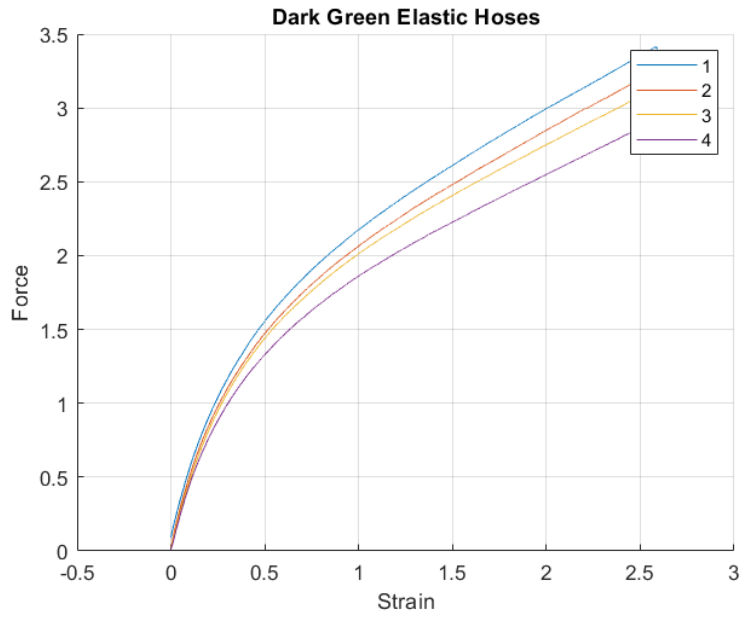

Fig. 10 Tensile test results of elastic hoses of the same color.

Tensile test – springs

Tensile tests are performed on self-manufactured spring samples to find the force strain curves for the modelling. The springs have a spring diameter of 4.5 mm and a wire thickness of 0.5 mm. However, the test data of multiple samples is not that neat, so these are excluded. One of the reasons for this is that it is difficult to keep the wires at a constant temperature. The most neat results are presented in Fig. 11, but for further research it would be good to do more tests in a more accurate way.

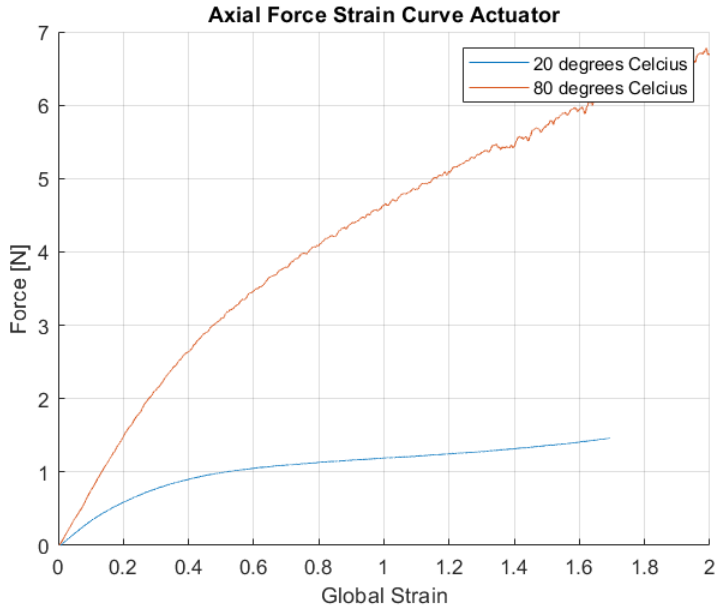

Fig. 11 Tensile test results of one unheated spring and one heated spring

A cyclic loading test at 80°C is performed as well. The testing system is now closed off with cardboards of to diminish the airflow around the spring. The results are shown in Fig. 12.

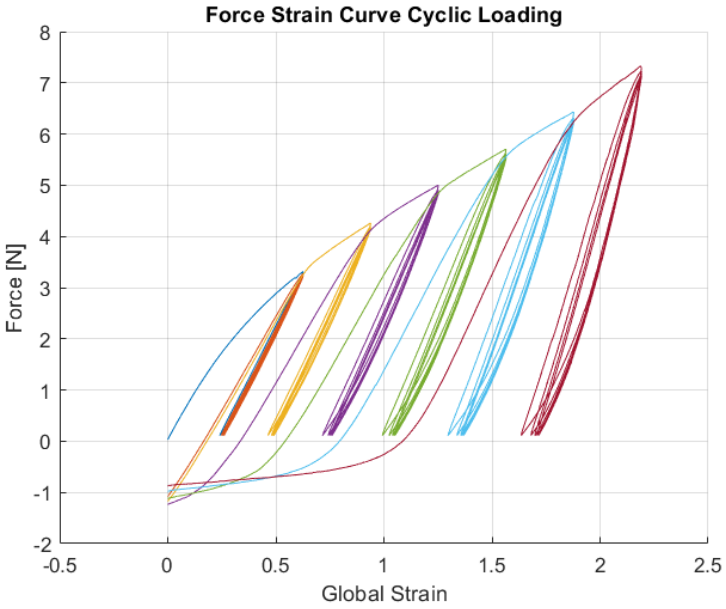

Fig. 12 Tensile test results for heated cyclic loading of one spring

After the load cycle up to 60% (orange), there is almost no degradation of the material, as can be seen from the fact that the load cycle up to 80% (yellow) follows about the same upward curve up to 60%. After the

load cycle up to 80%, the behavior of the material starts to change, as can be seen from the drift of the upward curve towards the right due to nearly zero stiffness at the beginning of the curve. This is due to the elongation of the sample which could be observed during the test. Is this elongation caused by plastic deformation or is it because the spring is actually not fully in austenite phase? To check this, a similar test is done on another sample. The initial force at zero displacement is 0.145 N. Then, the spring is strained up to 80% at a temperature of at 80°C. After going back to the initial displacement, the force is -1.205 N; the spring exerts a compressive force now, so it is elongated. At this point, the temperature is shortly heated up to 200 °C, upon which the force becomes -0.590 N, so the spring has shrunk, but not up to its original point. This means that there is probably some plastic deformation and some stress-induced martensitic transformation. To be careful, the spring should be kept in the linear region in the austenite phase.

Appendix IX – Ansys APDL code

```
/CLEAR,START
/CWD,'C:\Users\Kim\Documents\Graduation Project\'
/PREP7
!
ET,1,BEAM188                    !!! can be used for SMA

MP,DENS,1,744
MP,EX,1,10020
MP,PRXY,1,0.0165
MP,CTEX,1,0.05
TB,BISO,1
TBDATA,1,10020*0.9,10020/5*3
!
SECTYPE,1,BEAM,RECT,
SECDATA,0.015,0.0128
SECOFFSET,USER,0,0
!
!
*SET, X1,0                      !!! X coords parameters
.
.
.
*SET, X163,0.024315
!
!
*SET, Y1,0                      !!! Y coords parameters
.
.
.
*SET, Y163,0.0944400702826931
!
k,1,X1,Y1                       !!! make all keypoints
.
.
.
k,163,X163,Y163
!
TYPE,1                          !!! "SMA" elements
MAT,1
```

```
SECNUM,1
!
ALLSEL,ALL
L,2,8                          !!! draw lines between keypoints
.
.
.
L,133,163
LSEL,ALL
LESIZE,ALL,,,100               !!! number of elements
LMESH,ALL                      !!! mesh lines
!
ALLSEL,ALL
/ESHAPE,1
/VIEW,1,1,1,1
eplot
!
ET,7,MPC184,16                 !!! rigid elements
SECTYPE,8,JOINT,GENE,
SECJOINT,RDOF,1,2,3,4,5,6
SECJOINT,RDOF,1,2,3,4,5,6
TYPE,7
SECNUM,8
!
KSEL,S,KP,,1                   !!! get keypoints for connector
NSLK,S
*GET,ID_1,NODE,,NUM,MIN
KSEL,S,KP,,2
NSLK,S
*GET,ID_2,NODE,,NUM,MIN
KSEL,S,KP,,3
NSLK,S
*GET,ID_3,NODE,,NUM,MIN
KSEL,S,KP,,4
NSLK,S
*GET,ID_4,NODE,,NUM,MIN
KSEL,S,KP,,5
NSLK,S
*GET,ID_5,NODE,,NUM,MIN
KSEL,S,KP,,6
NSLK,S
```

```
*GET,ID_6,NODE,,NUM,MIN
KSEL,S,KP,,7
NSLK,S
*GET,ID_7,NODE,,NUM,MIN
!
!E,ID_2,ID_3                    !!! connect with rigid elements
E,ID_3,ID_4
E,ID_4,ID_5
E,ID_5,ID_6
E,ID_6,ID_7
E,ID_7,ID_2
!
.
.
.
!
KSEL,S,KP,,101
NSLK,S
*GET,ID_101,NODE,,NUM,MIN
KSEL,S,KP,,132
NSLK,S
*GET,ID_132,NODE,,NUM,MIN
KSEL,S,KP,,102
NSLK,S
*GET,ID_102,NODE,,NUM,MIN
KSEL,S,KP,,67
NSLK,S
*GET,ID_67,NODE,,NUM,MIN
KSEL,S,KP,,66
NSLK,S
*GET,ID_66,NODE,,NUM,MIN
KSEL,S,KP,,100
NSLK,S
*GET,ID_100,NODE,,NUM,MIN
KSEL,S,KP,,131
NSLK,S
*GET,ID_131,NODE,,NUM,MIN
!
!E,ID_132,ID_102
E,ID_102,ID_67
E,ID_67,ID_66
```

```
E,ID_66,ID_100
E,ID_100,ID_131
E,ID_131,ID_132
!
!
!
KSEL,S, , ,134                    !!! get boundary keypoints
NSLK,S
*GET,ID_134,NODE,,NUM,MIN
.
.
.
KSEL,S, , ,163
NSLK,S
*GET,ID_163,NODE,,NUM,MIN
!
ALLSEL,ALL
/ESHAPE,1
/VIEW,1,1,1,1
eplot
ALLSEL
!
!/OUT,SCRATCH
!
/SOLU
ANTYPE, 0
NSUBST,50,10000,50
NROPT,UNSYM
!NROPT,AUTO
!LNSRCH,AUTO
NLGEOM,ON
!CNVTOL,U,,
!CNVTOL,F,,
OUTRES,NSOL,LAST
!
TIME,1
D, ID_134, ALL, 0                 !!! constrain all DoF except in-plane
DDELE, ID_134, UX
DDELE, ID_134, UY
.
.
```

```
.
D, ID_163, ALL, 0
DDELE, ID_163, UX
DDELE, ID_163, UY
D, 3, ALL, 0                    !!! move center upward
DDELE, 3, UZ
D, 3, UZ, 0.01
D, 54, ALL, 0
DDELE, 54, UZ
D, 54, UZ, 0.01
D, 105, ALL, 0
DDELE, 105, UZ
D, 105, UZ, 0.01
D, 156, ALL, 0
DDELE, 156, UZ
D, 156, UZ, 0.01
D, 207, ALL, 0
DDELE, 207, UZ
D, 207, UZ, 0.01
D, 258, ALL, 0
DDELE, 258, UZ
D, 258, UZ, 0.01
BFUNIF,TEMP,0
ALLSEL,ALL
SOLVE
TIME,2                          !!! hold resulting boundary displacements
KBC,1
*GET,X_DISP_134,NODE,ID_134,U,X
*GET,Y_DISP_134,NODE,ID_134,U,Y
.
.
.
*GET,X_DISP_163,NODE,ID_163,U,X
*GET,Y_DISP_163,NODE,ID_163,U,Y
D, ID_134, UX, X_DISP_134
D, ID_134, UY, Y_DISP_134
.
.
.
D, ID_163, UX, X_DISP_163
D, ID_163, UY, Y_DISP_163
```

```
TIME,3                          !!! heat uniformly
BFUNIF,TEMP,0.1
ALLSEL
SOLVE
TIME,4
BFUNIF,TEMP,0.2
ALLSEL
SOLVE
TIME,5
BFUNIF,TEMP,0.3
ALLSEL,ALL
SOLVE
TIME,6
BFUNIF,TEMP,0.4
ALLSEL,ALL
SOLVE
TIME,7
BFUNIF,TEMP,0.5
ALLSEL,ALL
SOLVE
TIME,8
BFUNIF,TEMP,0.6
ALLSEL,ALL
SOLVE
TIME,9
BFUNIF,TEMP,0.7
ALLSEL,ALL
SOLVE
TIME,10                         !!! let go of center
DDELE, 3, ALL
DDELE,54, ALL
DDELE,105, ALL
DDELE,156, ALL
DDELE,207, ALL
DDELE,258, ALL
!ACEL,,,1
ALLSEL,ALL
SOLVE
TIME,11
BFUNIF,TEMP,0.8
ALLSEL,ALL
```

```
SOLVE
TIME,12
BFUNIF,TEMP,0.9
ALLSEL,ALL
SOLVE
TIME,13
BFUNIF,TEMP,1
ALLSEL,ALL
SOLVE
TIME,14
BFUNIF,TEMP,1.1
ALLSEL,ALL
SOLVE
TIME,15
BFUNIF,TEMP,1.2
ALLSEL,ALL
SOLVE
TIME,16
BFUNIF,TEMP,1.25
ALLSEL,ALL
SOLVE
TIME,17
BFUNIF,TEMP,1.3
ALLSEL,ALL
SOLVE
TIME,18
BFUNIF,TEMP,1.35
ALLSEL,ALL
SOLVE
TIME,19
BFUNIF,TEMP,1.4
ALLSEL,ALL
SOLVE
TIME,20
BFUNIF,TEMP,1.5
ALLSEL,ALL
SOLVE
TIME,21
BFUNIF,TEMP,1.6
ALLSEL,ALL
SOLVE
```

```
TIME,22
BFUNIF,TEMP,1.7
ALLSEL,ALL
SOLVE
TIME,23
BFUNIF,TEMP,1.8
ALLSEL,ALL
SOLVE
TIME,24
BFUNIF,TEMP,1.9
ALLSEL,ALL
SOLVE
TIME,25
BFUNIF,TEMP,2
ACEL,,,1                    !!! activate gravity
ALLSEL,ALL
SOLVE
TIME,26                     !!! heat ununiformly
LSEL, S,,,4,6,1
LSEL, A,,,10,11,1
LSEL, A,,,23,27,1
LSEL, A,,,38,39,1
BFL, ALL, TEMP, 2.1
ALLSEL, ALL
SOLVE
TIME,27
LSEL, S,,,4,6,1
LSEL, A,,,10,11,1
LSEL, A,,,23,27,1
LSEL, A,,,38,39,1
BFL, ALL, TEMP, 2.2
ALLSEL, ALL
SOLVE
.
.
.
(up to TEMP, 11, at some points smaller load steps are required)
```

Appendix X – Design Brief

The Design Brief starts on the next page.

DESIGN FOR our future

nieuw. 2

TU Delft

IDE Master Graduation

Project team, Procedural checks and personal Project brief

This document contains the agreements made between student and supervisory team about the student's IDE Master Graduation Project. This document can also include the involvement of an external organisation, however, it does not cover any legal employment relationship that the student and the client (might) agree upon. Next to that, this document facilitates the required procedural checks. In this document:

- The student defines the team, what he/she is going to do/deliver and how that will come about.
- SSC E&SA (Shared Service Center, Education & Student Affairs) reports on the student's registration and study progress.
- IDE's Board of Examiners confirms if the student is allowed to start the Graduation Project.

USE ADOBE ACROBAT READER TO OPEN, EDIT AND SAVE THIS DOCUMENT
Download again and reopen in case you tried other software, such as Preview (Mac) or a webbrowser

STUDENT DATA & MASTER PROGRAMME

Save this form according the format "IDE Master Graduation Project Brief_familyname_firstname_studentnumber_dd-mm-yyyy".
Complete all blue fields and upload the approved Project Brief in your Graduation Report as Appendix 1 !

family name
initials
student numb
street & n
zipcode & ci
country
phone
email k

Your master programme (only select the options that apply to you):

IDE master(s): ★ IPD ( ) DfI ( ) SPD
2nd non-IDE master: Mechanical Engineering
individual programme: - - (give date of approval)
honours programme: ( ) Honours Programme Master
specialisation / annotation: ( ) Medisign
( ) Tech. in Sustainable Design
( ) Entrepeneurship

SUPERVISORY TEAM **

Fill in the required data for the supervisory team members. Please check the instructions on the right !

** chair Kaspar Jansen dept. / section: IDE Emerging Materials

** mentor Regine Vroom dept. / section: 3ME - PME

2nd mentor Freek Broeren

organisation: 3ME - PME

city: country:

Chair should request the IDE Board of Examiners for approval of a non-IDE mentor, including a motivation letter and c.v..

Second mentor only applies in case the assignment is hosted by an external organisation.

comments (optional): There is a second mentor involved as the project is a double degree project and the supervisory team needs to fulfill the requirements of both masters.

Ensure a heterogeneous team. In case you wish to include two team members from the same section, please explain why.

Procedural Checks - IDE Master Graduation

TU Delft

APPROVAL PROJECT BRIEF

To be filled in by the chair of the supervisory team.

chair Kaspar Jansen date 18 - 3 - 2020 signature

CHECK STUDY PROGRESS

To be filled in by the SSC E&SA (Shared Service Center, Education & Student Affairs), after approval of the project brief by the Chair.
The study progress will be checked for a 2nd time just before the green light meeting.

Master electives no. of EC accumulated in total: _____ EC

Of which, taking the conditional requirements into account, can be part of the exam programme _____ EC

List of electives obtained before the third semester without approval of the BoE

YES all 1st year master courses passed

NO missing 1st year master courses are:

name _____ date - - signature _____

FORMAL APPROVAL GRADUATION PROJECT

To be filled in by the Board of Examiners of IDE TU Delft. Please check the supervisory team and study the parts of the brief marked **.
Next, please assess, (dis)approve and sign this Project Brief, by using the criteria below.

- Does the project fit within the (MSc)-programme of the student (taking into account, if described, the activities done next to the obligatory MSc specific courses)?
- Is the level of the project challenging enough for a MSc IDE graduating student?
- Is the project expected to be doable within 100 working days/20 weeks ?
- Does the composition of the supervisory team comply with the regulations and fit the assignment ?

Content: ✓ APPROVED ○ NOT APPROVED

Procedure: ✓ APPROVED ○ NOT APPROVED

second version approved

comments

name Monique von Morgen date 30-3-2020 signature MvM

Initials & Name K. M. L. Koudstaal Student number 4289234

Title of Project Design of 2D Material for Local Deformation in Out-Of-Plane Direction

Personal Project Brief - IDE Master Graduation

TU Delft

Design of 2D Material for Local Deformation in Out-Of-Plane Direction

project title

Please state the title of your graduation project (above) and the start date and end date (below). Keep the title compact and simple. Do not use abbreviations. The remainder of this document allows you to define and clarify your graduation project.

start date 25 - 05 - 2020

08 - 02 - 2021 end date

INTRODUCTION **

Please describe, the context of your project, and address the main stakeholders (interests) within this context in a concise yet complete manner. Who are involved, what do they value and how do they currently operate within the given context? What are the main opportunities and limitations you are currently aware of (cultural- and social norms, resources (time, money,...), technology, ...).

"Mechanical metamaterials are artificial structures with mechanical properties defined by their structure rather than their composition." (Mechanical metamaterial, n.d.) 3D printing makes it possible to produce complex structures in a cheap way. It has been proven mathematically that any stiffness can be designed. However, we still do not have a methodology to do so. This is what Freek Broeren is interested in. Kaspar Jansen is interested in emerging materials and their integration in design. An assignment has been formed of which the goal is to create a 2D material that can morph around any object upon an actuation force or upon an actuation temperature, see Figure 1.

An example application could be a cup holder inside of a car, see Figure 2. The cupholder would be a flat surface, but once a cup is placed upon it, it can morph around the cup. This could have aesthetical benefits. In addition, no dirt will gather inside of the holder, because the holder is a flat surface that can easily be cleaned when not in use. Also, the holder will always form perfectly around the cup, which will eliminate the risk of tilting of the cup.

Mechanical metamaterial. (n.d.). In Wikipedia. Retrieved January 12, 2020, from https://en.wikipedia.org/wiki/Mechanical_metamaterial

space available for images / figures on next page

introduction (continued): space for images

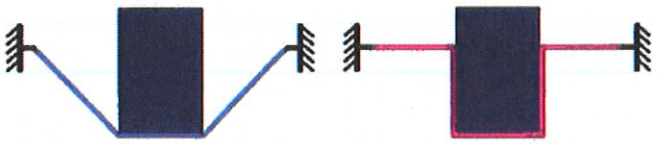

image / figure 1: left: generic material with "global" deformation, right: new material with "local" deformation

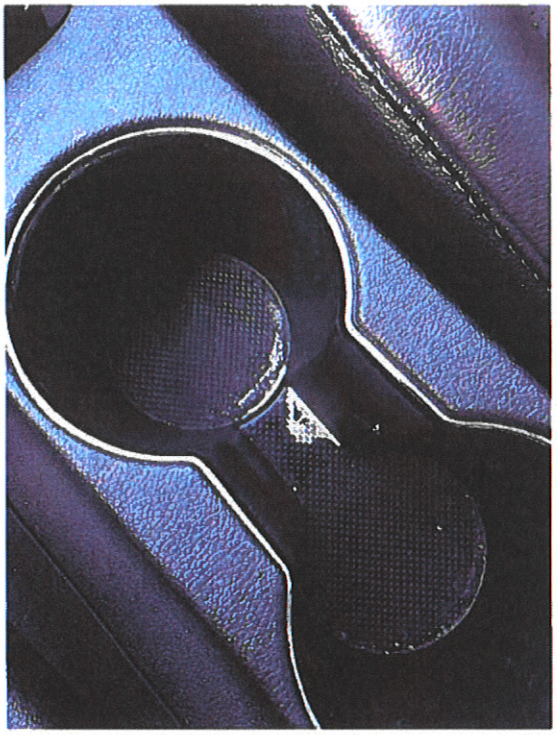

image / figure 2: https://www.yelp.com/biz_photos/car-wash-palace-orlando-2?select=1SsnrlSolZR_x6jEhum0gA

PROBLEM DEFINITION **

Limit and define the scope and solution space of your project to one that is manageable within one Master Graduation Project of 30 EC (= 20 full time weeks or 100 working days) and clearly indicate what issue(s) should be addressed in this project.

In the introduction, several problems were stated, such as dirt gathering inside of the cupholder. The proposed solution is the morphing material, which might also be useful for other applications. During the graduation project, the focus will be on the technical problem. Elastic materials that are spanned would not curve locally around an object that exerts a force upon it. These materials would bend globally. The goal of the project is to design a metamaterial that can do so, as it is expected that such a material can be useful for various applications and will enable new design opportunities. Throughout the project, the cupholder will be used as an example and focus application. The design decisions will be based on this specific application, but other applications will be explored as well.

ASSIGNMENT **

State in 2 or 3 sentences what you are going to research, design, create and / or generate, that will solve (part of) the issue(s) pointed out in "problem definition". Then illustrate this assignment by indicating what kind of solution you expect and / or aim to deliver, for instance: a product, a product-service combination, a strategy illustrated through product or product-service combination ideas, ... In case of a Specialisation and/or Annotation, make sure the assignment reflects this/these.

First, I will do a literature research (before the graduation project). Second, I will design a material and print the new material to examine it on the proposed functionality. I will design, print and test iteratively. In the end I expect to have a working prototype to demonstrate the functionality with a cup.
In addition, I will brainstorm about more applications.

The project will consist of four iteration cycles. The result of each cycle will be a material prototype. The fourth prototype will be a demonstrator.

An idea is to design a network of small springs made of shape memory alloys, which can either extend or contract, upon which the flat surface can morph out of plane. To be able to predict, based on the design of the network, how the surface will morph out of plane, is an interesting part for the ME component of the project. How to design the material as such that it can deform locally out of plane is interesting for the IPD component of the project as this is specifically related to the application of the cupholder.

Initials & Name K. M. L. Koudstaal Student number 4289234

Title of Project Design of 2D Material for Local Deformation in Out-Of-Plane Direction

PLANNING AND APPROACH **

Include a Gantt Chart (replace the example below - more examples c… 2) that shows the different phases of your project, deliverables you have in mind, meetings, and how you… te that all activities should fit within the given net time of 30 EC = 20 full time weeks or 100 wor… le a kick-off meeting, mid-term meeting, green light meeting and graduation ceremony. I… ining your approach, and please indicate periods of part-time activities and/or p… ct, if any, for instance because of holidays or parallel activities.

start date 25 - 5 - 2020 — 2021 end date

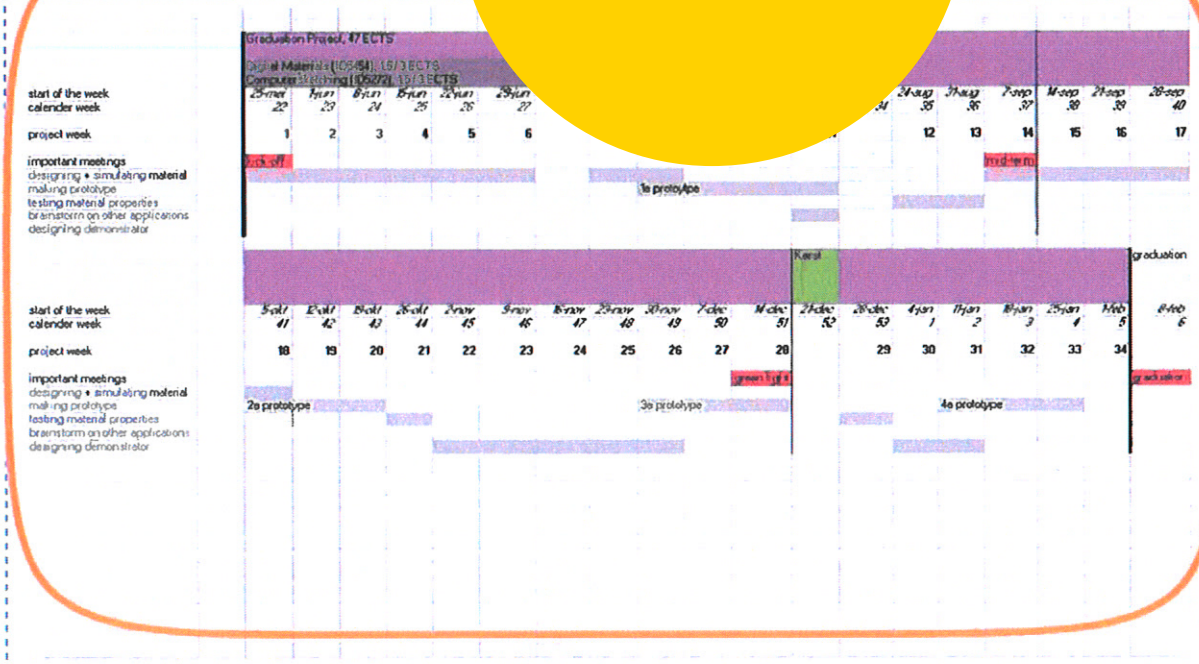

The graduation project is a combined graduation project, combining Mechanical Engineering and Integrated Product Design. In the Double Degree agreement, signed by Jana Stantcheva, it is stated that the graduation project should comprise 47 ECTS, which is about 32 weeks. Including 3 ECTS of electives, this becomes 34 weeks.

(Additionally, a literature study of 10 ECTS precedes the graduation project.)

Although a lot of aspects actually fit both and integrate IPD and ME, a distinction is made for clarity:
more Mechanical Engineering (blue in planning):
- designing + simulating material (designing predictable material = more ME)
- testing material properties

more Integrated Product Design (green in planning):
- designing + simulating material (designing for application = more IPD)
- making prototype
- brainstorm on other applications
- designing demonstrator

The iteration cycles (design, make, test) become shorter, as the adjustments become smaller. The fourth prototype is a demonstrator. There are two shades of grey in the planning: the focus in each time period is on the aspect with the darker shade.

Initials & Name K. M. L. Koudstaal Student number 4289234

Title of Project Design of 2D Material for Local Deformation in Out-Of-Plane Direction

MOTIVATION AND PERSONAL AMBITIONS

Explain why you set up this project, what competences you want to prove and learn. For example: acquired competences from your MSc programme, the elective semester, extra-curricular activities (etc.) and point out the competences you have yet developed. Optionally, describe which personal learning ambitions you explicitly want to address in this project, on top of the learning objectives of the Graduation Project, such as: in depth knowledge a on specific subject, broadening your competences or experimenting with a specific tool and/or methodology, ... Stick to no more than five ambitions.

I am interested in mechanical metamaterials, because of its relevance to the design profession and because of its mechanical challenges. In addition, I believe it to be a suitable application to integrate my background knowledge (compliant mechanisms, finite element method, optimization, modelling).

Also, I would like to become more acquainted with 3D printing through hands-on experience.

FINAL COMMENTS

In case your project brief needs final comments, please add any information you think is relevant.

The project is meant to graduate for a Double Degree.

Initials & Name K. M. L. Koudstaal Student number 4289234

Title of Project Design of 2D Material for Local Deformation in Out-Of-Plane Direction

Appendix XI – Literature Report

The Literature Report starts on the next page.

Shape-shifting shape memory alloy spring network

Literature Study Report

How can a shape memory alloy spring network be designed such that it is capable of deforming from a flat configuration in 2D into a couble curved configuration in 3D?

Kim Koudstaal (4289234)
coaches: Freek Broeren, Kaspar Jansen and Regine Vroom

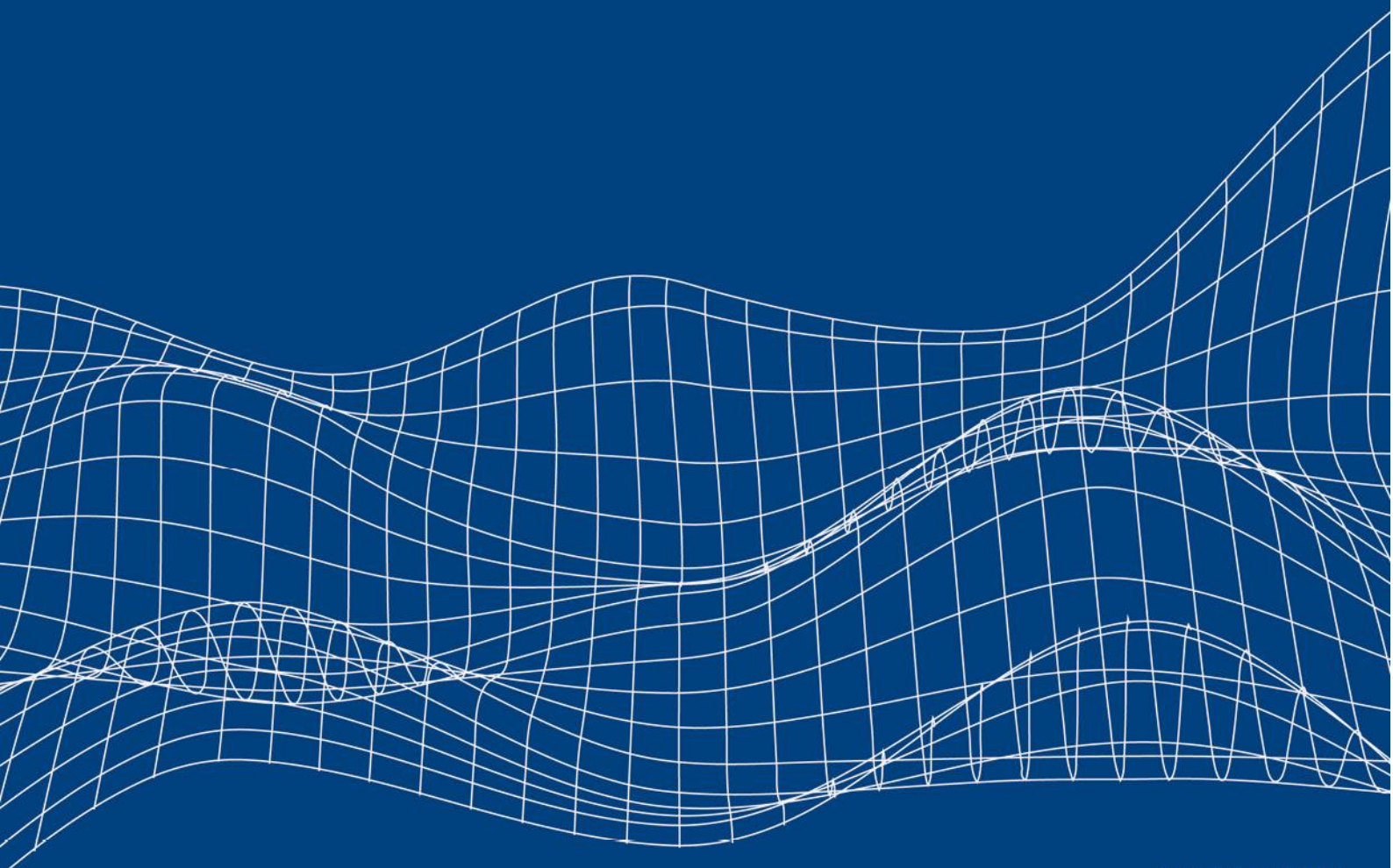

25-06-2020

Contents

1. Introduction

1.1 Why shape-shifting?

The interest in shape-shifting materials has increased over the past years (Dunbar, 2018). A part of this field concerns the shape-shifting of sheets that can morph from a flat configuration in 2D into a curved configuration in 3D. The shape-shifting technology can be used in various fields, on different length scales. Some example applications are discussed below.

Assembly

The shape-shifting technique can be used to let a product obtain its final shape. This could be useful to make 3D microstructures based on 2D microfabrication techniques. An example of this is shown in Fig. 1a (Gracias, 2002). The patterned surface causes the sheet to fold into a cube upon heating.

Using shape-shifting techniques for assembly could also be useful at larger scale. Creating complex shapes from single sheets could reduce the number of parts. Connecting fewer parts results in smoother surfaces, which would be a benefit in for example aviation, see Fig. 1b (Guseinov, 2020). In addition, assembly through activation could enable assembly at site. The initially flat sheets can be packaged, transported and stored efficiently, and can be activated where needed.

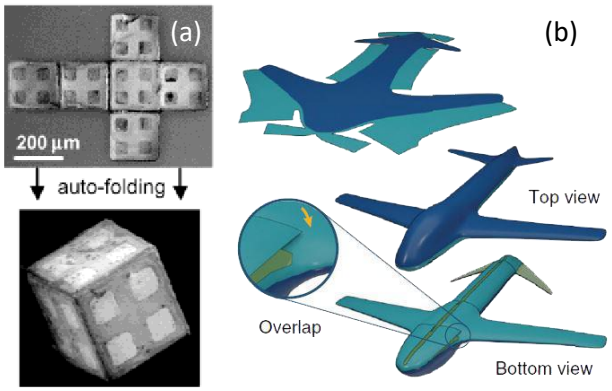

Figure 1. (a) A via 2D microfabrication patterned sheet folds into a cube upon heating (Gracias, 2002). (b) An idea to make a drone of a shape-morphing sheet for improved aerodynamics (Guseinov, 2020).

Function

Additionally, the shape-shifting properties could be a function of the product during its lifetime, meaning that the curvature can change over time. Several applications in which the shape-shifting technique is dynamically used at smaller scale are optical devices, sensors, biomaterials, smart surfaces and soft robotics (Ceron, 2018; Palleau, 2013). Regarding optics, controlling the curvature of sheets is for example used to create tunable mirrors (Liu, 2003), see Fig. 2a.

At larger scale, out-of-plane deformations are researched as a means to make digital information tangible (Hemmert, 2010; Wang, 2012). It is believed that this kind of feedback could help in remote collaboration, as the curving of a surface could also be used to touch and manipulate objects at a distance. In addition, the technology could be a ground for smart environments, in which a surface adapts to the human physically. For example, the surface of a table could tilt your tablet towards you or hold your pens (Follmer, 2013, 2015).

At even larger scale, shape-shifting sheets could be used in adaptable architecture as opposed to in general static architecture (Baseta et al., 2014). An example an application in this field is a “breathing façade”, in which a 2D initially closed structure opens up when it is moved out of plane by the wind. Dynamic shape-shifting can again also be used in aviation, e.g. flexible wings that alter their shape for the most efficient flight have been designed (NASA, 2019).

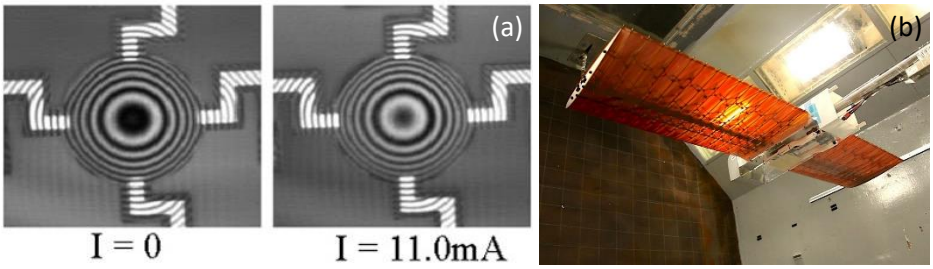

Figure 2. (a) The optical device is heated through resistive heating. The temperature relates to the expansion and therewith to the amount of curvature (Liu, 2003). (b) Adaptable wing for efficient flight (NASA, 2019).

1.2 Research goal

The goal of this project is to design a 2D network that can deform out-of-plane. The out-of-plane deformation of shape-shifting materials is limited by the maximum material stretch. An important advantage of shape memory alloys (SMA) springs, is that they deform substantially upon heating. (What SMA springs are exactly is discussed in the second chapter.)

The goal of this literature research is to gather information that is necessary to be able to design a shape-shifting sheet consisting of a SMA spring network. So, the main question of this literature research is: *How can a SMA spring network be designed such that it is capable of deforming from a flat configuration in 2D into a double curved configuration in 3D?* Throughout the report, the topic will shift from the material level to the network level. The following sub questions are discussed.

- *What are the important characteristics of an SMA spring?*
- *What mechanisms can be used for a transformation from flat to double curved?*
- *What lattices can be used and how can the ribs be connected?*
- *How can the required shape be translated to a sheet design?*

2. Shape Memory Alloy springs

Smart materials are materials that can change one or more of their properties substantially upon a certain stimulus. A shape memory alloy is an example of a smart material. Shape memory alloys can undergo large deformations that can be recovered from upon heating or stress reduction.

2.1 Shape Memory Alloy – material level

2.1.3 How does it work?

Discovery

The shape memory effect had been observed a few times throughout the 20th century in different alloys. A breakthrough in the field was the observation of the effect in a NiTi alloy (Buehler et al., 1963). The NiTi alloy was much more usable (safer, less expensive and better deformation-to-recovery ratio) than the materials that had been found before (Gilbertson, 1993).

Shape memory effect

A material deforms plastically if you exceed it yield strength. Plastic deformation is unrecoverable. However, in shape memory alloys (SMA), another type of nonelastic deformation exists. This type of deformation seems plastic, but is actually recoverable. Say, you have a SMA stick and you bend it "plastically". If you then heat it above its transition temperature, it will deform back to its original shape, see Fig. 3. The transition temperature is a characteristic for any type of SMA and lies between 100 °C and 100 °C, depending on the exact composition of the SMA (Stoekel, 1989).

A shape can be programmed into the material by heating the material in the desired shape above the annealing temperature, which is typically around 500 °C. Note that if you want to program a shape, you have to constrain it before you put it in the oven, as the transition temperature is lower than the annealing temperature. If you do not constrain it, the material will deform back to its original shape.

The difference between the two types of nonelastic deformations lies in the difference between the mechanisms on atomic level. Plastic deformation is caused by slipping of atoms. The recoverable deformation in shape memory alloys is caused by rearrangement of atoms without breaking connections between atoms. Initially, the atoms are packed tightly due to which there is room for substantial deformation without slipping. The atom arrangements are visualized in Fig. 3. At high temperature, the material is in the austenite phase. After cooling, the shape is still the same, but the material is in the twinned martensite phase. After applying a mechanical load to deform the shape, the material is in the detwinned martensite phase. Through heating the material, the original shape that is stored in the austenite phase can be retrieved (Chopra, 2002).

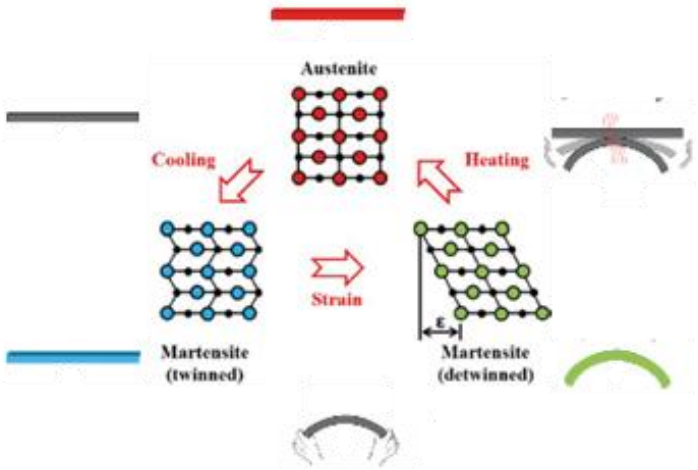

Figure 3. The three phases of an SMA material on a microscopic and a macroscopic level (Mettler & Toledo, n.d.; Barbarino, 2014, combined)

The temperature at which the transition from austenite to martensite happens is slightly different from the temperature at which the transition from martensite to austenite happens; there is hysteresis, see Fig. 4. The characteristic transformation temperatures are given from low temperature to high temperature: M_f is the martensite finish temperature, M_s is the martensite start temperature, A_s is the austenite start temperature and A_f is the austenite finish temperature. The transformation temperatures are affected by the mechanical load on the material; if there is a mechanical load, these transformation temperatures are slightly higher (Barbarino, 2014).

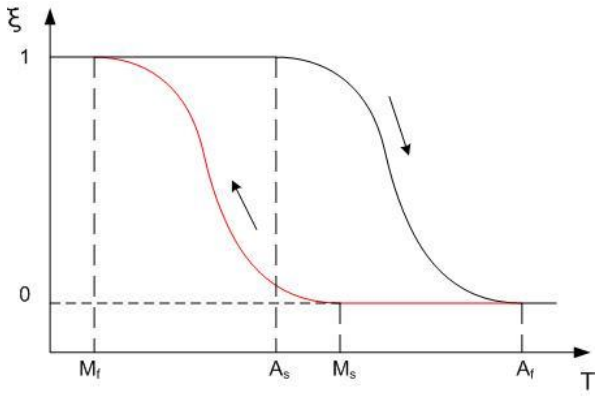

Figure 4. The heating and cooling under constant force (ζ=martensitic fraction, T=temperature) (Wikimedia Commons, 2006).

Like said, the transformation temperatures depend on the exact NiTi composition. In addition, contaminations of iron or oxygen can affect the transformation temperatures (Gilbertson, 1993), and adding Cu to the NiTi alloy decreases the A_s and the A_f substantially (Dilibal, 2013).

Pseudo-elasticity

Besides the shape memory effect, another effect which is called pseudo-elasticity (sometimes also called super-elasticity) exists. Pseudo-elasticity can be observed when the material is loaded while the temperature of the material is above the austenite finish temperature A_f. If you apply a load on the material above A_f, the atoms arrange according to the detwinned martensite phase. If you now take away the load (while the material is still heated above A_f), the material directly deforms back to its original shape (Barbarino, 2014). Both the shape memory effect and the super-elasticity are

visualized in Fig. 5. Fig. 5 shows the two extremes, whereas Fig. 6 shows what happens if you load not completely in austenite or martensite phase, but somewhere in between.

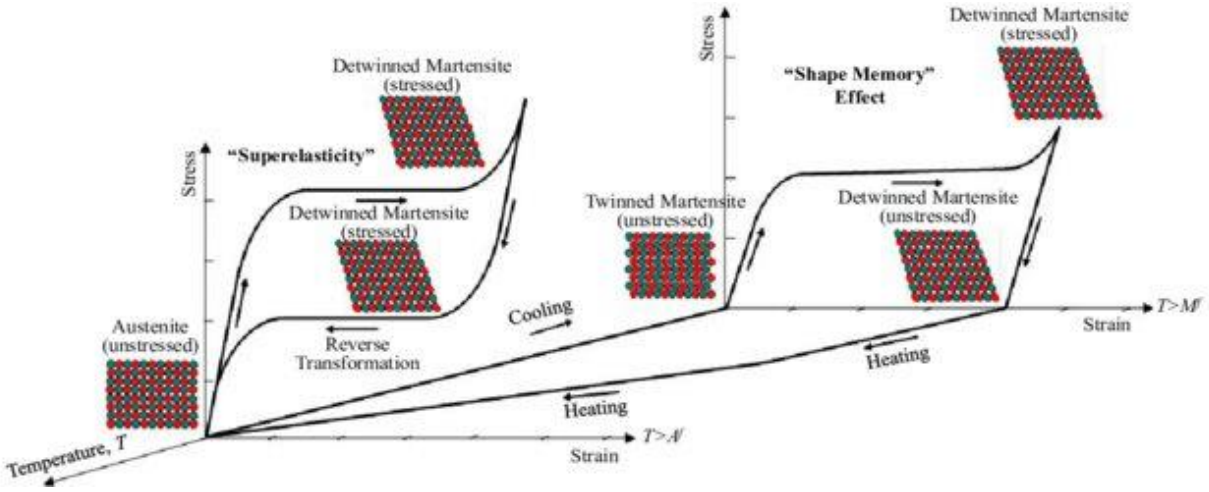

Figure 5. The loading cycles for both the shape memory effect and the super-elasticity (Seo et al., 2015).

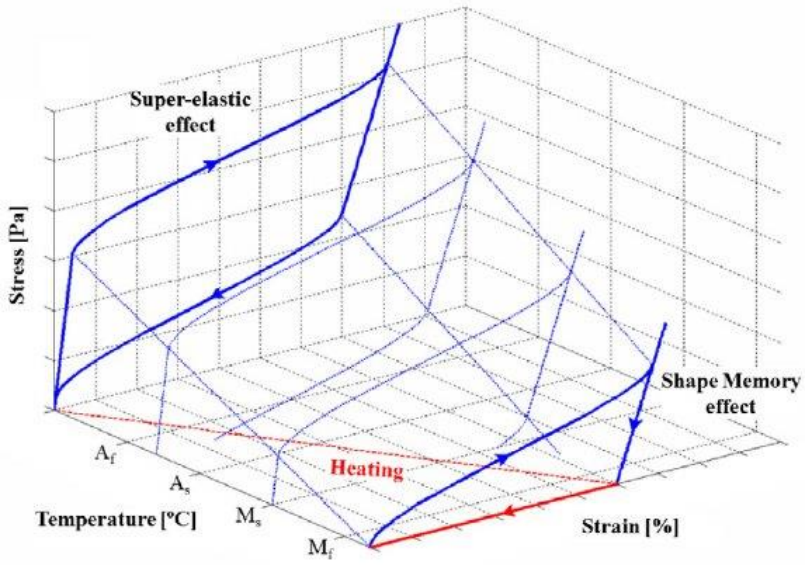

Figure 6. The loading cycles in between the shape memory effect and the super-elasticity (Barbarino, 2014).

One-way vs. two-way

The effects discussed above are one-way shape memory effects. In a one-way shape memory effect, the deformation has to be imposed by applying a load on the material and the original shape can be retrieved by heating the material. In a two-way shape memory effect, two different shapes can be stored at two different temperatures, so the material can be deformed back and forth by heating and cooling. The two-way shape memory effect is typically trained into materials with lower mechanical properties. The recovery force of two-way SMAs, which is the force they can exert upon heating, is lower than that of one-way SMAs, which makes them less suited for actuators (Barbarino, 2014). Another downside of two-way SMAs is that the training of a two-way SMA makes it a bit more labor-intensive to fabricate a two-way SMA compared to a one-way SMA.

2.1.3 Mechanical properties

The mechanical properties depend on the exact composition, but also on the annealing temperature (Kim, 2009). Here, some typical values for nitinol (Nickel Titanium Naval Ordnance Laboratory), which is an alloy of which the atomic distribution is 50:50, are given just to have an idea of the properties.

The elastic modulus is around 28 GPa in the martensitic phase, and around 75 GPa in the austenitic phase. The maximum recovery strain is 8%, but it is recommended to only use 3-5% of this for a maximum wire lifetime. The maximum recovery force is around 600 MPa (Gilbertson, 1993).

A final note on the properties is that it might be better to use as-drawn nitinol wires rather than off-the-shelf Flexinol wires. Flexinol actuator wires, or Muscle Wires is a trade name for NiTi SMA wires from Dynalloy, which is a big manufacturer in this field. The nitinol wires are not only much cheaper, but also have a larger deflection for a given force and spring geometry, and allow for a greater influence on the force-deflection characteristics of the springs by choosing the annealing temperature (Kim, 2009).

2.2 Shape Memory Alloy – geometry level (coil springs)

2.2.1 Why SMA coil springs?

For the described application, it is useful if the SMA can deform substantially. To increase the effective deformation length, SMA can be used in the form of coiled springs. (Waram, 1993). In Fig. 7 this effect is visualized. Both wire and coil have a free length of 30 mm. A material strain of 1% results in a stroke of 0.3 mm for the wire, whereas it results in a stroke of 60.3 mm for the coil. The formula that is used to calculate the deflection of the coil spring based on the strain is

$$\delta = \frac{\pi \gamma D^2 n}{d} \qquad \textit{Eq. 1}$$

in which γ is the strain, D^2 the outside coil diameter, n the wire turns and d the wire diameter. Note that this equation is purely geometrical and it does not take into account stresses. It is just to show the effect of using coil springs instead of straight wires.

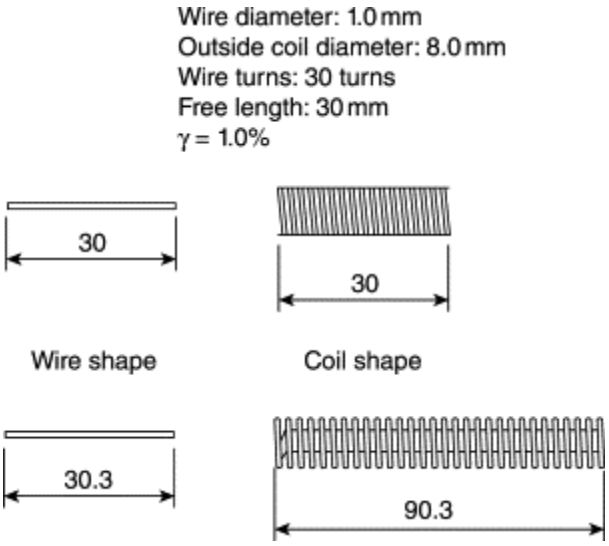

Figure 7. Comparison of strokes of SMAs between wire shape and coil shape (Ishii, 2011).

2.2.2 Design parameters

For the design of a SMA wire, two geometrical parameters need to be selected: the wire diameter determined by the needed force and the wire length determined by the needed deflection. For the design of a SMA spring, four parameters need to be determined, namely the wire diameter d, the spring diameter D, the number of active coils n and the pitch angle α. These determine the force-deflection curves of the austenitic and the martensitic phases of the material (An et al., 2012). The material properties, such as the shear modulus at austenite G_A, the shear modulus at martensite G_M, the maximum residual strain γ_L, the critical strain at the start γ_s^{cr} and at the finish γ_f^{cr} of the

detwinning influence the curves as well, but these are material parameters that are generally fixed. A design framework for the design process of an SMA coil spring is given in Fig. 8 (An et al., 2012). For more detailed information, for example about the equations that are referred to in the framework, the reader is referred to *An et al., 2012*. The framework is given here just to have an idea of the flow of the design process.

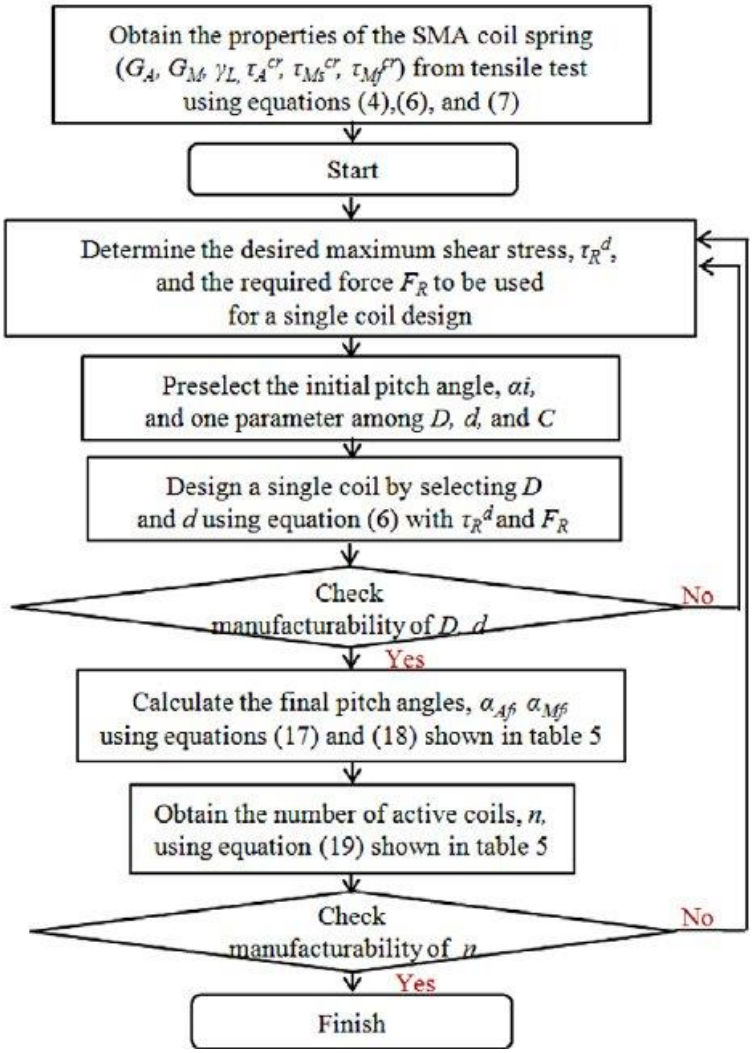

Figure 8. Design framework for SMA coil springs (An et al., 2012).

2.2.3 Fabrication

Off-the shelve springs are relatively expensive and offer a limited variation in springs (and it is even more expensive if one wants to order tailor made springs), so it is chosen to self-fabricate them. By making the springs ourselves, we can vary the spring parameters exactly as we want to. The winding, baking and training are discussed here.

Winding

A method to program an SMA wire into an SMA spring is displayed in Fig. 9. The wire is wound around a standard M1 bolt, of 1 mm in diameter and 0.25 mm in pitch (Kim et al., 2005). A drawback

of this method is that it makes use of a bolt, due to which it is difficult to adjust the pitch. If a smooth core guide is used, the pitch can easily be adjusted by stretching the NiTi wire over the core.

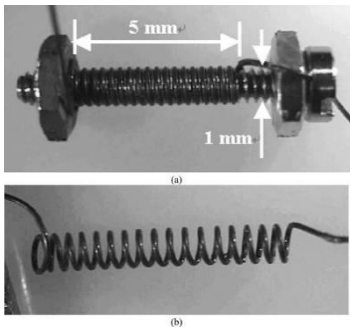

Figure 9. Fabrication of an SMA spring. Constrained SMA wire on a mandrel (above). SMA spring after "shape setting" heat treatment (below) (Kim et al., 2005).

A similar, yet slightly different method is visualized in Fig. 10. Instead of winding the wire around a bolt, the wire is wound around a smooth steel core by rotating the block.

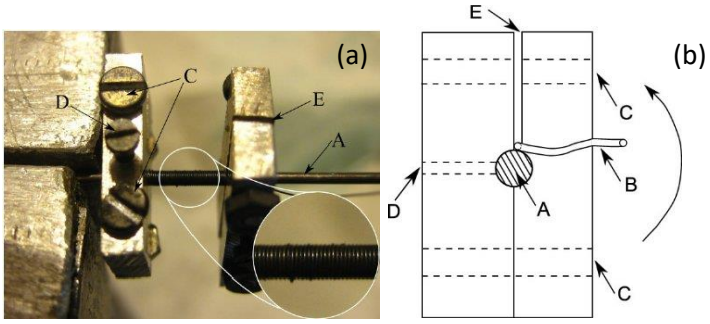

Figure 10. (a) Fabrication method of the SMA springs. The wire is wound around a steel bar and fixed by two aluminum elements. Refer to figure 10b for the meaning of the letters (Follador et al., 2012). (b) Aluminum device for winding the SMA wire around the steel core. A-steel core; B-SMA wire; C-holes for screw and nuts for fixing the two halves of the block; D-threaded hole for fixing the aluminum block on the steel bar; E-slot for the SMA wire (Follador et al., 2012).

A third method is shown in Fig. 11. Here, the winding is automated with the help of a drill press. The NiTi wire is guided by the metal tube coil guide. The core wire is kept under tension with a mass. This method is especially useful to make springs with a small spring diameter. After the winding, the end of the NiTi wire is fixated to the core wire and undergoes a heat treatment. A variation on this method has been effectively used as well (Holschuh et al., 2014).

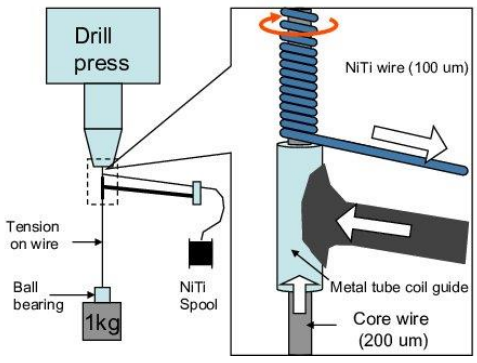

Figure 11. A simple manufacturing setup enables long strand coiled springs of NiTi muscle fiber. The core wire is under tension and NiTi is wound around the core. The guidance tube is slightly larger than core wire. The tension of NiTi is maintained by friction between the NiTi and the long bar (Kim et al., 2009).

Baking

After the NiTi wire is wound and fixated, it is baked to store the shape in the material. A typical annealing temperature is around 400 – 500 °C. The specific temperature affects the force-deflection curve. The lower the annealing temperature, the stiffer the spring, see Fig. 12 (Kim et al., 2009).

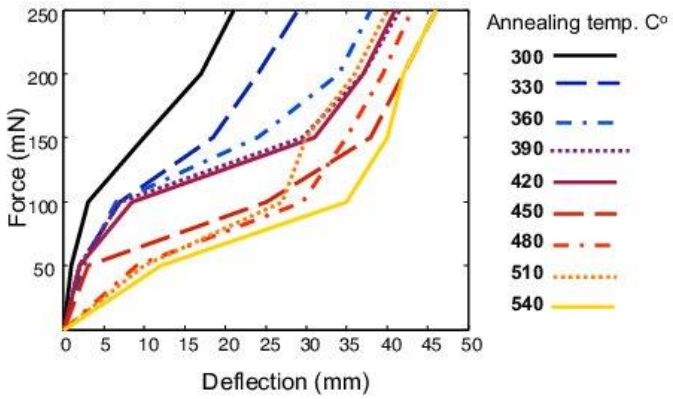

Figure 12. The effect of the annealing temperature on the stiffness of the spring (Kim et al., 2009)

Training

If the above steps are finished, the material can exhibit a one-way shape memory effect. (The difference between a one-way shape-memory effect and a two-way shape memory effect is described in the previous chapter.) If one wants to obtain a two-way shape memory effect (despite the inevitable sacrifice on the mechanical properties), training is needed. Various methods exist to program a two-way shape memory effect. A possible method is to deform the material below the martensite finish temperature M_f, constrain it, and then heat it above the austenite finish temperature A_f (not to be confused with the annealing temperature). The constrained material is then heated and cooled a couple of times (Zanaboni, 2008). The repetition of the steps is called the training of the two-way SMA. As said before, the performance of two-way SMA actuators is typically lower than the performance of one-way SMA actuators (Barbarino, 2014).

2.2.4 Spring model

It is useful to have an accurate model of the force-deflection curve based on the geometry of the SMA spring, because we want to be able to predict the behavior of the springs.

Conventional springs are designed to operate in their linear elastic region. SMA springs are designed to operate in their non-linear region as well. The detwinning of the SMA material drastically increases the recoverable deformation. However, the non-linear behavior makes it a bit more difficult to model the force-deflection curve. Here, two models are proposed and discussed.

Simple Static Two-State SMA Coil Spring Model

The displacement of an SMA spring is affected not only by the general spring effect, but also by the phase rearrangement of the molecules that occurs during a phase change (Kim et al., 2009). In addition, the phase change also influences the spring effect, as the spring constant in the austenite phase is around 2-3 times larger than in the austenite phase (Otsuka & Wayman, 1999). In the model discussed here, the general spring equation is modified. The spring deflection due to detwinning and the difference in shear modulus for the different phases are taken into account.

The possible spring displacements are visualized in Fig. 13 (Kim et al., 2009). A force is applied in the austenite phase, and the spring displacement is δ_H. If the force is then removed, the spring deforms back to its original length x_{A0} with zero residual displacement. However, if the same force is applied and removed at M_f, the spring deforms back to a length x_{M0} with a residual displacement δ_M.

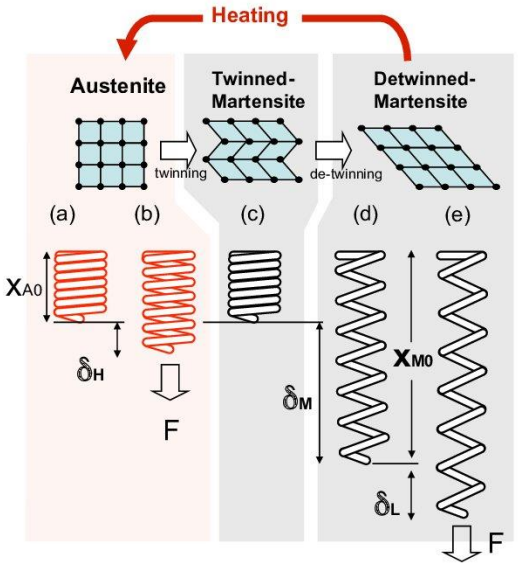

Figure 13. Five representative states of NiTi spring actuator. (a)full austenite without load, (b)-full austenite with load, (c)twinned martensite without load, (d)-fully detwinned martensite without load, (e)-fully detwinned martensite with load (Kim et al., 2009).

The spring deflection in the martensitic phase is

$$\delta_{martensite} = \delta_M + \delta_L$$

in which δ_M is the change in free length of the spring if it changes from austenite to martensite and δ_L is the general coil spring deflection in the martensitic phase, so

$$\delta_{martensite} = \frac{\pi\gamma D^2 n}{dk} + \frac{8FD_{eff}^3 n}{G_M d^4} \qquad \textit{Eq. 2}$$

in which γ is the shear strain of the spring, D the spring diameter, n the number of coils, d the wire diameter, k Wahl's stress correction factor, F an axial force and G_M the shear modulus in the martensitic phase. D_{eff} is the effective spring diameter, which depends on the amount of deflection. The effective spring diameter can be calculated with

$$D_{eff} = D\cos\theta$$

in which θ is the angle between the spring wire and the horizontal plane.

The spring deflection in the austenitic phase is

$$\delta_{austenite} = \delta_H$$

in which δ_H is the general coil spring deflection in the austenitic phase, so

$$\delta_{austenite} = \frac{8FD^3 n}{G_A d^4} \qquad \textit{Eq. 3}$$

in which G_A is the shear modulus in the austenitic phase.

The effective displacement, also called the stroke, is the displacement that can be realized, assuming that a constant force is applied. The effective displacement is

$$\delta_{effective} = \delta_M + \delta_L - \delta_H = \delta_{martensite} - \delta_{austenite} \qquad \textit{Eq. 4}$$

In this model, the deformation upon detwinning is added as a constant, but the force-deflection curve *during* the detwinning cannot be described with this model.

Advanced Static Two-State SMA Coil Spring Model

In the more advanced model, the equations have been modified to take into account the non-linear geometric effect of the SMA coil spring for large deformations (An et al., 2012).

The deformation can be described in terms of the initial pitch angle and the final pitch angle:

$$\delta = \frac{\pi n D}{\cos \alpha_i} (\sin \alpha_f - \sin \alpha_i)$$

The spring force in the martensitic phase is

$$F_M = \frac{G_M d^4}{8D^3 n} \left(\frac{\cos^3 \alpha_i}{\cos^2 \alpha_f \left(\cos^2 \alpha_f + \frac{\sin^2 \alpha_f}{1+v}\right)} \right) \delta - \frac{\pi d^3}{8D} G_M \gamma_L \zeta_{S\tau} \qquad \textit{Eq. 5}$$

in which α_i is the initial pitch angle, α_f the final pitch angle, v the Poisson's ratio, γ_L the maximum residual strain (see Fig. 14) and $\zeta_{S\tau}$ the detwinned martensitic fraction. At low temperature ($T < M_s$), the detwinned martensitic fraction can be calculated with

$$\zeta_{S\tau} = \frac{1}{2} \cos \left[\frac{\pi}{\tau_{Ms}^{cr} - \tau_{Mf}^{cr}} \left(\tau - \tau_{Mf}^{cr} \right) \right] + \frac{1}{2}$$

in which τ_s^{cr} and τ_f^{cr} are the critical shear stresses and the start and finish of the detwinning phase (see Fig. 14), respectively. The shear stress can be calculated with

$$\tau = \frac{8DF}{\pi d^3} \qquad \textit{Eq. 6}$$

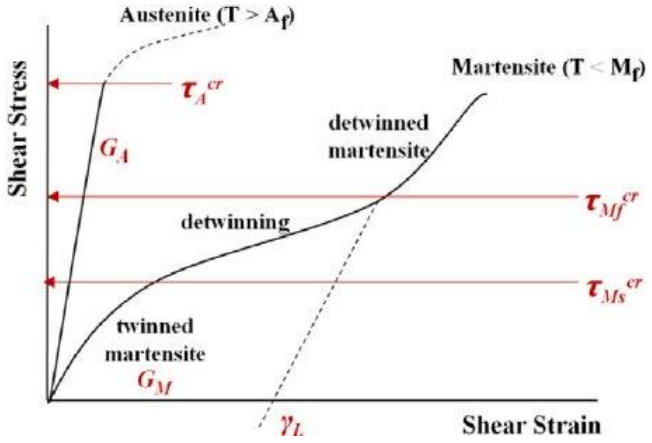

Figure 14. A clarification of the properties used in the formulas (An et al., 2012).

To calculate F_M with $\zeta_{S\tau}$, which depends on F itself, is a recursive problem, which brings along some computational difficulties. To make calculating F_M easier, the equation for the detwinned martensitic fraction can be rewritten in terms of shear strains rather than shear stresses (Koh, 2018). Typical values for γ_s^{cr} and γ_f^{cr} are 1% and 12% respectively.

$$\zeta_{S\tau} = \frac{1}{2}\cos[\frac{\pi}{\gamma_s^{cr} - \gamma_f^{cr}}(\gamma - \gamma_f^{cr})] + \frac{1}{2}$$

The spring force in the austenite phase is

$$F_A = \frac{G_A d^4}{8D^3 n}\left(\frac{\cos^3 \alpha_i}{\cos^2 \alpha_f \,(\cos^2 \alpha_f + \frac{\sin^2 \alpha_f}{1+v})}\right)\delta \qquad \textit{Eq. 7}$$

Matlab

The two models are put together in Matlab to see the differences in the force-deflection curves and to see what effect changing several spring parameters have on the force-deflection curves. The parameters that are used are put in the table below.

Table 1. Parameter values used in models

Geometry / Material parameter	**Value**
Geometry	
Number of coils n	12
Spring diameter D	5.0 mm
Wire diameter d	0.8 mm
Initial pitch angle α_i	0°
Material	
Shear modulus martensite G_M	4.7 GPa
Share modulus austenite G_A	11.26 GPa (Koh, 2018)
Poisson's ratio	0.33
Critical shear strain at start detwinning γ_s^{cr}	0.01 (Koh, 2018)
Critical shear strain at end detwinning γ_f^{cr}	0.12 (Koh, 2018)
Maximum residual strain γ_L	0.06 (Koh, 2018)

The plot containing the two models is shown in Fig. 15. As you can see, the detwinning in the martensitic phase is added as a constant in the simple model; the curve is shifted over the x-axis. This model could only be used for large spring deflections, after the detwinning phase. The advanced model takes into account the detwinning, so it can be used for any deflection. The austenite curves should be compared with real data to determine which one of the two fits the data best. For small deflections it does not matter whether the simple model or the advanced model is used.

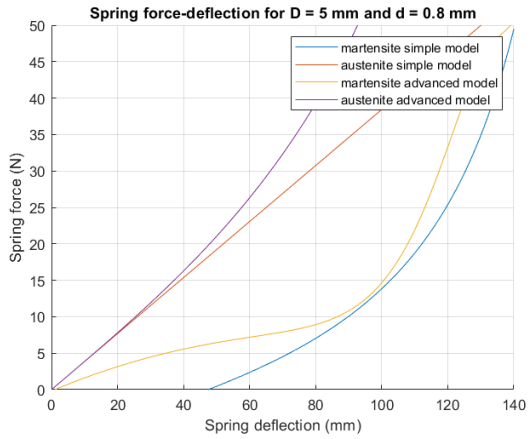

Figure 15. The force-deflection curves for the different phases and the different models. The used parameters can be found in Table 1.

By comparing the two plots below, you can see what happens if the spring diameter and the wire diameter are changed, but the ratio between them stays the same. As a larger spring can carry more load before plastic deformation, the detwinning phase also happens at a higher load.

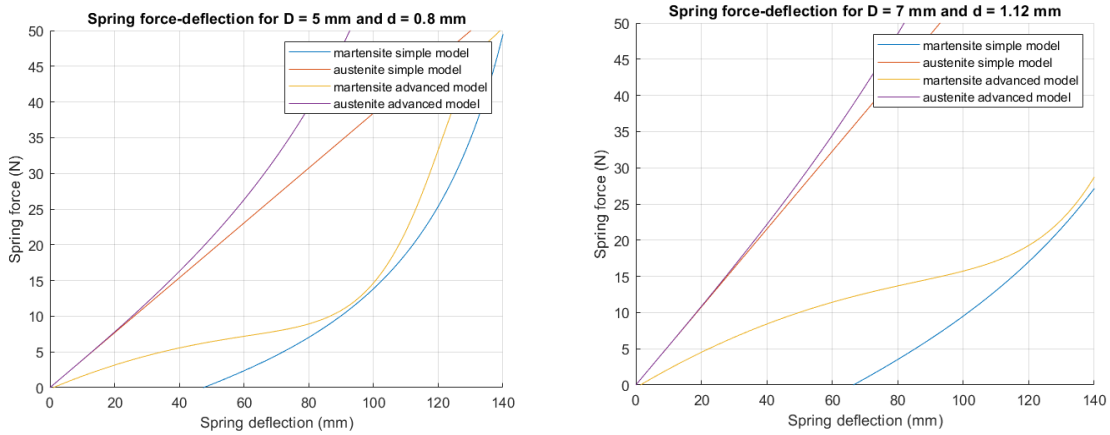

Figure 16. Force-deflection curves based on two models for different spring diameters and wire diameters, but same ratio

By comparing the two plots below, you can see what happens if the ratio is changed. As the ratio D/d, the spring index, decreases, the detwinning region is shortened, and occurs at a higher load. Also, the differences between the model become smaller.

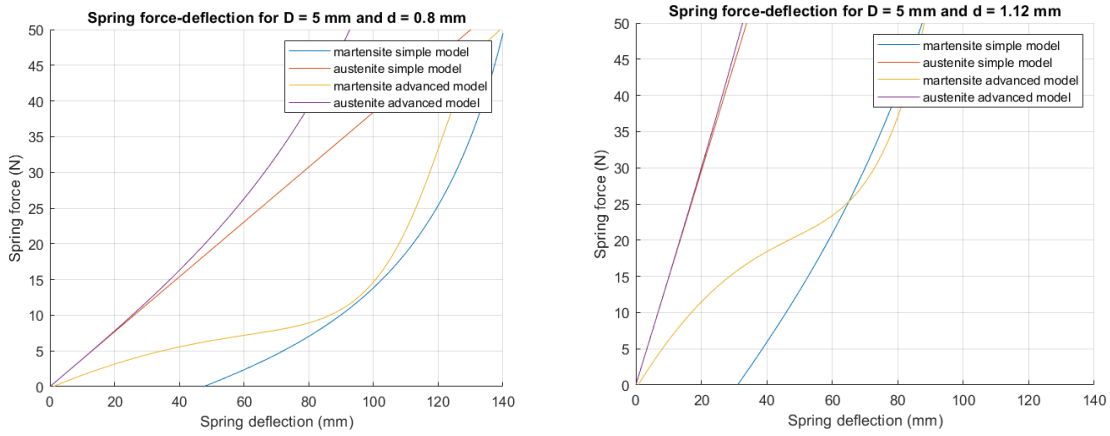

Figure 17. Force-deflection curves based on two models for different spring diameters and therewith different ratio

Stroke

SMA coil springs are used as actuators, typically in combination with a bias spring that brings it back to the unactuated shape, see Fig. 18 (Tai, 2010). The SMA coil spring is compressed when it is in the martensite phase. It pushes the bias spring when it is activated to the austenite phase. The stroke is influenced by the stiffness of the bias spring, see Fig. 19 (Ishii, 2011).

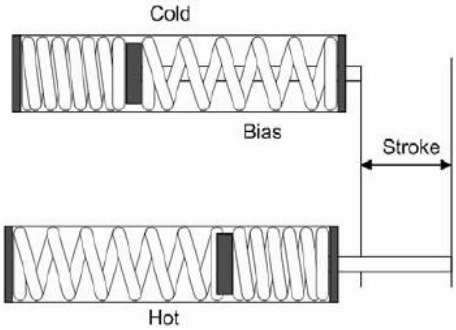

Figure 18. SMA coil springs (left) are typically used in combination with a bias spring (right) (Tai, 2010).

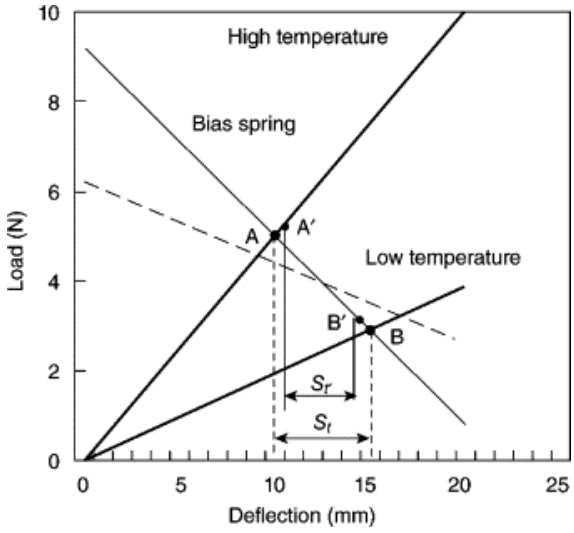

Figure 19. The stroke of the actuator is influenced by the stiffness of the bias spring (Ishi, 2011).

In order to increase the stroke, it would be best to strain the material as much as possible. However, if the strain is too high, the material could degrade, which would decrease the performance. A balance should be found. For cyclic loading, a maximum shear strain of 8% is recommended (Koh, 2018). The shear stress can be calculated from the axial force with Equation 6.

2.2.5 Activation

We distinguish two input types that can activate the SMA: external and control input. The difference is illustrated here with an example. Imagine that we want the SMA to deform when a hot cup of coffee is placed on it. The heat coming from the cup of coffee is an external input and it may be sufficient to achieve the desired deformation. If it is not sufficient, a control input (typically Joule heating) can be used to make up for the difference. Note that an external input can have many forms, such as a force or a sound.

The control input can also be used to accurately regulate the transition between the phases of the SMA material. This is the case for example if you want to create a cyclic motion. However, in our case, it is in the first instance only important that the material can shift from fully martensite to fully austenite upon heating. Therefore, it useful to know how we can heat it sufficiently without overheating, i.e. without reaching the annealing temperature at which the shape is programmed.

Heat source

Different types of energy can result in thermal energy that can be used to heat the SMA actuator. If we look at the heat transfer induced by temperature differences, the SMA actuator can be heated by means of convection, conduction and radiation. To heat it by means of convection, we could for example place it in a hot bath or use a hairdryer to heat it. To heat it by means of conduction, we could for example place a hot coffee cup upon it. If we just make sure that the heat source is not too high, overheating will not occur.

Joule heating

Another means to heat the SMA actuator is by means of Joule heating. In Joule heating, electrical energy is converted into thermal energy. In the case of Joule heating, it is trickier to not overheat the wire. How much energy can be converted per second can be calculated with

$$P = IV = I^2R = \frac{V^2}{R} \quad [W]$$

The resistivity of nitinol is about 100 $\mu\Omega \cdot \mathrm{cm}$ for austenite and about 80 $\mu\Omega \cdot \mathrm{cm}$ for martensite (Matthey, 2020). How much energy is needed to change the temperature of the wire can be calculated with

$$\Delta Q = cm\Delta T \quad [J]$$

If we neglect that the wire loses energy as well (which ensures that we are on the safe side), we can calculate the amount of time it takes to heat the wire with a certain temperature difference.

3. How can a flat sheet in 2D morph into a double curved sheet in 3D?

The goal of this chapter is to understand how a flat sheet can physically morph into a double curved sheet. First, some fundamental mathematical theory of differential geometry necessary for this is discussed (Gaussian curvature and Theorema Egrigium). Second, various mechanisms that realize the translation from flat sheet to double curved shape are discussed and categorized.

3.1 Gaussian curvature

Curved surfaces can be analyzed either extrinsically or intrinsically. In an *extrinsic* analysis the curvature of a surface is described based on the 3D coordinate system of the surrounding space in which the surface is located. In an intrinsic analysis the curvature of a surface is described based on the 2D coordinate system of the surface itself. An example that is used to explain the difference is that one could study the surface of the Earth either by walking over it (intrinsic analysis) or by looking at it from outer space (extrinsic analysis).

The *mean curvature* is an extrinsic measure of the curvature at a point on a surface. The mean curvature is the average of the principle curvatures:

$$H = \frac{1}{2}(k_1 + k_2)$$

The *Gaussian curvature* is a commonly used intrinsic measure of curvature at a point on a surface. The Gaussian curvature is the product of the principle curvatures:

$$K = k_1 \cdot k_2$$

The principle curvatures, see Fig. X, are the minimum and the maximum normal curvatures. The related directions are the principle directions (see X_1 and X_2 in Fig. 20). If the normal curvatures are equal, the point is called a *umbilical point*. The only two types of surfaces that consist solely of umbilical points are a flat surface and a sphere. Even though the principle curvatures are extrinsic measures, the Gaussian curvature can also be calculated based on the distances and the angles between points on a surface, and is therefore an intrinsic measure of the surface.

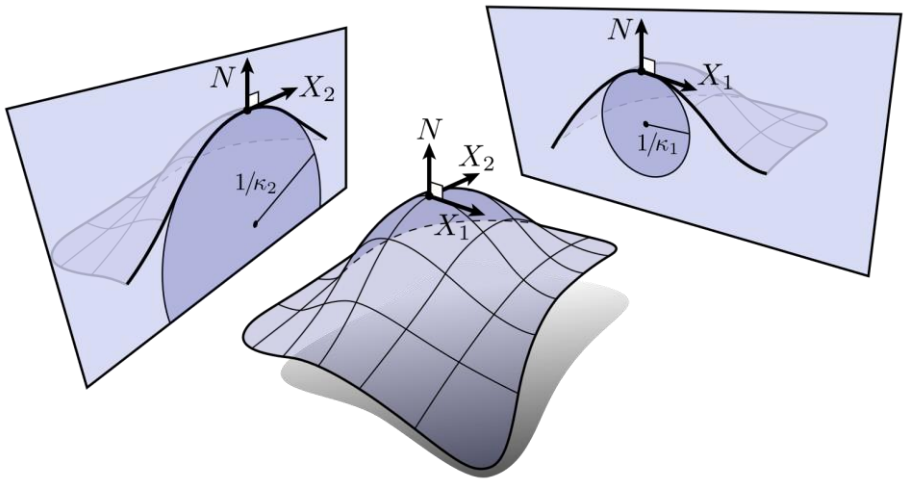

Figure 20. The principle curvatures k_1 and k_2 are the minimum and the maximum normal curvatures at a point on a surface. (Crane, n.d.)

If the Gaussian curvature is negative, it means that the principle curvatures are of different sign, and the point is a *hyperbolic point*. If the Gaussian curvature is zero, it means that one or both of the principle curvatures are zero, and the point is a *parabolic point*. If the Gaussian curvature is positive, it means that the principle curvatures are of the same sign (either both positive or both negative), and the point is an *elliptic point*.

If a surface has nonzero Gaussian curvature everywhere, either negative or a positive, it is called a *double curved*, *or intrinsically curved* surface. If a surface has zero curvature everywhere, it is called a *developable surface*. Examples of the types of surfaces are shown in Fig. 21.

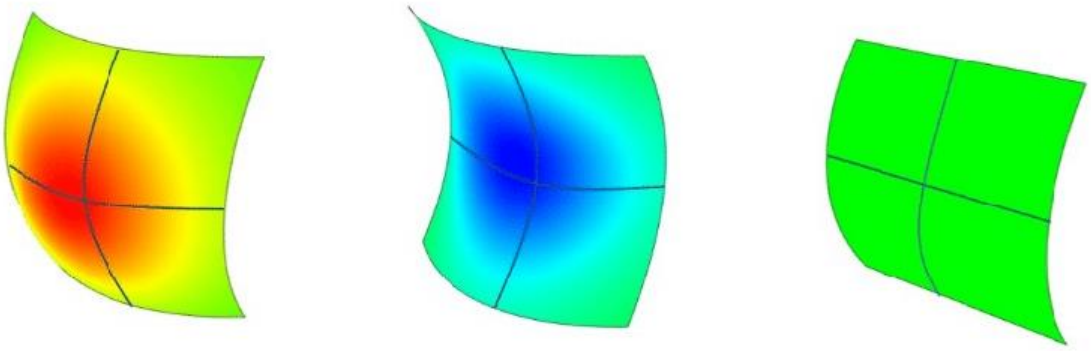

Figure 21. (a) A surface with $K > 0$. The surface consists of elliptic points. (b) A surface with $K < 0$ (a saddle). The surface consists of hyperbolic points. (c) A developable surface (one of the principle curves is a straight line). The surface consists of parabolic points. (Neugebauer, 2018)

A characteristic of a double curved surface is that the angles of a triangle drawn on that surface do not add up to π. The sum of the angles of a triangle on a surface with $K > 0$ is larger than π and the sum of the angles of a triangle on a surface with $K < 0$ is smaller than π.

3.2 Theorema Egrigium

If you would bend a sheet, you would change its extrinsic curvature, but not its intrinsic curvature. The Gaussian curvature would remain zero. You cannot change the intrinsic curvature of a flat sheet, or in other words bend it over its two axes simultaneously, with bending only. In fact, if you bend a sheet over a certain axis, the bending stiffness over the perpendicular axis increases. Therefore, a flat sheet of paper has a lower bending stiffness than a (slightly) curved sheet of paper.

The Theorema Egregium, which means Remarkable Theorem, is an important theorem in differential geometry, and is defined by Carl Friedrich Gauss. It is called remarkable because it can be quantified based on extrinsic measures, but is yet only dependent on intrinsic characteristics of the surface. The theorem states that if a surface deforms without nonuniform stretching, contraction or shear, the Gaussian curvature remains unchanged. You cannot create a sphere (positive Gaussian curvature) out of a flat sheet (zero Gaussian curvature) without nonuniform strain of the surface, or vice versa. That is why the distances on a map of the Earth are distorted compared to the distances on a globe.

That clarifies why the Gaussian curvature is an intrinsic measure of the curvature: it only changes if the distances between points on the surface change, which is a measure for which it is not necessary to know anything about the relationship between the surface and the surrounding space.

3.3 Mechanisms

In this chapter, a categorization is given for the type of mechanisms that can be used for shape-shifting from 2D to 3D. After the structure is given, several example designs categorized and discussed. The goal of the chapter is to have an idea of the different design strategies.

3.3.1 Bending versus buckling

Two major mechanisms that underlie out-of-plane deformation are bending and buckling (Manen, 2018). Bending happens gradually upon applying an out-of-plane bending moment. The out-of-plane bending moment can be realized by a gradient in stresses throughout the thickness of the sheet. Buckling happens suddenly when the critical in-plane compressive stresses are reached. The buckling direction is in theory arbitrary. However, in reality there are small imperfections in the material which impose a preferred direction. These “imperfections” could also be designed by for example applying a through-thickness gradient (Zhou, 2019).

3.3.2 Uniform activation versus nonuniform activation

For Gaussian curvature, in-plane nonuniform strain is required. In almost all of the example mechanisms named in this chapter, a nonuniform strain is preprogrammed in either the material distribution or the material structure. The input merely activates the target shape, but does not define it.

However, the input can influence the shape to some extent in some cases. The magnitude of the input could influence the level of development of the shape in the case of bending. (Buckling happens suddenly by definition, so there is no gradual development of the shape upon increasing the magnitude of the input; the input just has to have reached a certain magnitude.) For example, in Mechanism 5, a pressure difference between the two layers that is smaller than the final pressure difference necessary for a hemispherical shape results in a shape that is somewhere between a flat sheet and a hemispherical shape. The magnitude of the input does not always influence the level of the development though. For example, in the case of an activation temperature it is more like an on/off switch, and the level of development is only dependent on time.

Contrarily, a different type of strategy to realize nonuniform strain is to activate locally (Manen, 2018). The material could be uniform; just the input could realize an in-plane nonuniform strain.

3.3.3 Categorization

The categorization scheme in Table 2 is created. The columns concern whether there is control over the Gaussian curvature or over both the Gaussian curvature and the mean curvature. (No mechanisms with only control over the mean curvature are included, because we want to be able to affect the Gaussian curvature in the end.) Controlling the Gaussian curvature means that the in-plane strains are being regulated. Controlling the mean curvature means that the out-of-plane curvatures are being regulated. The rows concern a difference between a uniform sheet with nonuniform activation (the control is in the activation) and a nonuniform sheet with uniform activation (the control is in the design of the sheet, i.e. the sheet is preprogrammed).

The example mechanisms are categorized based on this scheme and are discussed separately hereafter. The type of activation (bending or buckling) is named apart from the scheme. Out-of-plane bending and buckling do in any case affect the mean curvature, but they do not necessarily affect the Gaussian curvature. For this, in-plane nonuniform strain is needed in addition.

Table 2. Schematic overview of type of curvature that is / are being controlled and how this type of curvature is controlled in each mechanism.

	Control over Gaussian curvature	+ Control over mean curvature
through sheet design	Mechanism 1 (buckling) Mechanism 2 (buckling) Mechanism 6 (bending) Mechanism 7 (buckling) Mechanism 8 (bending) Mechanism 4 (buckling) Mechanism 5 (bending) Mechanism 3 (buckling)	Mechanism 6 (bending) Mechanism 8 (bending) Mechanism 7 (buckling)
through nonuniform activation	Mechanism 3 (buckling)	Mechanism 4 (buckling) Mechanism 5 (bending)

3.3.3.1 Example mechanisms - control over Gaussian curvature

In this category all of the Gaussian curvatures are realized via the design of the sheet, except for one. For this one, the Gaussian curvature is realized via both the design and the activation of the sheet.

Through nonuniform sheet

Mechanism 1 (buckling)

The mechanism is an origami inspired mechanism that consist of rigid panels that are glued on a heat shrinkable polymer, see Fig. 22. The panels prevent the polymer to shrink uniformly. The only motion that is unconstrained is the rotation of the rigid panels towards each other. The shrinkage induces an angular defect and therewith a nonzero Gaussian curvature in the vertices (Cui, 2018).

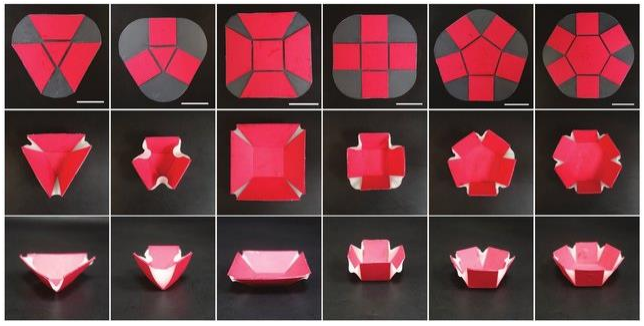

Figure 22. Origami inspired mechanisms that consists of rigid panels that are glued on a heat shrinkable polymer (Cui, 2018).

Mechanism 2 (buckling)

Different Gaussian curvatures are realized with soft hydrogel sheets with rigid inclusions. The patterns of the inclusions determine the final shapes as these inclusions cause nonuniform swelling. The shape is affected by the balance between the stretching energy and the bending energy, which depends on the thickness of the sheet. If one would want to accurately prescribe a complex shape, it is necessary to specify both mean and Gaussian curvature. (That makes sense if you just think of the mean curvature and the Gaussian curvature as two equations with two unknowns.) The mean curvature can be programmed by prescribing a through-thickness differential growth (Jeon, 2017).

Through nonuniform sheet & nonuniform activation

Mechanism 3 (buckling)

The mechanism is a sheet with a non-periodic cut pattern. Three types of cut patterns are used. The first type has a negative Poisson's ratio. The second type has a positive Poisson's ratio. The third type is stiff upon loading in tension. Combining different cut patterns in one sheet causes geometric frustration upon loading. In Fig. 23, the elasticity of the material gradually increases towards the center, where the two edges are kept stiff. The material is pulled in the transverse direction with respect to the gradient direction, and buckles out of plane. In Fig. 24, two islands of the auxetic type of cut pattern are enclosed in a sheet. They transform into two domes under a tensional load.

The buckled shapes depend on both the cut patterns and the loads. Also, if the thickness of the material is increased, more stretch is required for buckling and the shape is larger (Celli, 2018).

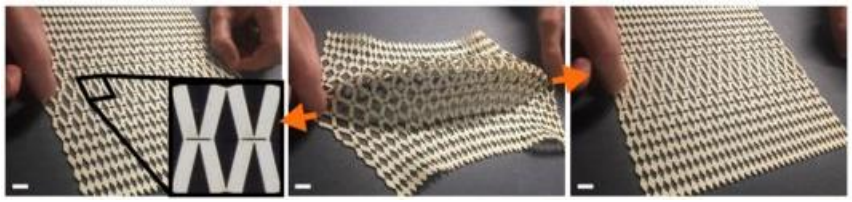

Figure 23. Cut pattern with gradually increasing elasticity towards middle. Scale bar: 12 mm (Celli, 2018).

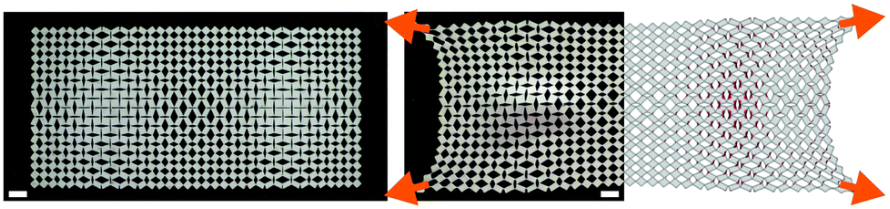

Figure 24. Cut pattern with auxetic island in center. Scale bar: 12 mm (Celli, 2018).

3.3.3.2 Example mechanisms – control over both Gaussian curvature and mean curvature

In this category all of the Gaussian curvatures are realized via the design of the sheet. The distinction between nonuniform activation or nonuniform sheet holds therefore for the mean curvature.

Through nonuniform activation

Mechanism 4 (buckling)

Different Gaussian curvatures are realized by prescribing nonuniform lateral swelling in hydrogel sheets. At a certain level of swelling, a flat sheet buckles into its target shape in 3D. Normally, the sheet would buckle into an arbitrary direction. However, by inducing a through-thickness gradient, the buckling direction can be specified. The through-thickness gradient is realized by exposing the sheet to UV light from either above or below (Zhou, 2019).

Mechanism 5 (bending)

The mechanism is inspired by how the leaves of the Dionaea Muscipula, see Fig. 25, change their Gaussian curvature to capture insects. In Fig. 26, the mechanism is visualized. The cell side lengths determine the amount of strain upon activation, so the inherent geometries of the cells determine the target shape. The mechanism is activated through a pressure difference between the two layers. If the mechanism is completely pressurized, it results in hemispherical shape (Pagitz, 2013).

Figure 25. The leaves of a Dionaea Muscipula can change their Gaussian curvature.

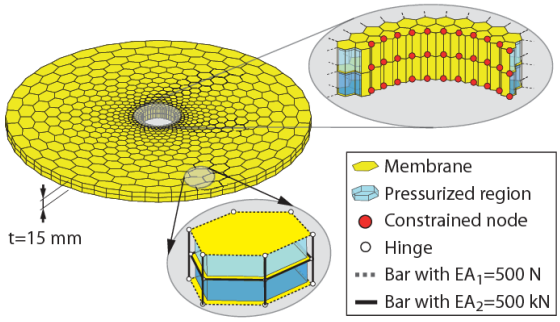

Figure 26. The mechanism consists of two layers of predefined unit cells and is activated by pressurizing the layers differently (Pagitz, 2013).

Only a global through-thickness gradient could be applied in the previous two mechanisms. The direction of the buckling or the bending could be specified with the direction of the gradient and the development of the shape could be specified with the magnitude of the out-of-plane bending moment imposed by the gradient. In the mechanisms below there is even more control of the mean curvature. In these mechanisms namely, the out-of-plane bending moments can be specified locally, and therewith the shape can be controlled to even greater extend.

Through nonuniform sheet

Mechanism 6 (bending)

Energy is stored in a prestressed elastic membrane that is sandwiched between two layers. The two layers both consist of non-periodic unit cells. The linkages between the unit cells consist of brackets and bumpers, see Fig. 27. Upon submersion in warm water, the brackets soften and the energy is (partially) released, so the unit cells are pulled together. Because the bumpers are asymmetric with respect to the midplane, they induce a certain curvature. The lengths of the unit cells, see Fig. 27, are variable, so that nonuniform contraction is possible. In addition, a varying thickness of the brackets allows for different softening rates and therewith for sequential folding (Guseinov, 2020).

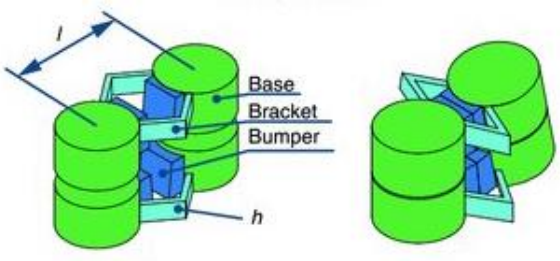

Figure 27. The unit cells of the sheet are connected with these brackets that soften upon submersion in water and bumpers that specify the curvature. The bumpers are pulled together because of a prestressed elastic membrane that is not visualized (Guseinov, 2020).

Mechanism 7 (buckling)

The mechanism is a heterogeneous lattice structure in which both the Gaussian curvature and the mean curvature are programmed for optimal shape control of complex shapes, such as a human face, see Fig. 28. The target shape is conformally (locally preserving angles, but not necessarily lengths) projected onto a plane. Therewith, the required growth per rib is calculated. The growth per rib is realized by a change in in-plane curvature. The change in mean curvature per rib is realized by a change in out-of-plane curvature. Both curvatures can be programmed as the ribs are bilayers in two directions, see Fig. 29. The structure is activated by globally heating the structure (Boley, 2019).

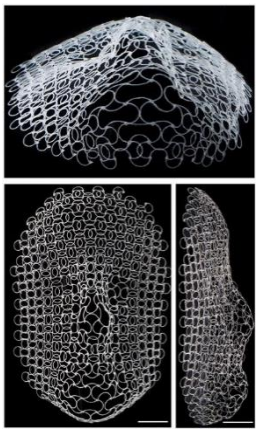

Figure 28. A lattice structure transformed into a human face through controlling both Gaussian and mean curvature (Boley, 2019).

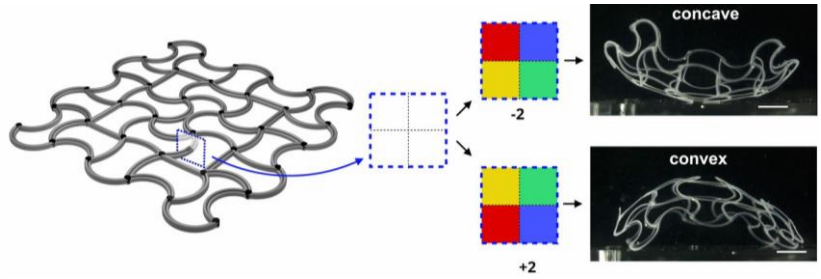

Figure 29. The curvature can be determined in two directions. In-plane curvature allows for in-plane strain, and therewith for determining Gaussian curvature. Out-of-plane curvature allows for out-of-plane curvature and therewith for determining mean curvature (Boley, 2019).

Mechanism 8 (bending)

The structure, see Fig. 30, consists of stretching and folding primitives, which are both activated upon submersion in water. By controlling both stretching and folding, both Gaussian and mean curvature can be specified. The amount of stretching and folding is programmed in the dimensions of the primitives. Note that the amount of programmed stretching is the same in each of the quadrants. The folding primitives determine whether the shape becomes convex or concave (Raviv, 2014).

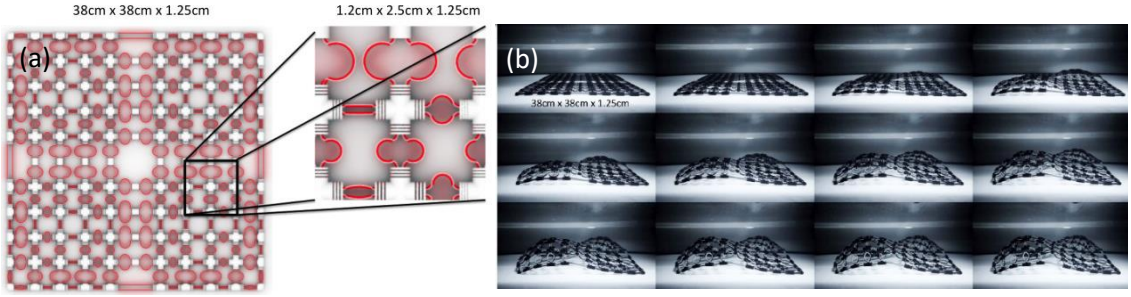

Figure 30. (a) A structure consisting of stretching (red) and folding primitives (white). The dimensions of the primitives determine the final shape. (b) A prototype activated upon submersion in water (Raviv, 2014).

3.4 Buckling in more detail

Recall that the goal is to design a planar network of SMA coil springs. In a planar network, the coil springs cause in-plane forces upon activation. The shape-shifting principle that uses in-plane forces is buckling. In the first instance, we will attempt to realize a shape-shifting network with the in-plane forces that can be realized by the springs, so without incorporating out-of-plane bending moments.

3.4.1 Minimal energy

A material sheet wants to adopt to the shape in which it has the least elastic energy. The elastic energy of a surface can be calculated by taking the surface integral of the elastic energy density function. The elastic energy density function for the one-dimensional case is:

$$w = \frac{1}{8}Et(g - \bar{g}) + \frac{1}{24}Et^3k^2$$

in which E is the material stiffness tensor, t the thickness of the sheet, $g - \bar{g}$ an expression for the amount of in-plane stretching and k the curvature of the sheet. As you can see in the function, the elastic energy of a flat sheet is composed of a stretching term and a bending term. The equation will be used to clarify buckling, but it should be noted that it is for a uniform material rather than for a network. Namely, the stretching and the bending in a network may arise in different structural parts in a designed network, which could have a different stiffness tensor and a different thickness.

The stretching energy scales with t and the bending energy scales with t^3. That means that when scaling down the thickness, the bending term decreases faster than the stretching term. Imagine that in-plane compressive forces strain the material ($g - \bar{g}$ is nonzero), but the sheet remains flat at first (k is zero). If now the thickness of the sheet is decreased or the load is increased, the stretching term becomes to high compared to the bending term at a certain point. At this point, the flat sheet adopts to its curved configuration to relax the stretching, which is called buckling. For an infinitesimal thickness, the bending term approaches zero, and the sheet will adopt to the curved shape that is defined by the prescribed amount of stretching ($g - \bar{g}$). However, in practice the thickness is finite, so the bending term does contribute to the elastic energy. Therefore, the shape is determined by a balance between the stretching and the bending term (Efrati, 2009; van Manen, 2018).

3.4.2 Design considerations for buckling

To allow for out-of-plane buckling upon relatively low in-plane forces, the bending stiffness should be low at least at certain points in the network. The points where the material bends could be at the springs, but also at the points where the springs are connected to each other. The geometries and the materials of the springs and the connectors are design parameters. For the springs, the buckling is mainly dependent on the spring geometry rather than the spring material (Patil, 2013).

The easiest way to connect the springs might be to connect them rigidly. In that case, the out-of-plane bending should be enabled by the springs. The bending stiffness, or the critical buckling load of the springs should be examined to determine if it is low enough for the force that the springs can generate *within the network*. The networks architecture affects the force upon a spring, so it is not

only about whether a spring can generate enough force to buckle itself. Namely, there can be losses within the network, in a sense that a spring deformation results in a deformation of the network rather than an in-plane stress. If it turns out that the springs within the network can generate sufficient force to overcome the critical buckling load of the springs, the springs could be rigidly connected. If not, a solution could be to localize the out-of-plane bending at the connectors. The springs would then cause the necessary in-plane stresses, but the connectors would enable the out-of-plane deformation. The out-of-plane bending can be localized at the connectors by decreasing the bending stiffness of the connectors. The bending stiffness of the connectors could be decreased by decreasing the thickness or decreasing the materials stiffness of the connectors. Another solution could be to increase the sheet size compared to its thickness.

4. Lattices

The lattice structure can be important for both creating the nonuniform strain and for creating the critical buckling stress. The properties of a lattice material are defined by its *material*, the *volume fraction* of the material and the *micro-architecture* of the network (Ashby, 2000), so these are design parameters. These parameters are for a network with solid material struts. Since our struts are springs, an extra design parameter is the geometry of the springs.

The nonuniform strain can be preprogrammed by alternating one or more of the design parameters along the sheet. If the nonuniform strain would be preprogrammed in a sheet by alternating the micro-architecture along the sheet, the shape is inherent to the structural design of the sheet. Imagine that the struts of such a sheet would somehow have the possibility to be activated nonuniformly. It might be difficult to generate different arbitrary shapes with the sheet with the nonperiodic micro-architecture. If a shape would be programmed in a sheet by alternating the properties of the struts, while having a periodic micro-architecture, the step towards using nonuniform activation to generate different arbitrary shapes in the future might be smaller. The nonuniform changes in lengths of the springs realized by alternating spring materials or geometries, may also be realized by nonuniform activation while using only one type of spring.

Therefore, the focus in this chapter is on sheets with periodic micro-architectures, e.g. lattice materials. The micro-architecture of the lattice affects how easily the stresses pile up so that the critical buckling stress is reached. First, some general theory regarding lattice materials is discussed. Second, some specific lattice structures that could be beneficial for our goal are discussed.

4.1 General

Fleck et al. (2010, p.7) describe lattice materials as “a cellular, reticulated, truss or lattice structure made up of a large number of uniform lattice elements (e.g. slender beams or rods) and generated by tessellating a unit cell, comprised of just a few lattice elements, throughout space”. Planar lattices can consist of either one type of polygon or a combination of multiple types of polygons.

An important distinction in lattices is that they can be either *bending-dominated* or *stretching-dominated*. Bending-dominated means that the collapse mechanism of the structure is dependent on the rotational stiffness of the connection points and the bending stiffness of the struts for its macroscopic properties. Stretching-dominated means that the collapse mechanism of the structure is dependent on the axial stiffness of the struts for its macroscopic properties. Stretching-dominated structures have a significantly higher elastic modulus than bending-dominated structures, as the axial stiffness of the struts is way higher than the bending stiffness of the struts.

Whether a lattice is bending-dominated or stretching-dominated depends on the nodal connectivity. For determining whether a lattice is bending-dominated or stretching-dominated, one can look at the lattice as a mechanism consisting of linkages and joints. If a 2D structure is statically and kinematically determinate, so not over-constrained, it should at least fulfill Maxwell’s equation:

$$b - 2j + 3 = 0$$

in which b is the number of linkages and j is the number of joints. If a structure is truly exactly constrained, the mechanism does not contain any mechanism or states of self-stress in addition. This

cannot be withdrawn from the equation above; it is possible that an architecture satisfies Maxwell's equation, but does contain a mechanism or a state of self-stress. The number of periodic collapse mechanisms and periodic states of self-stress, i.e. the kinematic and static properties, can be calculated from the kinematic and equilibrium matrix for the lattice structure (Hutchinson, 2005; Pellegrino, 1986). If it turns out that the lattice contains a collapse mechanism that generates macroscopic strain, the material is bending-dominated. If the lattice contains only periodic collapse mechanisms or no collapse mechanism, the material is stretching-dominated (Fleck, 2010).

4.2 Lattice mechanisms for shape-shifting

Lattice materials are of interest in the field of shape-shifting sheets. The Kagome lattice with periodic collapse mechanisms has for example been used for this. For this, some passive struts have been replaced with active struts. The fact that it contains mechanisms make it actually difficult to create stresses upon activation of the struts. Therefore, it is unlikely that a Kagome lattice will buckle out of plane. In the Kagome designs described below, the Kagome lattice is used differently. The activated mechanisms cause nodal displacements, upon which the strain happens in another layer.

The Kagome structure is an ideal architecture for 2D actuation, because of its in-plane isotropic elasticity, high stiffness and low energy requirement (Hutchinson, 2003). (The actuation energy of a lattice can be determine via a finite element analysis (Wicks, 2004).) Structures with similar properties useful for actuation exist (Nelissen, 2019). The low energy requirement in the Kagome lattice is due to the fact that it contains periodic collapse mechanisms.

The Kagome lattice benefits from the best of both worlds regarding the triangle lattice and the hexagonal lattice. The triangle lattice "provides" the stiffness, as it is a stretching-dominated structure that contains no collapse mechanism; it is kinematically determinate. It is impossible to create an architecture that is both statically and kinematically determinate at the same time (Guest, 2003). The fact that the triangle lattice is statically indeterminate means that it contains redundant struts. Resultingly, if the struts are actuated (to become shorter or longer), it results in a state of self-stress. The actuation energy goes into the struts rather than into a motion, which may be undesirable for actuation. The hexagonal lattice, a bending-dominated structure, "enables" the low energy requirement. It is kinematically indeterminate, so shortening or lengthening one or more of the struts results in a mechanism without deformation of other struts (Pronk, 2017). All of the supplied energy goes into the mechanism, and not into the deformation of the struts.

The Kagome lattice has been used for actuating in 2D to create curvature in 3D. Two designs are given in Fig. 31. The first one concerns one active Kagome layer and a passive solid sheet layer. The second one concerns two active Kagome layers. In both cases, the two layers are connected via a triangulated structure. The Kagome layers are actuated to induce displacements of the nodes of the Kagome structure. In the first design more energy has to be provided for shape-shifting, as high stretching forces are required to strain the passive solid sheet layer (Hutchinson, 2003).

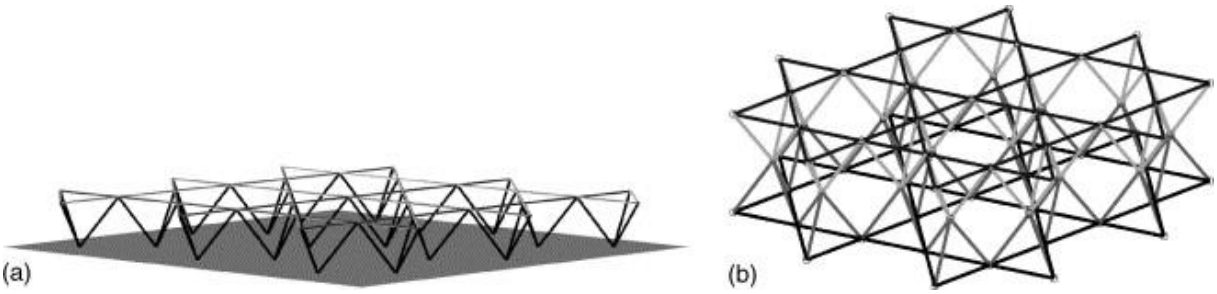

Figure 31. Two designs of planer Kagome lattices of which struts can be actuated for shape-shifting. (a) Active Kagome layer and passive solid sheet layer. (b) Two active Kagome layers (Hutchinson, 2003).

4.3 No lattice mechanisms for shape-shifting

Note that when using a Kagome lattice to actuate in 2D to create curvature in 3D, the actuation force is used to activate a mechanism without straining the struts. However, for buckling with one sheet it is actually desirable if stresses pile up within the architecture and that the only possible deformation is out of plane. In that case, you actually do not want your architecture to contain a mechanism. You want all actuation energy to be trapped inside of the material rather than be used for a motion, so you want the architecture to be kinematically determinate. As there exists no lattice architecture that is both statically and kinematically determinate (Guest, 2003), the lattice architecture will automatically be statically indeterminate. The actuation of the members will result in a state of self-stress.

What is the best statically indeterminate structure to use? A high in-plane stiffness is desirable, for generating high in-plane forces. A finite element analysis can be used to determine the effective stiffness of a lattice material (Nelissen, 2018). In general, the ratio between the effective elastic modulus and the elastic modulus of the is expressed with:

$$\frac{E}{E_S} = B\bar{\rho}^b$$

in which $\bar{\rho}$ is the relative density of the solid, and B and b are coefficients based on the architecture (Fleck, 2010). The in-plane stiffness of a stretching-dominated architecture scale with $\bar{\rho}$ and the in-plane stiffness of a bending-dominated architecture scales with $\bar{\rho}^3$ (Gibson, 1999).

In Table 3, the ratio B of some general stretching-dominated 2D lattice structures can be found (Zhang, 2008; Fleck, 2010). The values are normalized with the relative density r ($\bar{\rho}$ above).

Table 3. Comparison of mechanical properties for various 2D lattice structures (Zhang, 2008)

Unit cell	Triangular	Kagome	Mixed	SI-square	N-Kagome
$E^*/(rE_s)$	0.333	0.333	0.293–0.369	0.293–0.369	0.241

Since it is about stretching-dominated 2D lattie structures, the relative Young's modulus scales linearly with the relative density. This is visualized in Fig. 32. This figure shows the relative stiffnesses in the x-direction. Most of the lattices in the figure are orthotropic, so the stiffnesses are the same in the y-direction. Only for the lattice with the double hexagonal triangulation, which belongs to the bottom line in the figure, the stiffness in the y-direction is different (Elsayed, 2010).

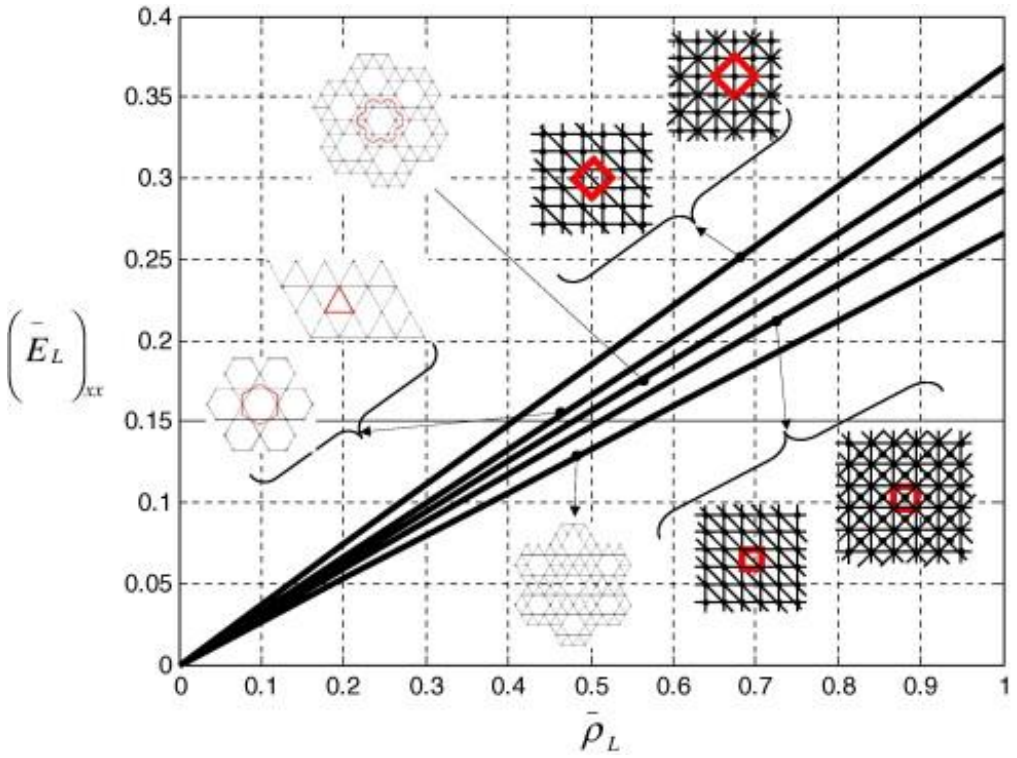

Figure 32. The relative stiffness of a stretching-dominated lattice scales linearly with the relative density (Elsayed, 2010).

5. Inverse design

Nonuniform stretching or contraction is necessary for Gaussian curvature. So, nonuniform lengthening or shortening of the springs is necessary. How much each strut in a lattice should grow or shrink is determined by the target shape. A method to determine the required deformations is conformal mapping, which was for example effectively used for Mechanism 7 of the previous chapter (Boley, 2019). In this chapter, the metric tensor is discussed, which is a basic concept in differential geometry that is used with conformal mapping, and thereafter conformal mapping is discussed.

5.1 Metric tensors

The metric tensor describes the distances between points on a surface. For example, for a flat disc in 2D, the distance between two points in a polar coordinate system (r, θ) is, see also Fig. 33:

$$dl^2 = dr^2 + r^2 d\theta^2$$

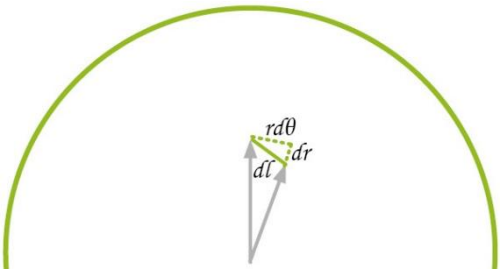

Figure 33. The distance dl between two points on a disk (only half shown) can be approximated with the vectors dr and $rd\theta$ for very small angles.

This can also be described as:

$$dl^2 = \begin{pmatrix} dr & d\theta \end{pmatrix} \begin{pmatrix} 1 & 0 \\ 0 & r^2 \end{pmatrix} \begin{pmatrix} dr \\ d\theta \end{pmatrix}$$

The related metric tensor is:

$$g = \begin{pmatrix} 1 & 0 \\ 0 & r^2 \end{pmatrix}$$

Any change in distance between two points changes the metric tensor (Sharon, 2010). Here, an example that clarifies the relation between the physical sheet and the theoretical metric tensor is given. The change in the metric has been realized physically by imposing nonuniform growth along the radius of a flat disc (Klein, 2007). The nonuniform growth along the radius is programmed in the gradient in the monomer concentration along the radius, see Fig. 34.

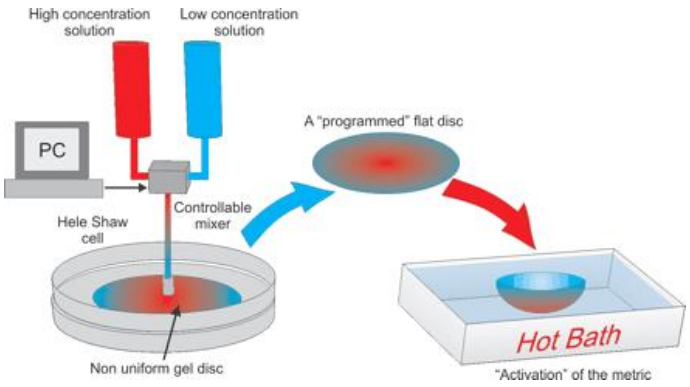

Figure 34. The nonuniform growth along the radius is programmed in the nonuniform material distribution along the radius (Klein, 2007).

The material stretches in both directions: each circle on the disk has a new radius and a new circumference. The material concentration depends on the radius: $\eta = \eta(r)$.

Due to the gradient in the monomer concentration, the radius does not stretch uniformly. The new radius of a circle on the disk can be calculated by adding up all of the small pieces of the old radius each multiplied with its linked growth factor: $\rho(r) = \int_0^r \eta(r')dr'$. The growth factor of the circumference of a circle on the disk depends on its new radius ρ. The growth factor of the circumference of the circle is given with $f(\rho)$ which depends on the material concentration at the new radius $\eta = \eta(\rho)$. The distance between two points on the disc is (Klein, 2007), see also Fig. 35:

$$d\bar{l}^2 = d\rho^2 + \rho^2 f(\rho)^2 d\theta^2$$

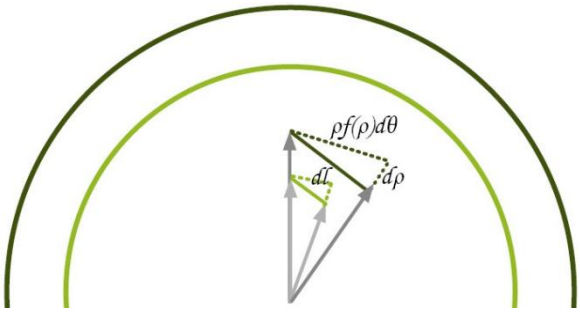

Figure 35. The sheet grows in both directions (light green = old disk outline, dark green = new disk outline). The new distance $d\bar{l}$ between two points on a disk (only half shown) can be approximated with the vectors $d\rho$ and $\rho f(\rho)d\theta$ for very small angles. $f(\rho)$ is the growth factor of the circumference of a circle on the disk, which is dependent on the new radius ρ, as the monomer concentration and therewith the growth factor has been varied over the radius of the disk.

This can also be described as:

$$d\bar{l}^2 = \begin{pmatrix} dr & d\theta \end{pmatrix} \begin{pmatrix} 1 & 0 \\ 0 & \rho^2 f(\rho)^2 \end{pmatrix} \begin{pmatrix} dr \\ d\theta \end{pmatrix}$$

The related target metric tensor is:

$$\bar{g} = \begin{pmatrix} 1 & 0 \\ 0 & \rho^2 f(\rho)^2 \end{pmatrix}$$

The Gaussian curvature K can be withdrawn from the metric tensor, which is in this case:

$$K = -\frac{1}{f(\rho)\rho} \frac{\partial^2 (f(\rho)\rho)}{\rho^2}$$

This can also be done vice versa: the metric tensor can be computed from the Gaussian curvature. The shape is inherent to the target metric tensor. Note that the metric tensor is radially dependent on the location on the disc. So, the Gaussian curvature can vary along the radius of the disk.

The amount of strain necessary to shape-shift between two configurations can be derived from the difference between the metric tensors (see also the energy density function in the text about buckling) (Sharon, 2010):

$$\epsilon = \frac{1}{2}(g - \bar{g})$$

5.2 Conformal mapping

A conformal map maps a grid to another grid while changing the lengths of the struts, but preserving the angles between the struts at the connection points, see Fig. 36. Other mathematical transformations exist as well to transform a surface to another surface, such as generalized multidimensional scaling (Bronstein, 2006). This method aims to map the points of a surface to another surface while preserving the lengths between the points as much as possible. However, the SMA springs can actually realize an axial deformation. Therefore, it is chosen to continue with the conformal mapping method. The springs are suited for the axial deformation of the struts and the connectors between the springs can be used to preserve the angles between the springs.

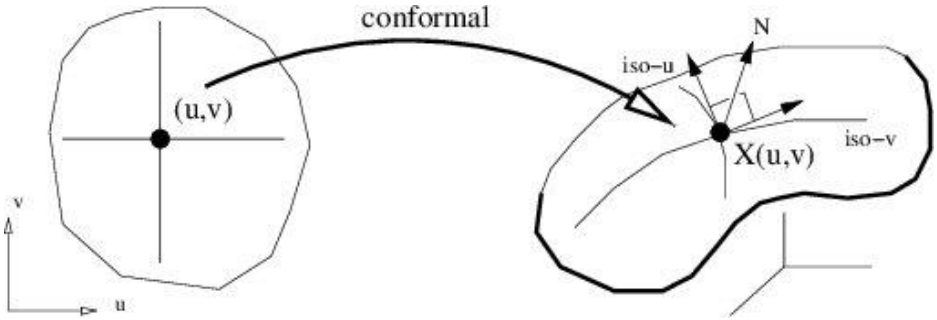

Figure 36. In conformal mapping the angles between the vectors (u and v) are preserved (Lévy, 2002).

The target shape can be conformally projected onto a plane. The Laplacian eigenmaps is a method that does this in a constraint-free way (Mullen, 2008), meaning that there are no constraints on the boundaries of the conformal map. However, it is also possible to impose constraints on the boundaries of the map. Both type of conformal maps are given in Fig. 37 for a face (Kittler, 2018).

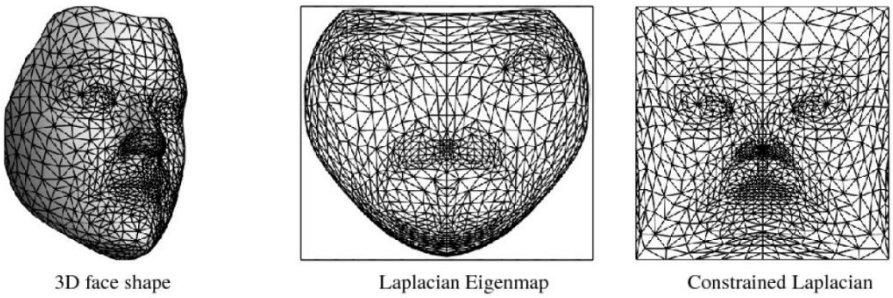

Figure 37. Two conformal maps (right) of the 3D face shape; one without constrained boundaries (left) and one with constrained boundaries (right) (Kittler, 2018).

The mesh in Fig. 37 is not necessarily the lattice structure. The lattice chosen structure can be placed over the conformal map, and the conformal map can be scaled to the size of the lattice. The conformal map provides a function $\boldsymbol{m}(r,\theta)$ that translates a point on the plane to a point on the surface in 3D. The target metric is actually a function of this mapping function (PNAS, 2019):

$$\bar{g} = d\boldsymbol{m}^T d\boldsymbol{m}$$

The required growth for a small vector $d\boldsymbol{u}$ in the plane is (PNAS, 2019, adjusted):

$$s = (d\boldsymbol{u}^T \bar{g} d\boldsymbol{u})/(d\boldsymbol{u}^T g d\boldsymbol{u})$$

So for the example in Chapter 5.1 this means that the growth factor of dl (see also Fig. 35) is:

$$s = \frac{(dr \quad d\theta)\begin{pmatrix}1 & 0\\ 0 & r^2\end{pmatrix}\begin{pmatrix}dr\\ d\theta\end{pmatrix}}{(dr \quad d\theta)\begin{pmatrix}1 & 0\\ 0 & \rho^2 f(\rho)^2\end{pmatrix}\begin{pmatrix}dr\\ d\theta\end{pmatrix}} = \frac{dl^2}{d\bar{l}^2}$$

However, lattices aren't small, so these growth factors cannot be computed in this way for the lattices directly. A solution to this is to compute the average growth field along the strut of a lattice, which represents the growth factor of the strut (PNAS, 2019).

5.3 Conformal mapping and buckling

For Gaussian curvature, nonuniform in-plane strain is necessary. For buckling, in-plane stresses are necessary. The two could be combined (Klein, 2007). The prescribed growth factors of the springs should induce the critical buckling forces when the deformation is still suppressed in plane.

What if you have calculated the growth factors and it turns out that these strains do not result in the required buckling forces? At least you could try tweaking the parameters of the springs such that the same deformation results in a higher force. Another option could be to increase the deformations of the springs. The mapping function could be scaled such that the largest required deformation of a spring is the largest deformation possible by a spring. However, this also magnifies the target shape.

6. Conclusion

Here, the research questions are repeated and the answers are briefly discussed.

What are the important characteristics of an SMA spring?

The background of shape memory alloys and their mechanical properties are discussed. The force-deflection curves of both material phases are important characteristics for the design of an SMA spring actuator. The force-deflection curves can be adjusted by changing the spring parameters: the wire diameter, the spring diameter, the number of coils and the initial pitch angle. Two models that describe the mechanical behavior were found. The advanced model takes into account the detwinning phase, and is therefore more veracious. The model can be used to estimate what spring parameters should be used for a certain force-deflection characteristic.

What mechanisms can be used for a transformation from flat to double curved?

Nonuniform planar strains are needed for Gaussian curvature according to Theorema Egregium. Both Gaussian and mean curvature can be controlled. Controlling the Gaussian curvature means that the in-plane strains are being regulated. Controlling the mean curvature means that the out-of-plane curvatures are being regulated. The control can be either in the design of the sheet or in the activation. Including control over mean curvature allows for greater shape control.

Out-of-plane deformations can be activated through bending or buckling. Bending happens upon applying an out-of-plane bending moment, which can for example be realized by a gradient in stresses through the thickness of the sheet. Buckling happens suddenly when the stretching energy exceeds the bending energy of the sheet. To make buckling happen, the stretching energy could be increased or the bending energy could be decreased. Various solutions to increase the likeliness of buckling came forward: increasing the axial stiffness of the springs via its material or its geometry (more effective), increasing the size of the sheet compared to its thickness, increasing the stiffness of the lattice (or include a stiff boundary), making the connectors bend instead of the springs and choosing a shape for which larger strains are required to begin with.

What lattices can be used and how can the ribs be connected?

The type of lattice is relevant as it influences the stress build-up in the structure, which is necessary for buckling. The background of lattices is discussed, clarifying the difference between bending-dominated and stretching-dominated structures. Stretching-dominated structures are more appropriate, as these are much stiffer than bending-dominated structures. The elastic modulii of several basic stretching-dominated lattices are presented, see Fig. 32. A kinematic model of the chosen lattice with the springs should be made so that the buckling can be simulated.

The second part of the question is not answered yet. It is chosen to find a solution for connecting the springs in a more practical way rather than in a literature research.

How can the required shape be translated to a sheet design?

A conformal map can be used to relate a desired shape to the required in-plane deformations. Conformal mapping is based on axial deformations of the struts, while preserving the angles between the struts at the connection points, which is appropriate for a spring network with rigid connectors. The length changes between two points on a surface that are described by a conformal map hold for

very small differences between the points on the surface. The growth factor of a relatively large strut in the lattice can be computed by taking the average growth factor over the length of the strut.

Project Approach

At first, it will be tried to use the nonuniform strains that are described by a conformal map in a multifunctional way, such that these strains also induce out-of-plane buckling when they are still suppressed in-plane. Several options are named above to enable buckling. If these do not work nonetheless in the end, or if greater control over the shape is desired, bending moments could be included by making the sheet double layered.

References

An, S. M., Ryu, J., Cho, M., & Cho, K. J. (2012). Engineering design framework for a shape memory alloy coil spring actuator using a static two-state model. *Smart Materials and Structures*, *21*(5), 055009.

Ashby, M. F., Evans, T., Fleck, N. A., Hutchinson, J. W., Wadley, H. N. G., & Gibson, L. J. (2000). *Metal foams: a design guide*. Elsevier.

Baseta, E., Tankal, E. and Shambayati, R. (2014). *Translated geometries.* https://iaac.net/project/translated-geometries/

Barbarino, S., Flores, E. S., Ajaj, R. M., Dayyani, I., & Friswell, M. I. (2014). A review on shape memory alloys with applications to morphing aircraft. *Smart materials and structures*, *23*(6), 063001.

Boley, J. W., van Rees, W. M., Lissandrello, C., Horenstein, M. N., Truby, R. L., Kotikian, A., ... & Mahadevan, L. (2019). Shape-shifting structured lattices via multimaterial 4D printing. *Proceedings of the National Academy of Sciences*, *116*(42), 20856-20862.

Bronstein, A. M., Bronstein, M. M., & Kimmel, R. (2006). Generalized multidimensional scaling: a framework for isometry-invariant partial surface matching. *Proceedings of the National Academy of Sciences*, *103*(5), 1168-1172.

Buehler, W. J., Gilfrich, J. V., & Wiley, R. C. (1963). Effect of low-temperature phase changes on the mechanical properties of alloys near composition TiNi. *Journal of applied physics*, *34*(5), 1475-1477.

Celli, P., McMahan, C., Ramirez, B., Bauhofer, A., Naify, C., Hofmann, D., ... & Daraio, C. (2018). Shape-morphing architected sheets with non-periodic cut patterns. *Soft matter*, *14*(48), 9744-9749.

Ceron, S., Cohen, I., Shepherd, R. F., Pikul, J. H., & Harnett, C. (2018). Fiber embroidery of self-sensing soft actuators. *Biomimetics*, *3*(3), 24.

Chopra, I. (2002). Review of state of art of smart structures and integrated systems. *AIAA journal*, *40*(11), 2145-2187.

Cui, J., Poblete, F. R., & Zhu, Y. (2018). Origami/Kirigami-Guided Morphing of Composite Sheets. *Advanced Functional Materials*, *28*(44), 1802768.

Dilibal, S., & Adanir, H. (2013, May). Comparison and Characterization of NiTi and NiTiCu Shape Memory Alloys. In *Safety is Not an Option, Proceedings of the 6th IAASS Conference* (Vol. 715).

Dunbar, M. (2018, September 27). Emerging technology insights: Shape-shifting materials. *CAS*. Retrieved May 22, 2020 from, https://www.cas.org/blog/emerging-technology-insights-shape-shifting-materials

Efrati, E., Sharon, E., & Kupferman, R. (2009). Buckling transition and boundary layer in non-Euclidean plates. *Physical Review E*, *80*(1), 016602.

Elsayed, M. S., & Pasini, D. (2010). Analysis of the elastostatic specific stiffness of 2D stretching-dominated lattice materials. *Mechanics of Materials*, *42*(7), 709-725.

Fleck, N. A., Deshpande, V. S., & Ashby, M. F. (2010). Micro-architectured materials: past, present and future. *Proceedings of the Royal Society A: Mathematical, Physical and Engineering Sciences*, *466*(2121), 2495-2516.

Follador, M., Cianchetti, M., Arienti, A., & Laschi, C. (2012). A general method for the design and fabrication of shape memory alloy active spring actuators. *Smart Materials and Structures*, *21*(11), 115029.

Follmer, S., Leithinger, D., Olwal, A., Hogge, A., & Ishii, H. (2013, October). inFORM: dynamic physical affordances and constraints through shape and object actuation. In *Uist* (Vol. 13, No. 10.1145, pp. 2501988-2502032).

Follmer, S. (2015, October). *Shape-shifting tech will change work as we know it* [Video]. TED Conferences. https://www.ted.com/talks/sean_follmer_shape_shifting_tech_will_change_work_as_we_know_it?language=en#t-465934

Gibson, L. J., & Ashby, M. F. (1999). *Cellular solids: structure and properties*. Cambridge university press.

Gilbertson, R. (1993). Muscle Wires Project Book (San Rafael CA: Mondo-Tronics).

Gracias, D. H., Kavthekar, V., Love, J. C., Paul, K. E., & Whitesides, G. M. (2002). Fabrication of Micrometer-Scale, Patterned Polyhedra by Self-Assembly. *Advanced Materials*, *14*(3), 235-238.

Guest, S. D., & Hutchinson, J. W. (2003). On the determinacy of repetitive structures. *Journal of the Mechanics and Physics of Solids*, *51*(3), 383-391.

Guseinov, R., McMahan, C., Pérez, J., Daraio, C., & Bickel, B. (2020). Programming temporal morphing of self-actuated shells. *Nature Communications*, *11*(1), 1-7.

Hemmert, F. (2010, February). *The shape-shifting future of the mobile phone* [Video]. TED Conferences. https://www.ted.com/talks/fabian_hemmert_the_shape_shifting_future_of_the_mobile_phone?language=en

Holschuh, B., Obropta, E., & Newman, D. (2014). Low spring index NiTi coil actuators for use in active compression garments. *IEEE/ASME Transactions on Mechatronics*, *20*(3), 1264-1277.

Hutchinson, R. G., Wicks, N., Evans, A. G., Fleck, N. A., & Hutchinson, J. W. (2003). Kagome plate structures for actuation. *International Journal of Solids and structures*, *40*(25), 6969-6980.

Hutchinson, R. G., & Fleck, N. A. (2006). The structural performance of the periodic truss. *Journal of the Mechanics and Physics of Solids*, *54*(4), 756-782.

Ionov, L. (2013). Biomimetic hydrogel-based actuating systems. *Advanced Functional Materials*, *23*(36), 4555-4570.

Ishii, T. (2011). Design of shape memory alloy (SMA) coil springs for actuator applications. In *Shape Memory and Superelastic Alloys* (pp. 63-76). Woodhead Publishing.

Jeon, S. J., Hauser, A. W., & Hayward, R. C. (2017). Shape-morphing materials from stimuli-responsive hydrogel hybrids. *Accounts of chemical research*, *50*(2), 161-169.

Kim, B., Lee, S., Park, J. H., & Park, J. O. (2005). Design and fabrication of a locomotive mechanism for capsule-type endoscopes using shape memory alloys (SMAs). *IEEE/ASME transactions on mechatronics*, *10*(1), 77-86.

Kim, S., Hawkes, E., Choy, K., Joldaz, M., Foleyz, J., and Wood, R. (2009). “Micro artificial muscle fiber using niti spring for soft robotics,” in *IEEE/ RSJ International Conference on Intelligent Robots and Systems* (Kobe: IEEE), 2228–2234.

Kittler, J., Koppen, P., Kopp, P., Huber, P., & Rätsch, M. (2018, February). Conformal mapping of a 3D face representation onto a 2D image for CNN based face recognition. In *2018 International Conference on Biometrics (ICB)* (pp. 124-131). IEEE.

Klein, Y., Efrati, E., & Sharon, E. (2007). Shaping of elastic sheets by prescription of non-Euclidean metrics. *Science*, *315*(5815), 1116-1120.

Koh, J. S. (2018). Design of shape memory alloy coil spring actuator for improving performance in cyclic actuation. *Materials*, *11*(11), 2324.

Lévy, B., Petitjean, S., Ray, N., & Maillot, J. (2002). Least squares conformal maps for automatic texture atlas generation. *ACM transactions on graphics (TOG)*, *21*(3), 362-371.

Liu, W., & Talghader, J. J. (2003). Current-controlled curvature of coated micromirrors. *Optics letters*, *28*(11), 932-934.

van Manen, T., Janbaz, S., & Zadpoor, A. A. (2018). Programming the shape-shifting of flat soft matter. *Materials Today*, *21*(2), 144-163.

Matthey, J. (2020). Nitinol technical properties. Retrieved from https://matthey.com/en/markets/pharmaceutical-and-medical/medical-device-components/resource-library/nitinol-technical-properties

Mettler & Toledo (n.d.). Characterization of shape Characterization of Shape Memory Alloys by DSC and DMA, Part 1: DSC Analysis. Retrieved June 9, 2020 from, https://www.mt.com/be/nl/home/supportive_content/matchar_apps/MatChar_UC403.html

Mullen, P., Tong, Y., Alliez, P., & Desbrun, M. (2008, July). Spectral conformal parameterization. In *Computer Graphics Forum* (Vol. 27, No. 5, pp. 1487-1494). Oxford, UK: Blackwell Publishing Ltd.

NASA, Earth Science Communications Team. (2019, April 5). What is MADCAT? Flexing Wings for Efficient Flight. *NASA*. https://climate.nasa.gov/news/2858/what-is-madcat-flexing-wings-for-efficient-flight/

Nelissen, W. E. D., Ayas, C., & Tekõglu, C. (2019). 2D lattice material architectures for actuation. *Journal of the Mechanics and Physics of Solids*, *124*, 83-101.

Neugebauer, J., Wallner-Novak, M., Lehner, T., Wrulich, C., & Baumgartner, M. (2018, May). Movable thin glass elements in façades. In *Challenging Glass Conference Proceedings* (Vol. 6, pp. 195-202).

Otsuka, K., & Wayman, C. M. (Eds.). (1999). *Shape memory materials*. Cambridge university press.

Pagitz, M., & Bold, J. (2013). Shape-changing shell-like structures. *Bioinspiration & biomimetics*, *8*(1), 016010.

Palleau, E., Morales, D., Dickey, M. D., & Velev, O. D. (2013). Reversible patterning and actuation of hydrogels by electrically assisted ionoprinting. *Nature communications*, *4*(1), 1-7.

Patil, R. V., Reddy, P. R., & Laxminarayana, P. (2013). Buckling Analysis of Straight Helical Compression Springs Made of ASTM A229 Gr-II, ASTM A313 Materials (Type 304 & 316). *Int J Eng Res Technol (IJERT)*, *2*(6), 978-986.

PNAS. (2019). Supplementary information for shape-shifting structured lattices via multi-material 4D printing. Retrieved June 13, 2020 from, https://www.pnas.org/content/suppl/2019/10/02/1908806116.DCSupplemental

Pronk, T. N., Ayas, C., & Tekõglu, C. (2017). A quest for 2D lattice materials for actuation. *Journal of the Mechanics and Physics of Solids*, *105*, 199-216.

Pellegrino, S., & Calladine, C. R. (1986). Matrix analysis of statically and kinematically indeterminate frameworks. *International Journal of Solids and Structures*, *22*(4), 409-428.

Raviv, D., Zhao, W., McKnelly, C., Papadopoulou, A., Kadambi, A., Shi, B., ... & Raskar, R. (2014). Active printed materials for complex self-evolving deformations. *Scientific reports*, *4*, 7422.

Seo, J., Kim, Y. C., & Hu, J. W. (2015). Pilot study for investigating the cyclic behavior of slit damper systems with recentering shape memory alloy (SMA) bending bars used for seismic restrainers. *Applied Sciences*, *5*(3), 187-208.

Sharon, E., & Efrati, E. (2010). The mechanics of non-Euclidean plates. *Soft Matter*, *6*(22), 5693-5704.

Stoekel, D. (1989). Thermal Actuation with Shape Memory Alloys. *Raychem* Corporation, p 3.

Tai, N. T., Kha, N. B., & Ahn, K. K. (2010). Predictive position and force control for shape memory alloy cylinders. *Journal of mechanical science and technology*, *24*(8), 1717-1728.

Tanaka, H. (2019, April 22). "*Breathing Façade" by 3D-Printed Auxetic Pattern with Shape Memory Polymer (SMP)* [Video]. https://www.youtube.com/watch?v=Syn7TaX90Ik

Wang, H., Kaleas, D., Ruuspakka, R., & Tartz, R. (2012, March). Haptics using a smart material for eyes free interaction in mobile devices. In *2012 IEEE Haptics Symposium (HAPTICS)* (pp. 523-526). IEEE.

Waram, T. (1993). *Actuator design using shape memory alloys*. San Rafael, CA: Mondotronics.

Wicks, N., & Guest, S. D. (2004). Single member actuation in large repetitive truss structures. *International Journal of Solids and Structures*, *41*(3-4), 965-978.

Wikimedia Commons. (2006, January 19). SMA wire. Retrieved June 13, 2020 from, https://en.wikipedia.org/wiki/Shape-memory_alloy#/media/File:Sma_wire.jpg

Crane, K. (n.d.). A quick and dirty introduction to the curvature of surfaces. Retrieved May 22, 2020 from, wordpress.discretization.de/geometryprocessingandapplicationsws19/a-quick-and-dirty-introduction-to-the-curvature-of-surfaces/

Zanaboni, E. (2008). One Way and Two Way-Shape Memory Effect: Thermo-Mechanical Characterization of NiTi wires. 2008. 81f. *Magistrale in Ingegneria Biomedica, Dipartimento di Meccanica Strutturale, Università Degli Studidi Pavia, Itália*.

Zhang, C., Zee, R. H., & Thoma, P. E. (1996, August). Development of Ni-Ti based shape memory alloys for actuation and control. In *IECEC 96. Proceedings of the 31st Intersociety Energy Conversion Engineering Conference* (Vol. 1, pp. 239-244). IEEE.

Zhang, Y. H., Qiu, X. M., & Fang, D. N. (2008). Mechanical properties of two novel planar lattice structures. *International Journal of Solids and Structures*, *45*(13), 3751-3768.

Zhou, Y., Duque, C. M., Santangelo, C. D., & Hayward, R. C. (2019). Biasing Buckling Direction in Shape-Programmable Hydrogel Sheets with Through-Thickness Gradients. *Advanced Functional Materials*, *29*(48), 1905273.